SVAŠEK HYDRAULICS
COASTAL, HARBOUR AND RIVER CONSULTANTS

Long-term EIA morphological modelling of the MOG2 island

Modelling the long-term morphological effect of the EIA island on Natura2000 and gravel beds

Final

2094/U22319/E/AKR

November 3rd 2022

Kratonkade 23
3024 ES Rotterdam
The Netherlands
Ⓣ +31 - 10 - 467 13 61
Ⓔ office@svasek.com
Ⓘ www.svasek.com

Document title	Long-term EIA morphological modelling of the MOG2 island Modelling the long-term morphological effect of the EIA island on Natura2000 and gravel beds
Short document title	Long-term modelling EIA MOG2
Status	Final
Date	November 3rd 2022
Project name	MOGII Island modelling study
Project number	2094
Client	ELIA ASSET NV/SA
Reference	2094/U22319/E/AKR

Author	Yannick Steenman, Anna Kroon
Checked by	Bas van Leeuwen, Bram Bliek

TABLE OF CONTENTS

1 INTRODUCTION

1.1 The Project

The Modular Offshore Grid 2 (MOG2) project aims at developing and building new grid infrastructure in the Belgian part of the North Sea, following the definition by the Belgian government in the Marine Spatial Plan 2020-2026 of new zones for production and transmission of electricity. The MOG2 shall connect the envisaged new Belgian windfarms situated within the "Princess Elisabeth Windfarm zone".

Part of the potential infrastructure is an Energy Island to receive and convert energy coming from the Windfarm zone and to connect to the shore. In this report the impact of such an energy island on the local tidal flow and sediment balance is addressed as part of the comprehensive Environmental Impact Assessment (EIA) works for this project.

1.2 Purpose of the Report

The purpose of this report is to compare the environmental impact of the MOG2 island for three distinct island locations in the full context of the assumptions, uncertainties, sensitivities, and limitations that were addressed along the way. This includes the model calibrations and validations, comparisons between numerical software's, and uncertainty statements.

1.3 Approach

The impact of the MOG2 island on the local sediment balance and the resulting morphological changes is assessed using numerical models. For this purpose, the inhouse model FINEL of Svašek Hydraulics is employed, as was also the case in the MOG2 island metocean modelling and the MOG2 morphological study for the tender design (IMDC, CDR, Svašek. (2022a, 2022d)). The model assesses the impact of the tidal current around the island and the response of the bathymetry on changes in this tidal flow. The morphological impact of the MOG2 island as calculated by the FINEL model simulations is used to gain insight in the to-be-expected environmental impact of the MOG2 island on the local erosion and sedimentation, the Natura2000 area, and the potential gravel bed locations as described on the EDEN 2000 webpage[1].

Especially for the gravel bed impact uncertainties in the model predictions are highly relevant, because sedimentation of only 1 or 2 cm can already be significant. Therefore a sensitivity analysis is caried out, that focusses on the gravel bed sedimentation, to get additional confidence in the predictions.

For the purpose of the EIA, several potential island locations are considered within this report, being the West1, West2 and North island locations.

Finally, the results from the FINEL models deliver the input for the sediment plume computations, as set-up by IMDC for the EIA IMDC (2022).

1.4 Reading Guide

The starting assumptions are outlined in Chapter 2, the FINEL software package is explained in Chapter 3, followed by the morphological model inputs in Chapter 0. The hydrodynamic results of the FINEL model are tested in Chapter 5 followed by a description of the hydrodynamic impact of the island on currents, waves in chapter 0. The morphological impact of the island on sediment

[1] https://www.health.belgium.be/nl/eden2000-studies

concentration, local scour and deposition, and impact on gravel bed locations and the corresponding model sensitivity is presented in Chapter 0. Finally, the conclusions and recommendations are highlighted in Chapter 8.

2 STARTING MODEL ASSUMPTIONS

2.1 Island locations and available bathymetry data

Bathymetry data in the Belgian part of the North Sea is available on the 20 m grid of the Belgium continental shelf dataset. Those datasets are made available by the Flemish government (more specifically, Agentschap Maritieme Dienstverlening en Kust, Afdeling Kust') on the website "https://bathy.agentschapmdk.be/bathy/". An overview of this bathymetry is shown in Figure 2-1.

Within the EIA three island locations are considered, being the West1 location (465168 UTMx, 5708697 UTMy), the West2 location (466500 UTMx, 5710500 UTMy), and the North location (469678 UTMx, 5716008 UTMy). An overview of the three island locations is given in Figure 2-1.

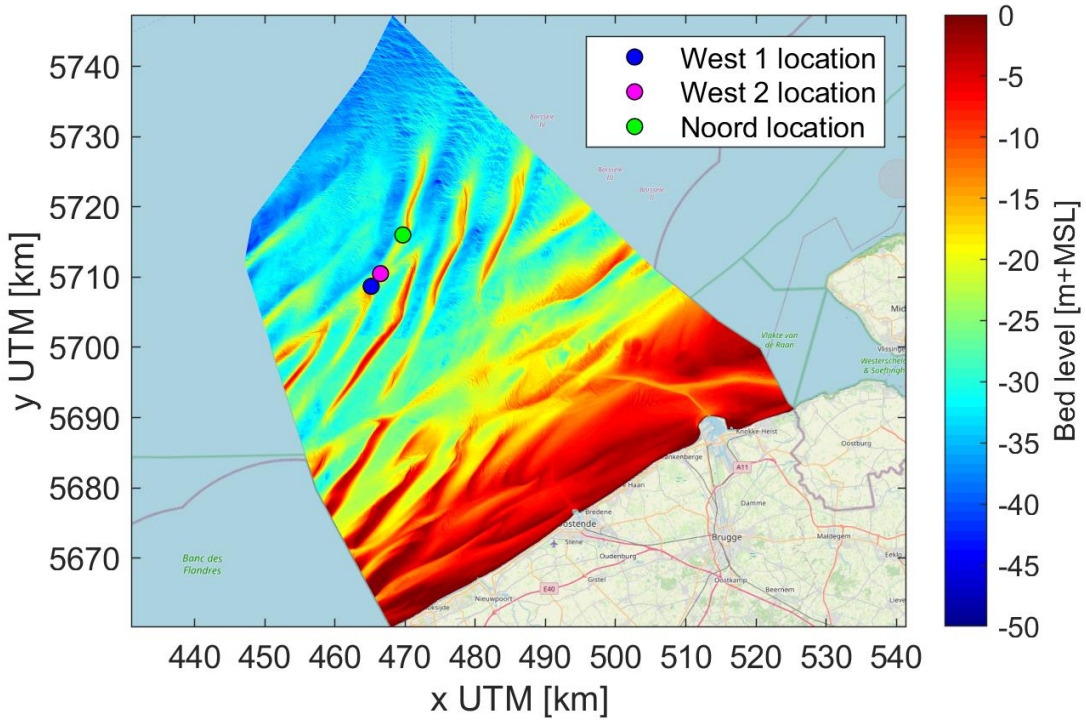

Figure 2-1: MOG2 island locations considered in the MER simulations in the context of the Belgian part of the North Sea

2.2 Island design

To maintain optimization flexibility for the tender process, an island design slightly wider compared to the island tender design was used within the EIA model simulations. However, the same rectangular shape is considered. Including the caisson structures, the dimensions of the island are 500 x 260 m. These dimensions are kept constant for all three island locations.

The base of the caisson structures is located at -17 m+LAT for all three island locations. For the West1 location, this position coincides with the average level of the bathymetry. However, for the West2 and North locations, an artificial sand platform is created to heighten the bed up to -17 m+LAT, see Figure 2-2.

Next to the caisson structures, a toe structure is built to ensure the stability of the caissons. This toe spans a height of 5 m and a width of 15 m, with the base located at -17 m+LAT. Next to the toe, a

horizontal buffer zone of 30 m is maintained to ensure dredging practices are carried out at a safe distance from the toe, see Figure 2-2. For the West2 and North locations, the bed lowers at a slope of 1:10 until the existing bed is reached.

2.3 Island orientations

To minimise the blocking effect of the island on the surrounding flow, the island is preferably oriented in such a way that it aligns the island's long sides with the predominant ebb and flood flow directions. If this is done perfectly, the blocking effect of the island is solely determined by the width of short-side of the island, which is 260 m in the current design. In any other case, the blocking width of the island is larger.

Within the scope of this project, the orientation of the island is kept constant at 30°N at all three island locations, as the perfect alignment is not known for all three islands. This leaves room for improvement for a contractor to optimise this project, making the produced environmental impact in this report conservative. Nevertheless, earlier preliminary work (Svasek, 2022c) showed the orientation of 30°N is especially unfavourable for the Noord location compared to the West1 and West2 locations. Thus, for the Noord location, a more favourable orientation of 50°N is also considered in a small sensitivity analysis.

2.4 Pre-dredge and scour protection design

Pre-dredging is the process where sediment is dredged from the expected erosion holes before the structure is placed. Within the scope of the MOG2 island, pre-dredging is carried out for two primary reasons: 1) to limit the amount of sediment released in the water column due to erosion, and 2) to use the pre-dredged sediment for the construction of the island.

The pre-dredge holes and the scour protection for all three locations are designed by **CDR**. The pre-dredge hole is created with a 1:10 slope downwards from the island. For the West2 and North location, this is essentially an extension of the downward slope from the platform. Between the three island locations, the depth of the pre-dredge holes varies due to the varying bed levels for the three locations. The pre-dredged volumes, depths, and scour protection lengths are shown in Table 2-1**.** A sketch of the pre-dredge design as it is implemented for the West2 and North locations is shown in Figure 2-2. Note that the design for the West1 location is similar, except that the existing bed is already located at -17 m+LAT.

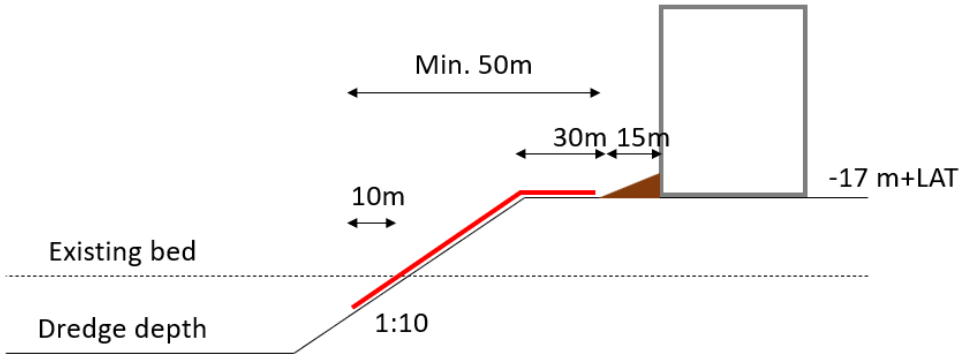

Figure 2-2: Sketch of the MOG2 island design for the West2 and North locations including the pre-dredge design and the bed protection (in red). The design for the West1 location is identical, except that the existing bed is already located at -17 m+LAT.

Table 2-1: Pre-dredge hole and scour protection characteristics for the three potential MOG2 island locations as used in the simulations.

Location	Pre-dredged volume [Mm^3]	Pre-dredge hole depth [m+LAT]	Length of scour protection [m]
West1	2.43	-20.70	50
West2	2.23	-23.90	79
North	2.30	-22.85	62

The islands for all three locations including pre-dredge holes as placed in the numerical grids are shown in Figure 2-3, Figure 2-4, and Figure 2-5 for locations West1, West2 and North respectively.

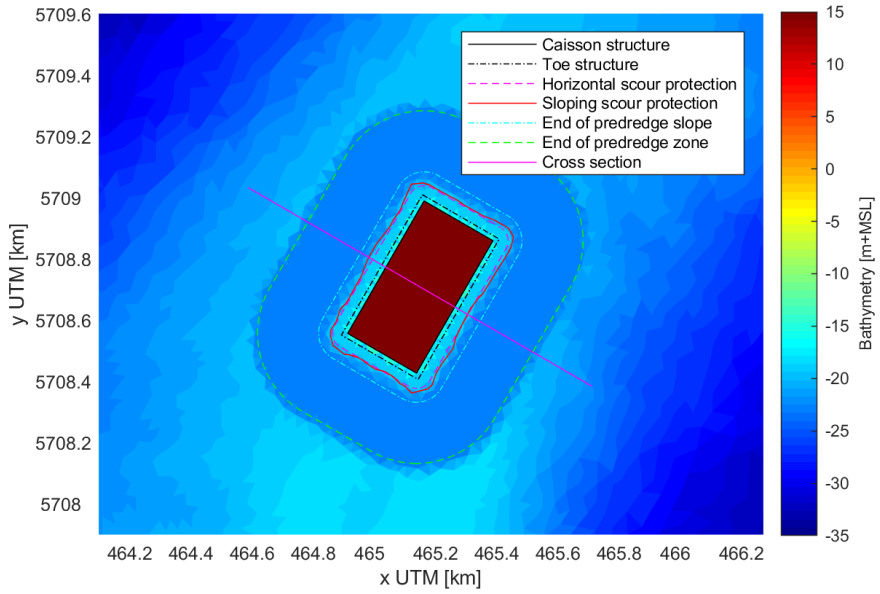

Figure 2-3: MOG2 island EIA design including pre-dredge holes as placed in the numerical grid for the West1 location.

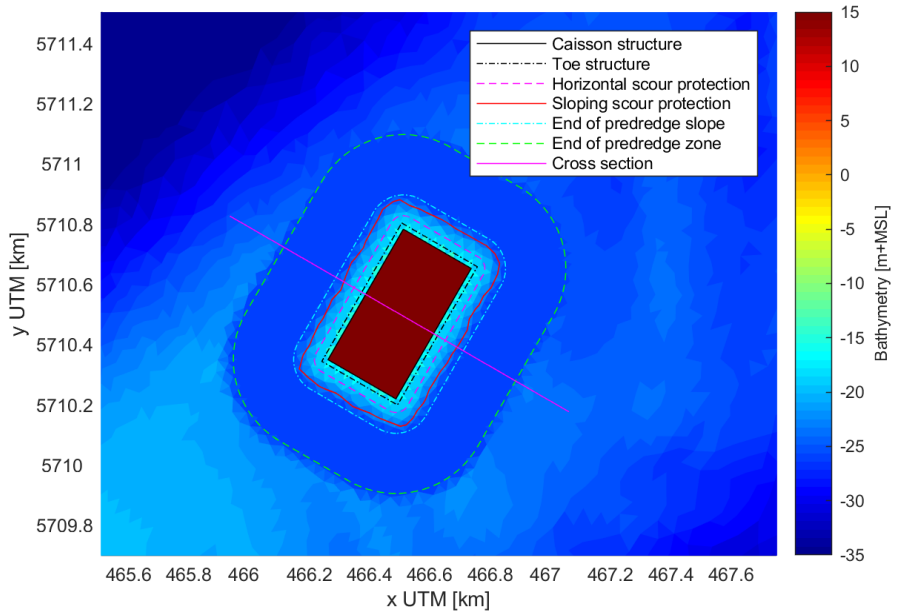

Figure 2-4: MOG2 island MER design including pre-dredge holes as placed in the numerical grid for the West2 location.

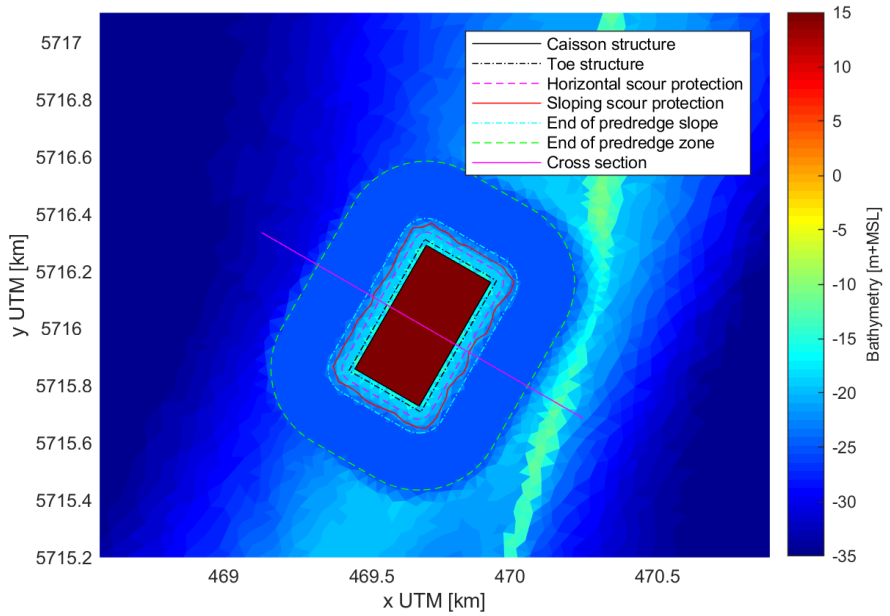

Figure 2-5: MOG2 island MER design including pre-dredge holes as placed in the numerical grid for the Noord location.

2.5 Natura2000 area

The Princess Elisabeth Windfarm zone is located close to Natura 2000 (N2000) area, Figure 2-6. To be able to responsibly allow wind farm activities close to N2000 areas the Belgian government initiated a programme called EDEN2000 - “Exploring options for a nature-proof Development of offshore wind farms inside a Natura 2000 area”.

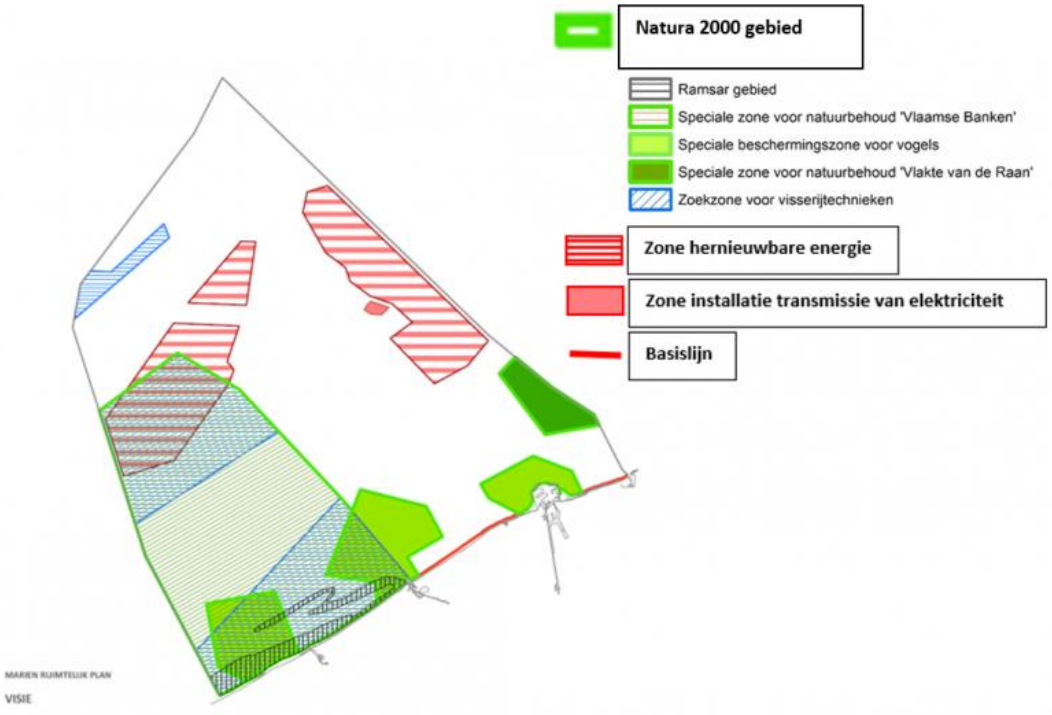

Figure 2-6: Natura 2000-areas and zones for renewable energie, MRP 2020-2026 (source: https://www.health.belgium.be/nl/eden2000-studies).

2.6 Gravel beds

The EDEN2000 research identified three types of gravel bed areas (Figure 2-7). Type 1 contain surfaced gravel with a high likelihood, type 2 contain surfaced gravel and coarse sand with a high likelihood, and type 3 contain surfaced gravel with a low likelihood.

These zones are wider polygons drawn around irregular contours of gravel areas, as can be seen in Figure 2-7. Indicating that especially at the edges of these areas the likelihood of surfaced gravel might be lower. This study primarily focusses on sedimentation due to the placement of the MOG2 island on the type 1 and type 2 gravel beds as described in the EDEN2000 research.

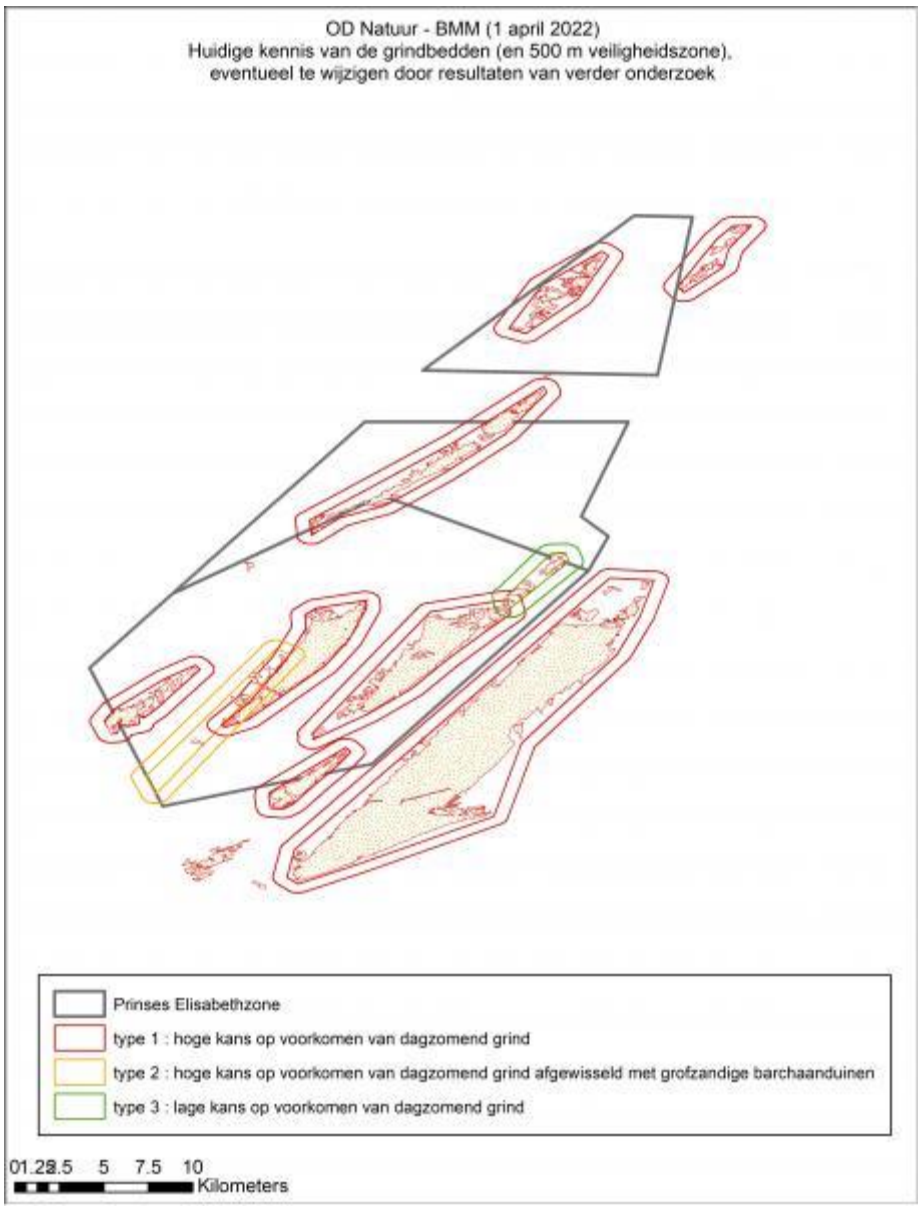

Figure 2-7: Gravel bed areas according to the EDEN2000 study (source: https://www.health.belgium.be/nl/eden2000-studies).

3 SOFTWARE & MODEL EXPLANATIONS

This chapter serves to highlight the employed numerical software within the scope of this project, and the framework of the numerical model used in this report. Hydrodynamic and morphological simulations are carried out using the computational flow software FINEL, which has been developed in-house by Svašek Hydraulics. The FINEL software package, separated in the FINEL-explicit and FINEL-implicit packages, is explained in Section 3.1.

The basis of the numerical model set-up in this report was created in the MOG2 island tender design study, see *IMDC, CDR, Svašek (2022d*). The details and adaptations made to this model to fit the purpose of a morphological impact analysis of the island is explained in Section 3.2.

3.1 Used numerical software

In this study, two distinct numerical software types are employed. In this section, a concise summary of both software types is given.

3.1.1 Hydrodynamic model FINEL2D with explicit solver

FINEL2D-explicit is a two-dimensional numerical flow model based on the finite element method. The underlying equations are the shallow water equations in combination with a hydrostatic pressure assumption and a constant density. The continuity and impulse equation read:

$$\frac{\partial h}{\partial t} + \frac{\partial uH}{\partial x} + \frac{\partial vH}{\partial y} = 0$$

$$\frac{\partial Hu}{\partial t} + \frac{\partial Hu^2}{\partial x} + \frac{\partial Huv}{\partial y} - fHv + \frac{H}{\rho}\frac{\partial p}{\partial x} - \frac{1}{\rho}\left(\tau_{x,b} + \tau_{x,w} + \tau_{x,r}\right) = 0$$

$$\frac{\partial Hv}{\partial t} + \frac{\partial Huv}{\partial x} + \frac{\partial Hv^2}{\partial y} + fHu + \frac{H}{\rho}\frac{\partial p}{\partial y} - \frac{1}{\rho}\left(\tau_{y,b} + \tau_{y,w} + \tau_{y,r}\right) = 0$$

In which:

H	= $h+z$ the water depth (m)
h	= water level (m+MSL)
z	= bottom level (m+MSL)
u, v	= depth averaged velocity in x- and y-direction (m/s)
f	= Coriolis parameter (s^{-1})
ρ	= density of water (kg/m^3)
p	= $p_{atm}+\rho gH$
p_{atm}	= atmospheric pressure (N/m^2)
g	= acceleration of gravity (m/s^2)
$\tau_{x,y\,b}$	= bottom shear stress (N/m^2)
$\tau_{x,y\,w}$	= wind shear stress (N/m^2)
$\tau_{x,y\,r}$	= wave forces (N/m^2)

The finite element method works with triangular elements. Discontinued Galerkin (*Hughes*, 1987) is applied to solve the above differential equations. Within every element, the water level and velocity are assumed constant. The solution is found with a Riemann solver named Roe, see *Glaister* (*1993*).

In mathematical terms the Roe solver in FINEL2D-explicit is a first order upwind scheme. This method guarantees strict mass and momentum conservation, but suffers from some numerical diffusion in stream-wise direction. To maintain acceptable levels of diffusion within the software, the physical

diffusion term is not resolved in the Shallow Water Equations. Thus, the software does not resolve physical, turbulent diffusion, but rather numerical diffusion that is dependent on the grid size. As a result, the diffusion within the model is not controlled with a turbulence model. The implications of this limitation of the model within the current project will be addressed in a later chapter. An explicit time integration scheme is used. As this method restricts the time step, the time step is controlled automatically for optimum performance. This allows the model to simulate long distances within long timeframes.

Apart from the commonly known tidal harmonic boundary conditions along open sea boundaries, FINEL2D-explicit has the option of applying a tidal potential to the water mass that is present within the model area. Tidal potential accounts for the net effect of direct tidal forces exerted on the Earth by Sun and Moon; this net tidal force consists of gravitational as well as centrifugal forces, and its variation is influenced by both the motion of Sun and Moon and the rotation of the Earth. In terms of hydrodynamic modelling, tidal potential may become important as soon as the total water mass becomes so extensive that its tidal behaviour is not fully governed by mere boundary conditions anymore. This is the case if the sea/ocean model exceeds a size of typically a few 100 km's (or equivalently, a few tidal wave lengths). Physically, tidal potential is a function of a large amount of given astronomical and geophysical parameters. Two implementations of tidal potential forces are included in the FINEL package, *Hervouet* (*2007*) and *Schrama* (*2020*). For this project, the second implementation is used in the modelling of the flow conditions in the North Sea.

3.1.2 Morphological module FINEL2D-explicit

The morphological module of FINEL2D-explicit uses current velocities and orbital velocities and/or (depending on the formula used) bottom shear stresses by currents and waves to calculate sand transport. Several transport formulas are available in FINEL2D-explicit, including *Engelund, F., & Hansen, E.* (*1967*), *Soulsby* and Van Rijn (Soulsby, *1997*), and *van Rijn* (*1984*).

Sediment fluxes are determined every hydrodynamic time step and translated to bottom changes. These bottom changes are multiplied by the morphological acceleration factor and used to calculate the new bed level. The new bed level is used for the hydrodynamic calculation on the next time step.

3.1.3 Hydrodynamic model FINEL2D with implicit solver

FINEL2D-implicit is a two-dimensional, parallel, non-hydrostatic flow solver based on the Finite Element Method (FEM), suitable for the computation of (shallow) water flow and transport processes in rivers and coastal waters. FINEL2D-implicit is based on the shallow water equations. The primary difference between FINEL2D-implicit and FINEL2D-explicit is the inclusion of the diffusion term within the shallow water equations, and thus the inclusion of turbulence.

The scientific basis of FINEL2D-implicit is given by research work by *Labeur* (2009) and *Labeur & Wells* (2012), who developed a 3D Navier-Stokes solver based on the novel Galerkin Interface Stabilization approach, which yields an advantageous combination of accuracy, stability and efficiency requirements. The implementation of FINEL2D-implicit applies these scientific concepts, but the model was further developed in-house by Svašek Hydraulics.

FINEL2D-implicit employs a flexible mesh of triangles (or tetrahedra in 3D mode), which can be built by various mesh generators. It is possible to use the same grid in 3D mode as for the 2-dimensional shallow water flow model FINEL2D-implicit; such a 2D mesh can be extended to a 3D mesh by adding element layers over the vertical (possibly locally refined). This method offers almost unlimited flexibility in grid generation: special features in the area of interest can be accurately incorporated within the model.

FINEL2D-implicit can deal with flow over weirs and barriers, drying-/wetting events and density effects resulting from (combined) cold-warm and salt-fresh interactions, as well as many other physical processes and boundary conditions.

3.2 North Sea model set-up

The basis of the numerical models used in this report stems from the MOG2 island Metocean Report (*IMDC, CDR, Svasek, 2022a*) carried out previously. Below, a short summary of the relevant information from the MOG2 island Metocean Report is given, including adaptations made for the environmental impact study of the MOG2 island. For more information regarding the model set-up, consult *IMDC, CDR, Svasek (2022a*).

3.2.1 Computational grid

The model domain of the FINEL North Sea flow model consists of the full European Continental Shelf, see Figure 3-1, ensuring that the tidal currents are well captured by the model, and allowing the possibility to incorporate meteorological effects in the model. FINEL employs an unstructured triangular mesh, which enables the user to fit boundaries accurately within the model and to increase resolution in the region of interest in a flexible way, without the need for nesting of grids. The grid resolution at ocean boundaries is between 8000 - 12000 m and refines to approximately 4000 m in the West part of the North Sea and the English Channel.

For the three island locations, being West1, West2 and North, the model template is adapted to increase the resolution of the model close to the considered island location. At least 20 km from the island location, the grid refines to approx. 400 m, which slowly continues to decrease to 90 m at 5 km from the island. At 2 km from the island the grid is set at its highest resolution of approx. 40 m. The general scale of the model is depicted in Figure 3-1, with close-ups around the individual island locations shown in Figure 3-2.

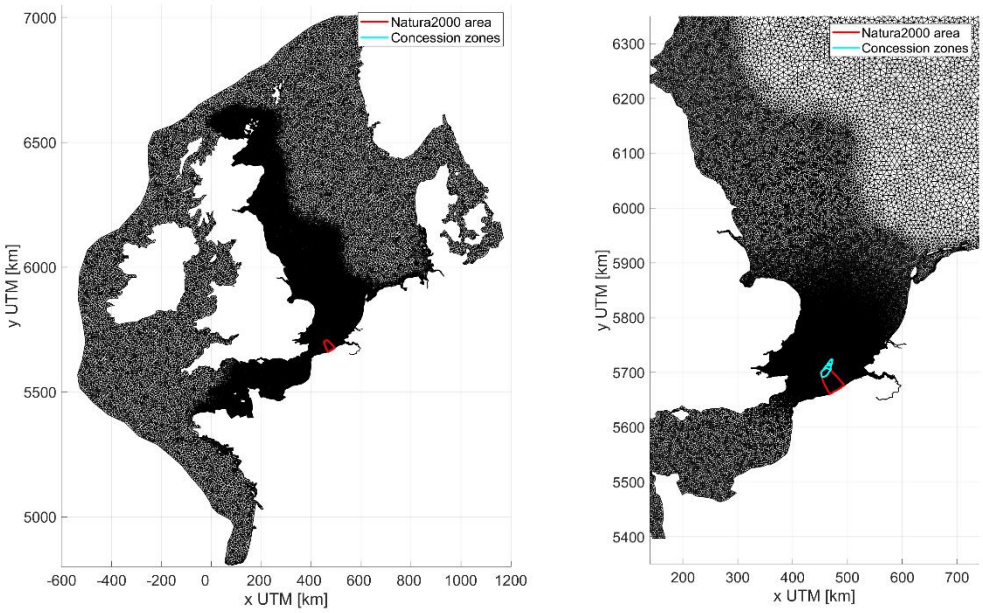

Figure 3-1: Computational grid (2D view) of FINEL North Sea flow model.

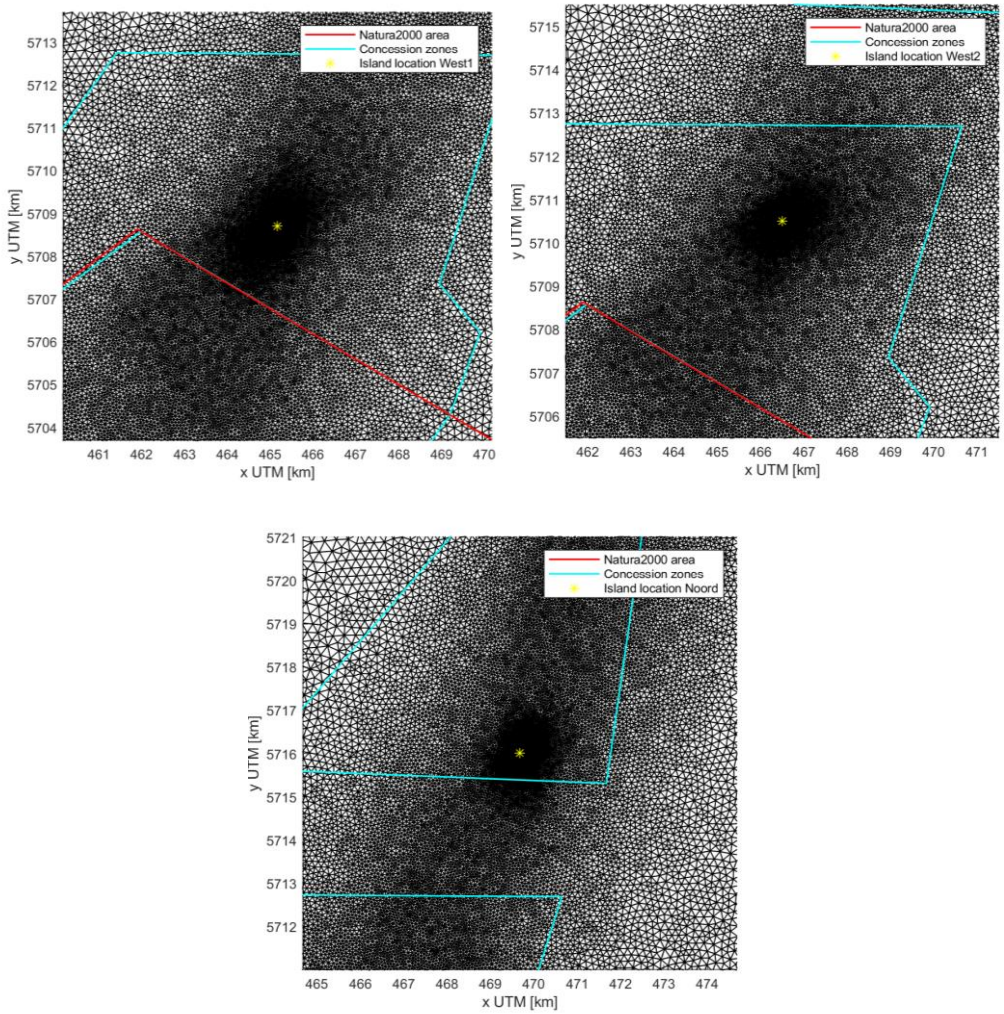

Figure 3-2: Zoom-in of the numerical grids around the three island locations.

3.2.2 Boundary conditions

The tidal amplitudes and phases used as harmonic tidal boundary conditions are extracted from the global FES2014a (32 harmonic components, 1/16° grid) world tide database.

Additional boundary conditions are applied to accurately implement the discharge from the Rhine and Meuse River. The Eastern-Scheldt barrier is included in the model with barrier formulations including energy loss coefficients.

3.2.3 Calibrated roughness

The FINEL North Sea model is calibrated using the OpenDA automated calibration software. In OpenDA the DUD (Does not Use Derivative) algorithm (*Ralston and Jennrich*, 1978) is used to evaluate and optimize uncertain model parameters for a nonlinear least square problem. This is done by minimizing a quadratic cost function by adjusting model parameters. The roughness parameter values corresponding to the minimum value of the cost function are considered as the optimal roughness parameter values for the given problem. The resulting roughness field is shown in

Figure 3-3. For more information regarding the calibration of the model, see *IMDC, CDR, Svasek* (2022a).

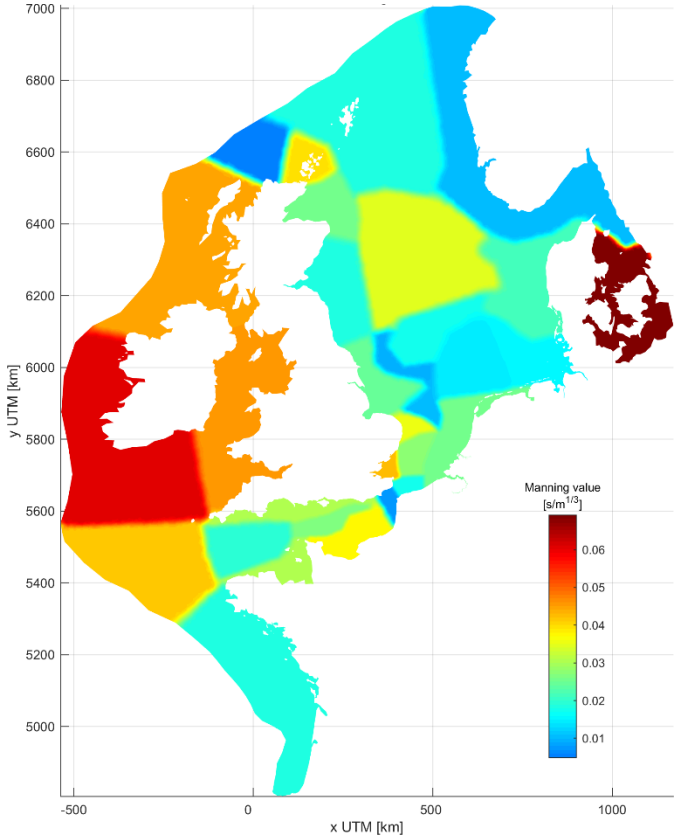

Figure 3-3: Resulting calibrated roughness map.

3.2.4 Hydrodynamic model inputs

For the hydrodynamical computations, FINEL2D version 7.30 (released 9 February 2021) is used. The most important model settings are summarised in Table 3-1. The calibration parameter of the FINEL flow model is the manning roughness.

Table 3-1: FINEL North Sea model settings

Parameter	Calibration setting	Validation setting
Manning roughness	Spatially variable	Spatially variable
Water density	1025 kg/m^3	
Water temperature	10 ˚C	

3.3 Model validation

The FINEL North Sea flow model including CFSR wind and air pressure fields is validated for a storm period of two months, for a calm period of two months, and for available sailing measurements near the MOG2 project location. The validated two-month storm period, December 2017 to January 2018, consists of a northwest storm (around 7 December), a southwest storm (around 3 January) and calm periods in between. Only water level measurements are available for validation in this period. For the two-month calm period, June to July 2012, both water levels and current measurements are

available. For the sailing measurements, only current measurements are available. The sensitivity of the current direction on model grid resolution is checked by validation of the applied grid and a refined grid.

3.3.1 Validation tide during storm conditions

In Figure 3-4 the water level comparison for December 2017 to January 2018 is presented at Westhinder Meetpaal. The timeseries and scatterplot for this period is presented for FINEL and the observations. The figures show that the FINEL model is well capable of reproducing the water level during storm conditions. A high correlation is visible, with a root mean square error of 11 cm.

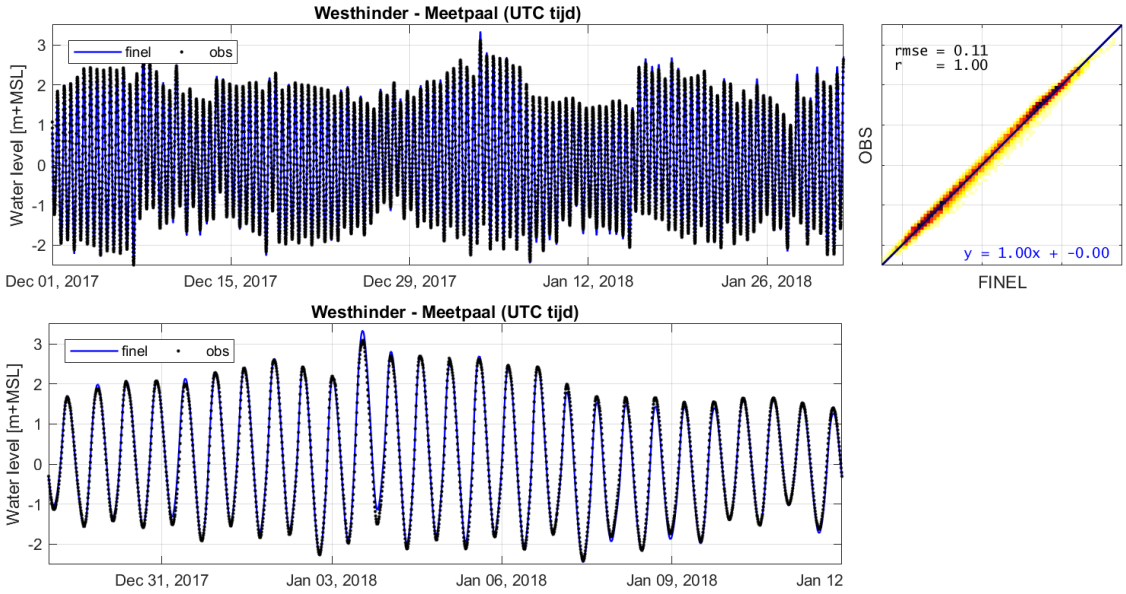

Figure 3-4: Water level and scatterplot comparison between FINEL and observations at Westhinder Meetpaal for December 2017 to January 2018.

3.3.2 Validation tide during calm conditions

In Figure 3-5 the water level comparison for 17 June to 11 August 2012 is presented at Westhinder Meetpaal. The timeseries and scatterplot for this period is presented for FINEL and the observations. The figures show that the FINEL model is well capable of reproducing the water level during calm conditions. A high correlation is visible, with a root mean square error of 9 cm.

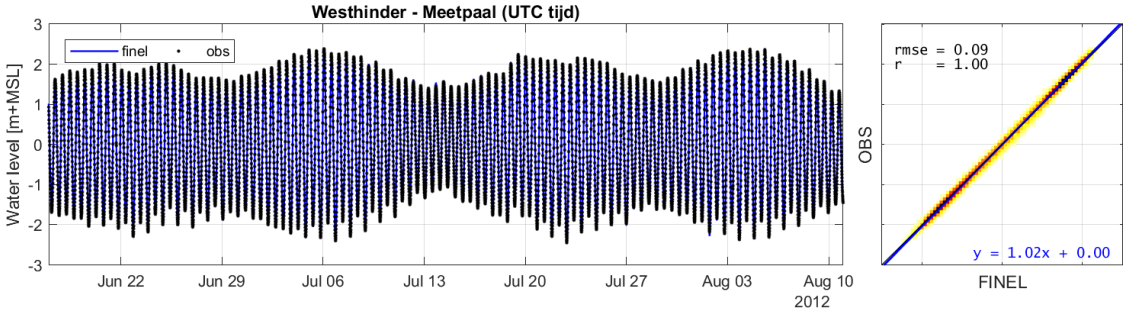

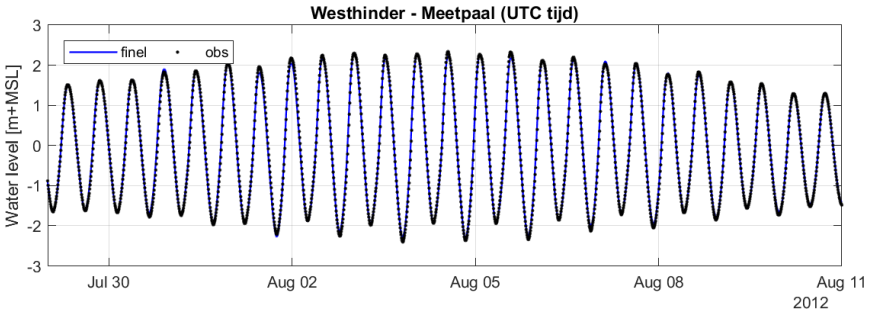

Figure 3-5: Water level and scatterplot comparison between FINEL and observations at Westhinder Meetpaal for 17 June to 11 August 2012.

3.3.3 Validation currents during calm conditions

In Figure 3-6 the current comparison for 17 June to 11 August 2012 is presented for Westhinderbank Noord, and a close up for the last 2 weeks can be found in Figure 3-7. This measurement station is located just east of the shallow and relatively steep Westhinderbank, see Figure 3-8. This influences the current speed and direction. A few observations can be made:

- The current speed shows a root mean square error of 14 cm/s for this period. The ebb current speed is modelled relatively well, while the flood current speed is overestimated in FINEL.
- The FINEL current direction is oriented approximately Southwest (ebb current) to Northeast (flood current) and rotates counter clockwise during the entire measurement period. The measurement direction is oriented approximately West (ebb current) to Northeast (flood current) and rotates around the North during the largest part of the measurements period.
- After August 4th, the measured directions and rotation suddenly change and match FINEL predictions well. As no apparent cause for this shift in current directions was found, it may indicate some uncertainty in the measurements.

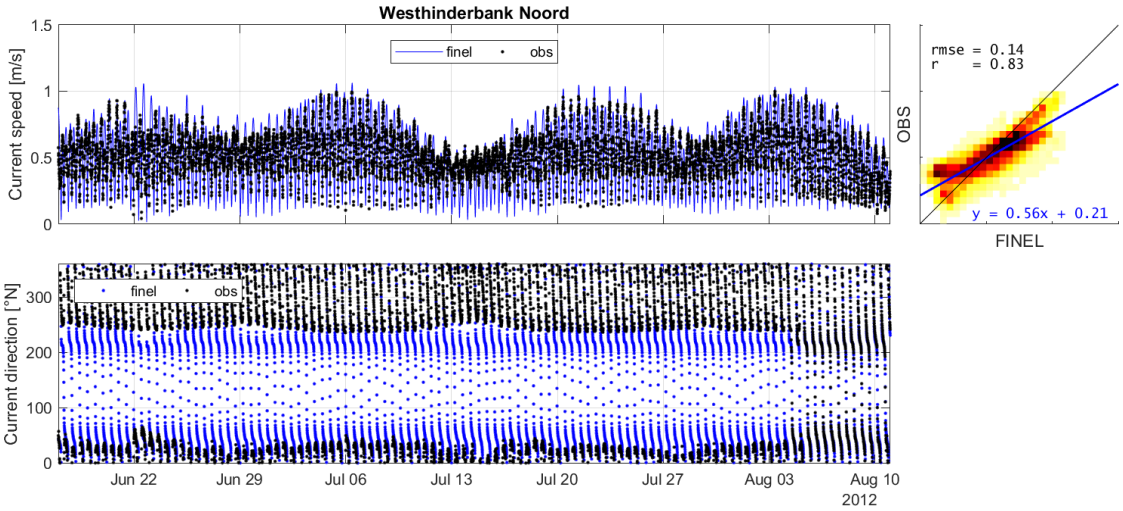

Figure 3-6: Current speed timeseries and scatterplot comparison and current direction timeseries comparison between FINEL and observations at Westhinderbank Noord for 17 June to 11 August 2012.

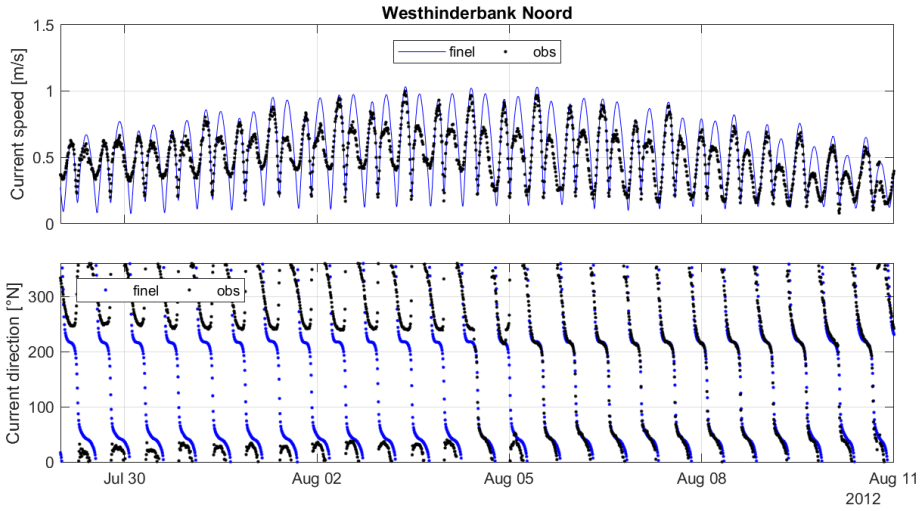

Figure 3-7: Current speed timeseries and current direction timeseries comparison between FINEL and observations at Westhinderbank Noord for July 30 to 11 August 2012.

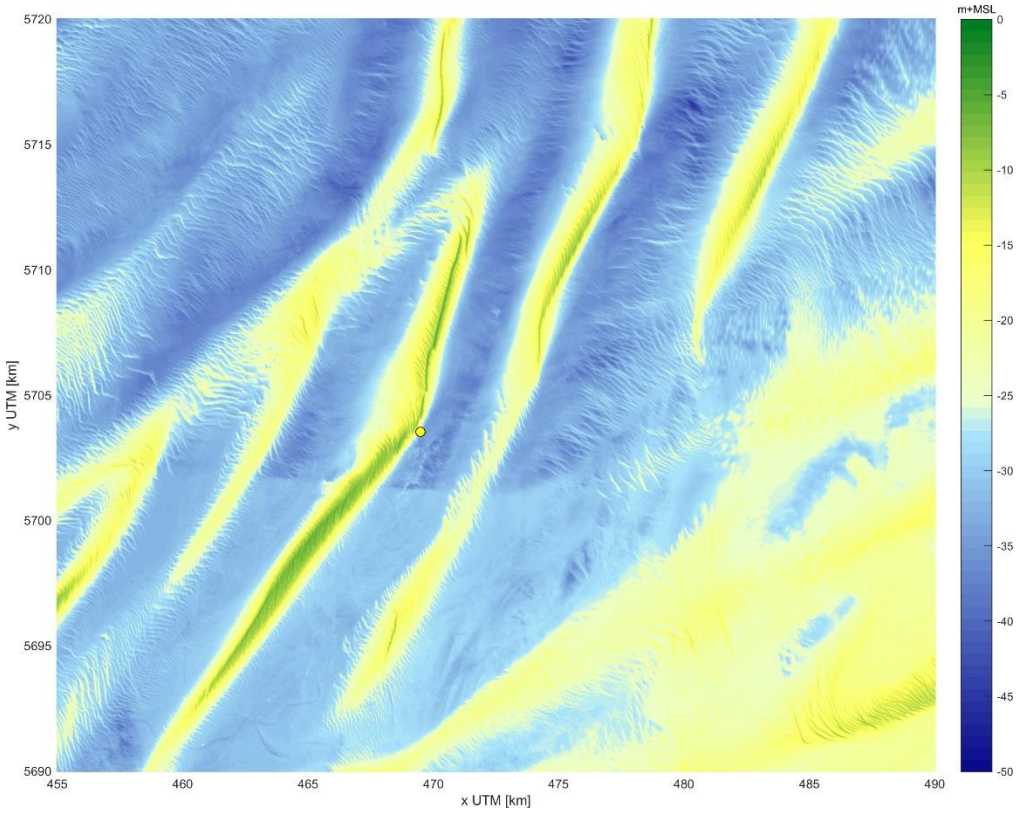

Figure 3-8: Location of Westhinderbank Noord measurement station, indicated by the yellow dot.

The validation for this current series gives an adequate match, but not as good as may be expected based on water level performance. On the one hand there are some uncertainties regarding the measurements, with some unexplained discontinuities in the flow directions and magnitude. On the other hand, it should be acknowledged that the measurement station is located at an especially complex location when it comes to hydrodynamics. The considered MOG2 island location is simpler, with a smoother deeper bank without a sharp crest, see Figure 3-8.

Note that no validation of currents during storm conditions is performed since no measurements are available for such periods.

3.3.4 Validation using sailing measurements

In *Van Lancker and Baeye (2015)* an autonomous wave glider was deployed to measure sediment concentrations and hydrodynamic conditions in the Hinderbank area. The wave glider also contained an Acoustic Doppler Current Profiler (ADCP) to measure velocities. Thus, another dataset with which to validate the numerical model is present. The measurement location of the waveglider is shown with the magenta line in Figure 3-9**.**

The ADCP data from Van Lancker and Baeye (2015) is not stationary due to the movement of the wave glider, and instead has approximately 30.000 unique data points in space. As it is unfeasible to maintain this many output locations in the numerical model, it was decided to place output points at a spatial interval of 200 x 200 m around the measurement area. At the time of each measurement, the velocity as simulated at the same time was sampled from the nearest FINEL output point. The resulting comparison between the ADCP data and FINEL is shown in Figure 3-10.

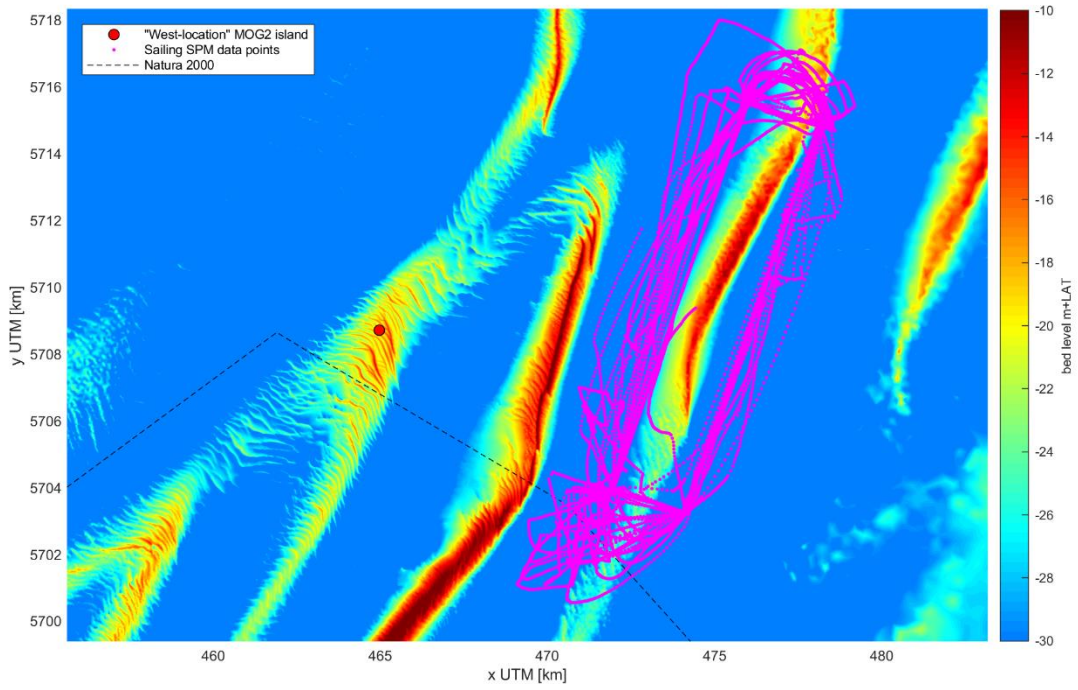

Figure 3-9: Sailing waveglider measurement locations from Van Lancker and Baeye (2015) with respect to the west-location and the Natura2000 area.

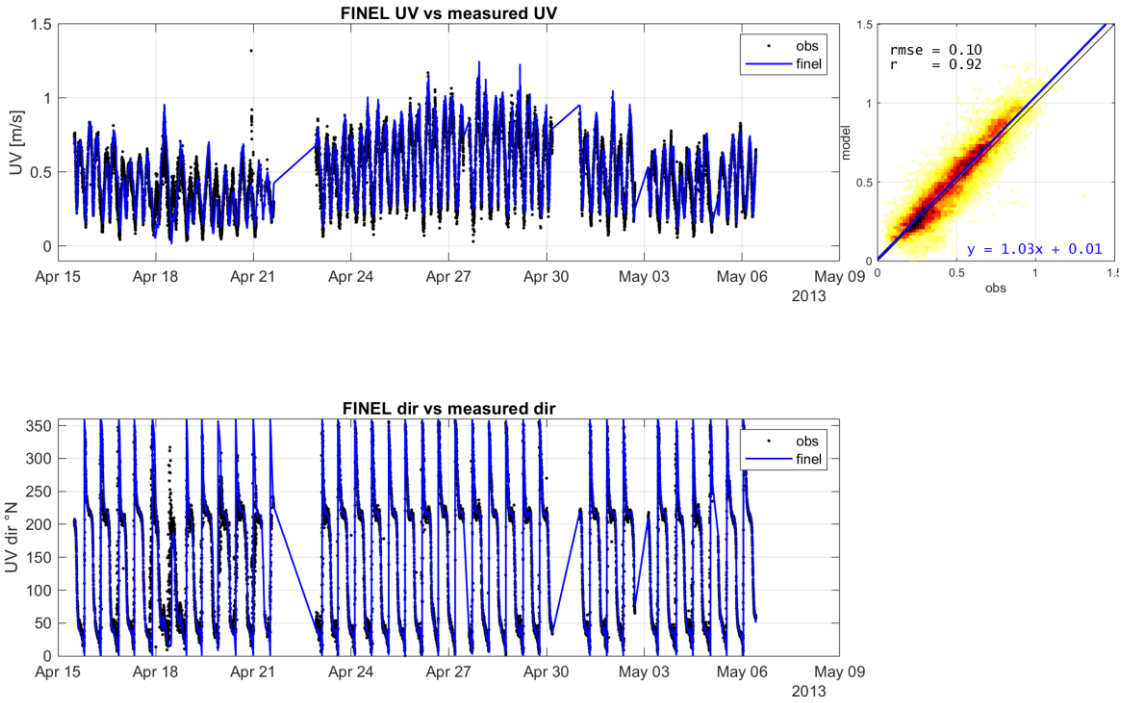

Figure 3-10: ADCP data from Van Lancker and Baeye (2015) compared to FINEL for the same time period.

It can be seen the FINEL velocities match adequately to the measured velocities. The error between FINEL and the measurements increases with increasing magnitude. Thus, FINEL has the tendency to over-estimate the flow velocities, which becomes more evident at higher flow velocities.

Considering the directions, the FINEL data matches the measured data well.

3.4 Implicit solver specific settings

The model set-up as presented so far has applied only the explicit solver as explained in Section 3.1. The implicit model uses the exact same model boundaries and input. This section explains the specific additional inputs and model validation for the North Sea model with the implicit solver.

Within the scope of this project, the FINEL2D-implicit simulations are employed to increase confidence in the FINEL2D-explicit simulation results. The primary difference between both software packages is the inclusion of the diffusion term in the shallow water equations in FINEL2D-implicit, and thus the inclusion of turbulence.

The inclusion of turbulence in FINEL2D-implicit allows an alternating eddy train to form on the leeside of the island, whereas in the FINEL2D-explicit model this effect will be limited. This comparison is performed for the West1 location, and is assumed to be applicable for all three island locations. It should be noted that detailed modelling of turbulence around the sharp edged of the caissons of the MOG2 island is not considered within this comparison, as this would require high resolution modelling unsuited for spatial scales and dynamics affecting long-term changes around the island. Furthermore, the FINEL2D-implicit model is strictly hydrodynamic, and will be compared to a hydrodynamic FINEL2D-explicit model. No morphological module is available for the FINEL2D-implicit software package.

Except for the inclusion of turbulence, the exclusion of the morphological module, and the simulation time, the model set-up of the FINEL2D models is identical to that of the FINEL2D-explicit model as discussed in Chapter 3.2.

3.4.1 Turbulence model

A two-dimensional horizontal Smagorinsky Large-Eddy-Simulation (LES) is performed to resolve eddies with equal of larger lengths with respect to the size of grid elements (40 m). As a result, the large-scale eddy-trains on the leeside of the island will be resolved, whereas the lower-scale turbulence is accounted for within the sub-grid scale Smagorinsky model. Furthermore, an Elder model is employed to account for the vertical eddy viscosity within the 2DH model. The LES model was chosen to yield higher accuracies around the island, due to the higher resolution of the mesh, while minimizing the impact of the turbulence model further away from the island. The results of the LES simulation were compared with a simulation with constant turbulent eddy viscosity ($\nu_t = 0.1 \ / \ 0.01 \ / \ 0.001$ [m^2/s]), and a simulation with lower grid resolution around the island in a small sensitivity analysis. The model was shown to be relatively unsensitive to the choice of turbulence model in general.

3.4.2 Model validation

The results of the implicit solver are compared to the results of the explicit model and measurement data. For the water levels, a section of the calm conditions at Westhinder Meetpaal are considered in Figure 3-11 (see also Chapter 3.3.2). It shows a good match between both FINEL solvers.

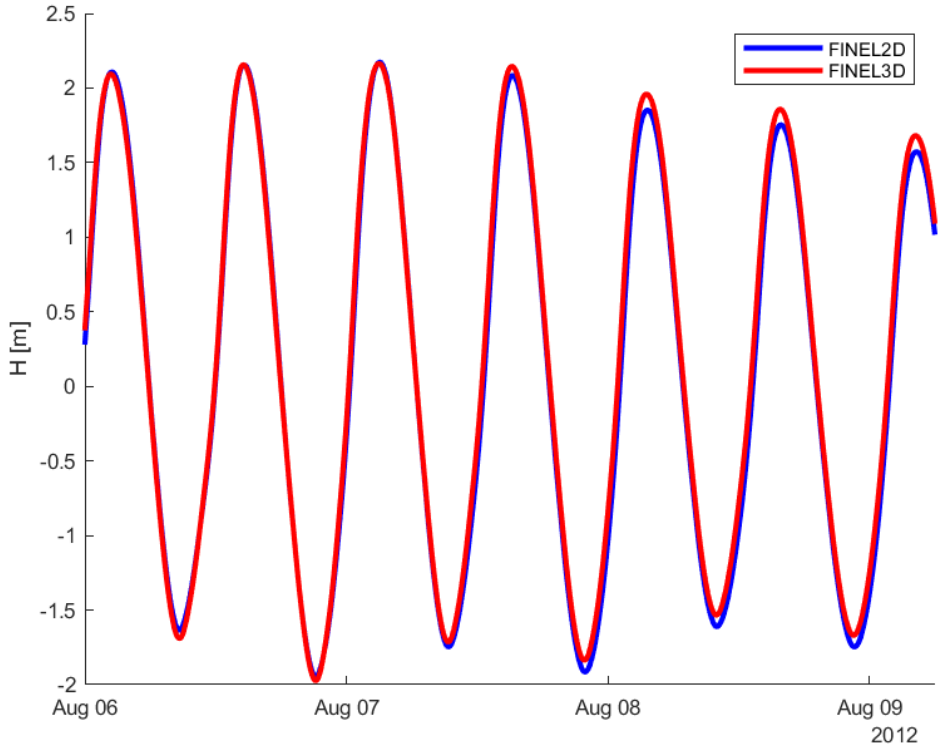

Figure 3-11: Water level comparison between FINEL2D-implicit (red), FINEL2D-explicit (blue), and observations at Westhinder Meetpaal for 6 August to 9 August 2012.

The velocities from both models are compared at the Westhinderbank Noord (Chapter 3.3.3) in Figure 3-12. The FINEL2D-implicit model yields lower flow velocities compared to the FINEL2D-explicit model. The differences are most apparent around peak flood velocities, while peak ebb velocities are quite similar. Nevertheless, given the good match in water levels both models are considered appropriate tools to model the hydrodynamics around the island locations.

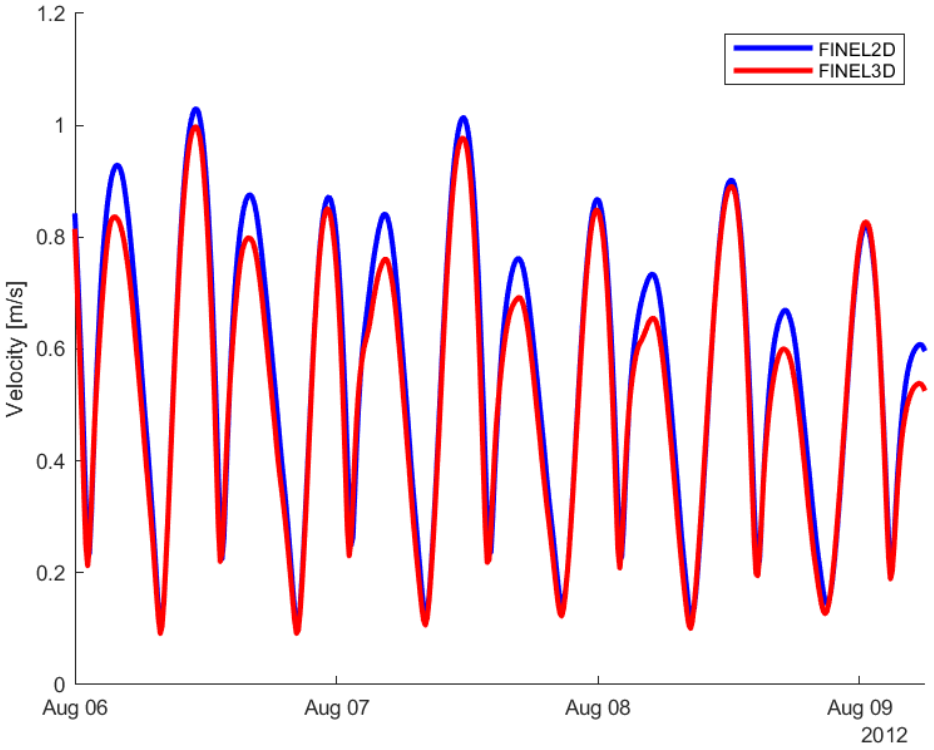

Figure 3-12: Current speed timeseries comparison between FINEL2D-explicit (blue), FINEL2D-implicit (red), and observations at Westhinderbank Noord for 6 August to 9 August 2012.

3.5 Wave model set-up

A local wave model is set-up to assess the impact of the island on the wave field and to assess the sensitivity of the morphological changes to the occurrence of the waves. The SWAN model comprises dimensions of 21 km in the islands short axis direction and 44 km in the islands long axis direction. The grid size is 500 m at the edges of the grid and it has a resolution of 25 m at a distance of about a kilometer from the island. To ensure a smooth transition several grid cells of 100 m are situated in between, Figure 3-13. The island itself is included as a reflective boundary with a reflection coefficient of 0.9.

SWAN version number 41.41 is used and the physical model settings are summarized in the text box below:

```
GEN3 KOMEN
BREAKING CON 1 0.73
FRICTION JONSWAP CFJON=0.038
```

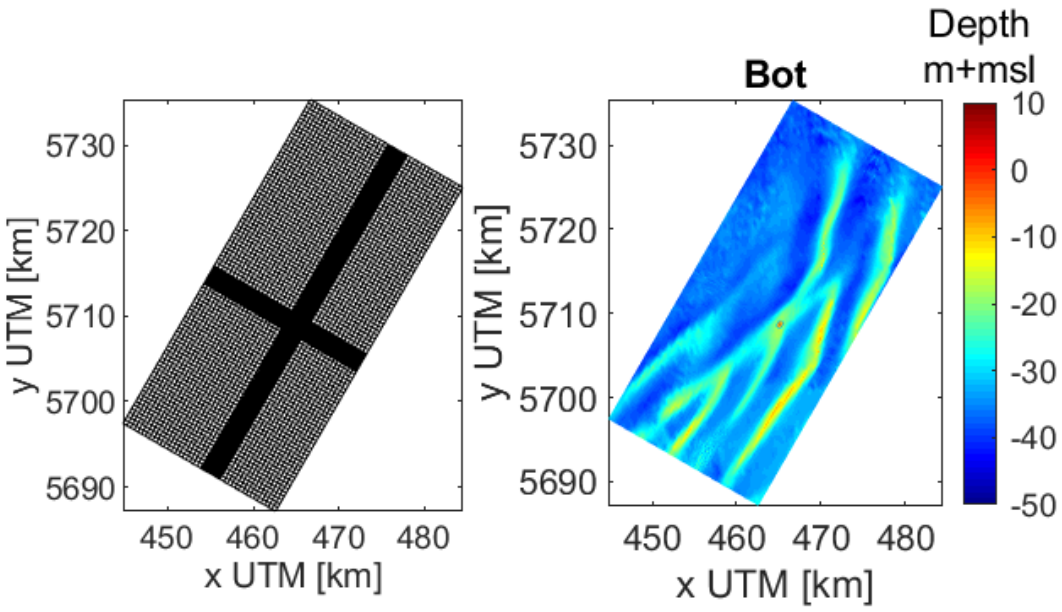

Figure 3-13: SWAN computational grid and bathymetry.

4 MORPHOLOGICAL MODEL INPUTS

The correct input parameters are crucial for the accuracy of the numerical morphological simulations. In this chapter an overview is given of the morphology related model input. The available data from the Gap Analysis (*IMDC, CDR & Svašek Hydraulics*, 2021) serves as a starting point for this.

First, the used sediment transport input is presented consisting of the applied transport formula and selected sediment grain sizes based on the available sediment data. Afterwards, the input for the model bathymetry and the implementation of the island design are described. This is followed by the choices made regarding the hydrodynamic forcing included in the morphological model. Finally, the selected modelling period and some general choices regarding the morphological model settings are presented.

4.1 Sediment transport model input

4.1.1 Sediment transport formula

In the morphological modelling report of the tender design (*IMDC, CDR, Svasek*, 2022d), the sensitivity of the FINEL model to the employed sediment transport formula is investigated by comparing results using the Soulsby-Van Rijn equation and the Engelund-Hansen equation. It is shown that the Engelund-Hansen equation showed significantly lower transport compared to the Soulsby-Van Rijn equation. The result of the lower transport is visible in the time-development towards a new morphological equilibrium around the island, where the simulation with the Soulsby-Van Rijn equation seems to reach that equilibrium on a lower time-scale compared to the Engelund-Hansen equation.

To maintain a conservative approach to the present study, the Soulsby–Van Rijn (*Soulsby*, 1997) equation is employed in the numerical model. Soulsby-Van Rijn calculates bed and suspended load transport under currents and waves on horizontal and sloping beds. Bed load calculations result directly in (bed load) sediment flux. Suspended load calculations result in equilibrium sediment concentration which feeds in to the Galappatti advection for suspended sediment to account for the time lag effect. For more information regarding the Soulsby-Van Rijn equation, see Soulsby (1997).

4.1.2 Sediment grain size

Vibrocore data (TILES data portal) are available at various locations around the Hinderbanks. For the North location and the West1/West2 locations, two separate datasets are used. An overview of the considered datapoints around the West1 and West2 locations is given in Figure 4-1, and an overview of the considered datapoints around the North location is given in Figure 4-2. The vibrocore samples were taken at various depths at the various locations. As the scour hole depths are expected to be larger than the maximum measurement depth below the bed level of 5 m, the data was depth-averaged to obtain representable values for the entire erodible bed.

West1 and West2 locations

The water depth at which the vibrocores were sampled around the West locations varies between 21.4 m and 39.3 m. As is visible in Figure 4-1, most measurements were sampled on the sand waves near the West1 and West 2 locations, and three measurements (5, 10, 12, red in Figure 4-1) were sampled towards the east of the sand waves. These three measurements were sampled with local water depths between 29.4 m and 39.3 m, which is significantly deeper compared to the average depth around the island. As the local water depth has significant influence on the sediment in the

bed, vibrocores 5, 10, and 12 are treated as outliers and neglected for the determination of the nominal grain size at the West location.

The average of all remaining vibrocores was taken to determine a representable nominal diameter for the West1 and West2 locations. The resulting depth-averaged and spatially-averaged d50 equals approximately 400 µm. A similar approach was taken for the determination of the d90, which equals approximately 1400 µm

It should be noted that gravel was found in several vibrocores samples. This is not portrayed in the current d90 value employed in the numerical model, which represents coarse sand. Additional physical processes such as armouring can become relevant with the inclusion of gravel. These processes are likely to have a positive effect on the computed scour volumes/depths around the island and thus the source of erodible sediment. As these processes are not included in the numerical simulations, the result is conservative.

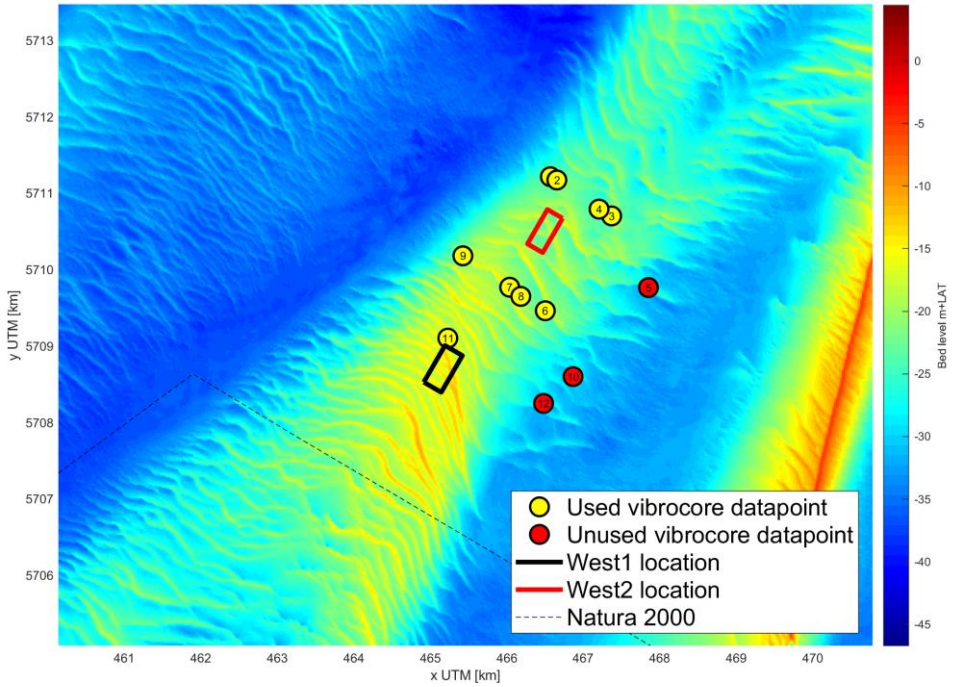

Figure 4-1: Overview of the vibrocore sample locations for the West1 and West2 locations.

Noord location

The water depth at which the vibrocores were sampled around the Noord location varies between 14.5 and 35.7 m. As is visible in Figure 4-2, most measurements were sampled near the crest of the Noordhinderbank, with one outlier at deeper depths toward the west (point 11). Contrary to the West locations, this outlier at 35.7 m water depth is representative for a section of the predicted erosion area around the island. The island at the Noord location is positioned closer to deeper water depths along its Western side. Thus, it was chosen to keep all datapoints around the Noord island, as all datapoints are considered representative of the sediment around the island.

The average of all vibrocores was taken to determine a representative nominal diameter for the Noord location. The resulting depth-averaged and spatially averaged d50 equals approximately 310

μm. A similar approach was taken for the determination of the d90, which equals approximately 580 μm.

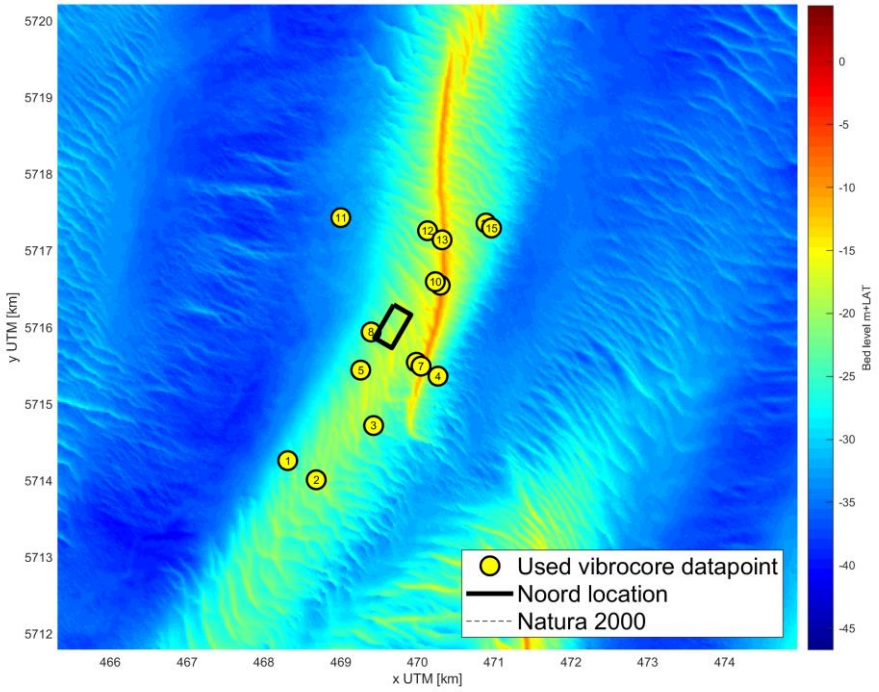

Figure 4-2: Overview of the vibrocore sample locations for the Noord location

Conclusion

Vibrocore datasets around the West locations and the Noord location are considered to determine proper model values for the nominal diameter d50 and the 90%-exceedance diameterd90. For the West locations, a representative nominal diameter of d50= 400 µm and a d90= 1400 µm is found. For the Noord location, a representative nominal diameter of d50= 310 µm and a d90= 580 µm is found.

For the determination of the erosion hole depths and eroded volumes around the island, which serve as input for other numerical simulations such as the 3d plume simulations (not presented in this report), it is important to use the locally representative grain size. For the West locations this means values of d50= 400 µm and d90= 1400 µm are used, and for the Noord location the values d50= 310 µm and d90= 580 µm are used.

For the larger spatial scale effect of the islands on its surroundings, the expected sedimentation and erosion patterns are expected to exceed the direct vicinity of the island. Furthermore, the sediment present in the water column can originate from different sections of the North Sea. Therefore, conservative realistic values of the vibrocore analyses are applied for every island location. Thus, a smaller grainsize that is easier transported over long distances, with a value of d50= 310 µm and d90= 580 µm are used within the scope of the EIA. The employed values are summarized in Table 4-1.

Table 4-1: Sediment characteristics for all three island locations from the measurements (vibrocores), as employed within the plume input simulations, and as employed for the large-scale island effect simulations.

Location	Grain size parameter	Measurement data [nm]	Simulation for plume input [nm]	Simulation for large-scale island effect [nm]
West1	d_{50}	400	400	310
	d_{90}	1400	1400	580
West2	d_{50}	400	400	310
	d_{90}	1400	1400	580
Noord	d_{50}	310	310	310
	d_{90}	580	580	580

4.2 Model bathymetries and island design implementations

4.2.1 Focus on results relative to reference situation

The seabed is always mobile, both in reality and in the model, with and without an artificial island. The seabed development without the island is excluded from the model results by, for each island location, comparing a simulation with the MOG2 island to a simulation without the MOG2 island. In this way we visualize only the effects of the island itself.

4.2.2 Autonomous bathymetries

A common problem within large-scale morphological models of seas and oceans, is an accurate reproduction of bedforms. Bedforms are (often) dynamic, and their migration is a complex coupling of detailed three-dimensional hydrodynamics and morphodynamics. A larger-scale two-dimensional numerical model is incapable of reproducing these effects[2]. Instead, the bedforms are seen as erodible sills within the water column, where at the upstream side of the bedform the flow accelerates, and at the downstream side of the bedform the flow decelerates. Coupled to the morphology within the model, the result is a smoothing of bedforms rather than migration of bedforms.

As a result, even without the placement of the island, the bathymetries within the models are highly dynamic due to the smoothing of these bedforms. This process is denoted as the 'autonomous effect' of the models. To reduce the impact of this spin-up effect, the bathymetries around the MOG2 island are pre-smoothed. These pre-smoothed bathymetries are created by running simulations without the island for a morphological period of two years with a set morphologically active area within which the bedforms could smoothen freely. Essentially, this can be considered a morphological spin-up time of 2 morphological years. Within the morphologically active area, locations with a water depth shallower than 15 m were set as non-erodible to ensure the crests large-scale bedforms (such as the Westhinderbank) remain untouched. The differences between the measured bathymetries and the autonomous bathymetries for the West1, West2 and North locations are shown in Figure 4-3, Figure 4-4, and Figure 4-5 respectively.

In short, the unrealistic smoothing of bed forms in the simulation impacts the simulated effect of the island. This is prevented by largely removing the bed forms from the simulation altogether, by 'pre-smoothing' the bed. The sensitivity of the model to this assumption is discussed in (*IMDC, CDR, Svasek*, 2022d).

[2] Even with very high resolution dedicated 3D models reproducing the formations and migration of bedforms is a challenge (Overes. 2021).

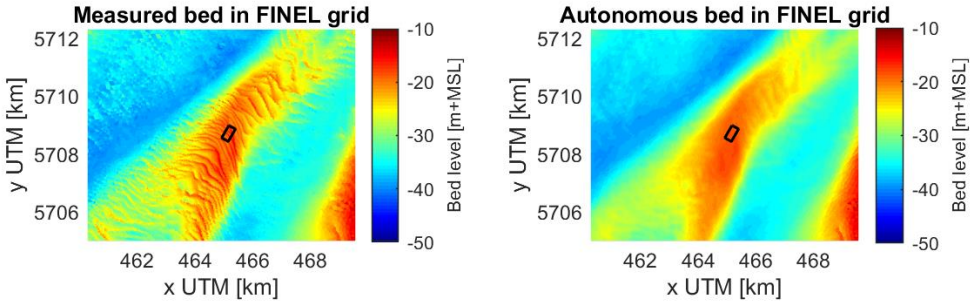

Figure 4-3: Measured vs pre-smoothened bed in FINEL for the West1 location.

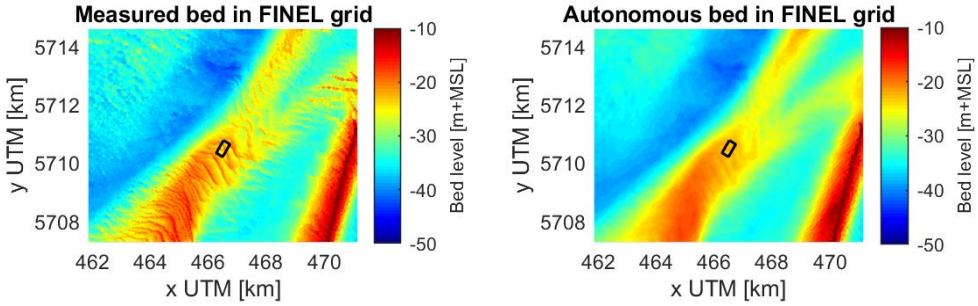

Figure 4-4: Measured vs pre-smoothened bed in FINEL for the West2 location.

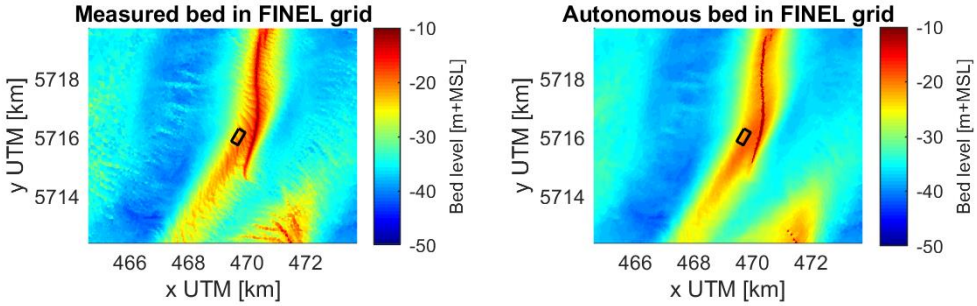

Figure 4-5: Measured vs pre-smoothened bed in FINEL for the North location.

4.3 Verification of autonomous bottom changes at gravel areas

This study focusses on morphological changes at the gravel bed areas. The gravel areas are relatively stable areas compared to the surrounding sandy bed with migrating ripples, dunes and banks. The coarse grain size of the gravel prevents erosion, and if natural sedimentation would occur at the location of the gravel beds, the gravel beds would not be exposed. To verify this behavior in the model, a simulation with erodible gravel beds and with non-erodible (type 1) gravel beds[3] is performed. From the simulation with erodible gravel beds (Figure 4-6, left) it can be seen that the majority of the gravel beds would erode if the bed would consist of sand instead of gravel. This

[3] All gravel beds of type 1 are considered non-erodible. Note that the type 2 gravel bed (indicated with #6) will likely be less mobile than assumed in these computations.

indicates that the locations of the gravel beds as simulated in the model are unstable for the simulated grain sizes, and thus that it is likely that a coarser sediment like gravel is positioned in the top layer of the bed material. At the edges of most of the gravel areas some sedimentation zones are predicted by the model. In the simulation with non-erodible gravel beds (Figure 4-6, right) these zones are still present at some locations. Especially at the southern end of the gravel bed 3 and the northern end of gravel beds 2, 4, and 5, some sedimentation can be observed. This sedimentation is either an indication of reduced model quality in these areas or an indication of a local inaccurate demarcation of the estimated gravel bed areas. Note that when comparing Figure 4-6 with Figure 2-7 these sedimentation areas seem to coincide with areas within the gravel bed polygons but outside the highlighted gravel bed areas.

The bed behavior with non-erodible type 1 gravel beds is considered most realistic, therefore this model setting is applied in the remainder of this study. The type 2 gravel bed is considered erodible, because there is also a chance that this area consists of sand. However, this assumption does not affect the outcome of the analysis in this report because of its distant location with respect to the island locations.

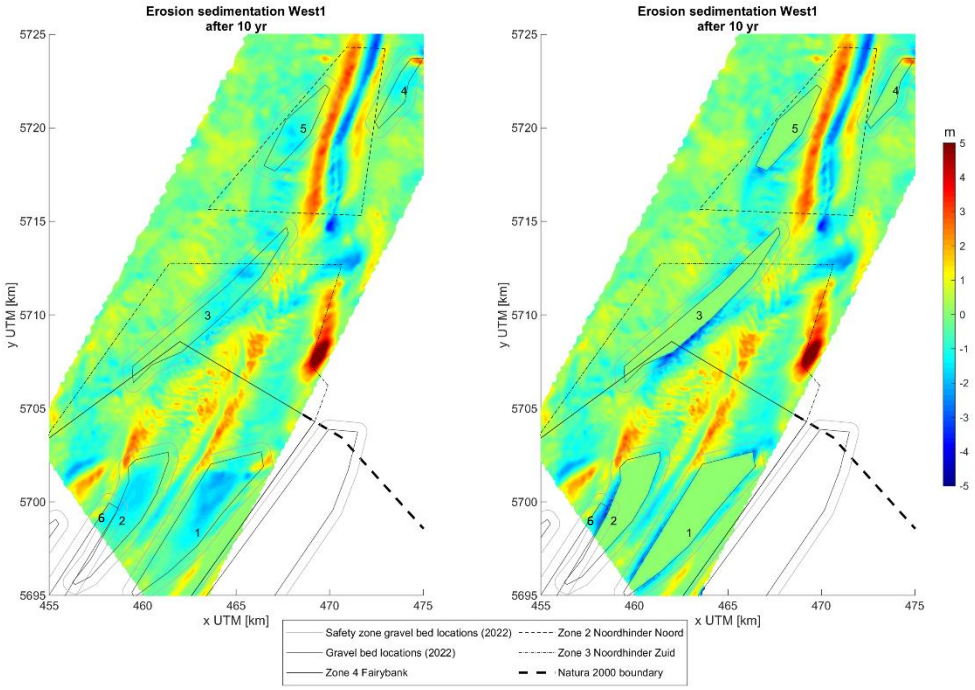

Figure 4-6: Autonomous bottom change after 10 years with erodible gravel beds (left) and with non-erodible gravel beds (right).

4.4 Modelled time frame

4.4.1 Morphological acceleration factor

The aim of the model simulations is to determine the morphological development over a long time period of 10 years. To speed up the morphological simulation and maintain acceptable computation times, a morphological acceleration factor is used.

Sediment fluxes are determined at every hydrodynamic time step and translated to bottom changes. These bottom changes are subsequently multiplied by the morphological acceleration factor and used to calculate the new bed level. The new bed level is used for the hydrodynamic calculation on the next time step.

Two sets of morphological acceleration factors are applied within the simulations. First, a morphological acceleration factor of 25 is applied over a modelled hydrodynamic period of approximately 30 days. In the morphological modelling study of the tender design in (*IMDC, CDR, Svašek* 2022d), it was shown the development of the erosion holes around the island is the most significant in the initial years. Thus, it is decided to apply a lower morphological acceleration factor in the initial part of the simulations to monitor the initial development closely. A hydrodynamic period of 30 days combined with a morphological acceleration factor of 25 yield a morphological period of approximately 2 years.

After the first two morphological years, the simulations continue with a morphological acceleration factor of 50 over a hydrodynamic period of approximately 60 days. The resulting morphological simulation period equals 8 years, for a total of 10 years of morphological simulation time.

Additionally, at the start of the simulation a spin-up period of 2 hydrodynamic days is applied before bed level changes are computed.

The mentioned model settings above are summarized in Table 4-2.

Table 4-2: General input parameters of the morphological model.

Parameter	Value
Morphological acceleration factor	25 / 50
Simulation time (morphological)	10 yrs
Simulation time (hydrodynamic)	90 days
Hydrodynamic spin-up time	2 days

4.4.2 Hydrodynamic modelling period

The modelled hydrodynamic simulation time is only a fraction of the actual modelled morphological time due to the morphological acceleration factor. This means, however, that the modelled hydrodynamic period needs to be representative in terms of hydrodynamic forcing and resulting morphological development.

In (*IMDC, CDR, Svasek*, 2022d) it was found that for the West1 location the influence of meteorological conditions (and wave conditions) on the morphological transport rates is limited, and that the astronomical tidal conditions are the main morphological driver at the island location. The selected representative astronomical tidal period of 90 days for this morphological study is based on an assessment where the selected period is representative for the yearly average sediment transport rates over 19 years[4].

To this end, a long-term timeseries (19 years) at the West1 island location of astronomical water levels and current velocities (*IMDC, CDR, Svasek, 2022a*) is translated to yearly sediment transport rates for all possible 90-day periods in this timeseries. This is done using the Soulsby and Van Rijn transport formula. The results of this analysis are presented in Figure 4-7. The blue line shows the sediment transport fluctuations for all possible 90-day periods within the 19-year timeseries. The green line indicates the average effect of the 18.6-year cycle on the transport fluctuation. And the red line indicates the average transport over the complete 19-year timeseries.

Finally, a realistic conservative 90-day period starting from 31th of December 2019 till 27th of March 2020 is selected. The transport rate of this period is indicated with the black dotted line in Figure 4-7, and accounts for a similar transport to the average transport rates.

[4] An astronomical timeseries of 19 years is used as this sufficiently long to account for the fluctuations of the 18.6 year cycle.

It is, however, not unlikely that construction of the Island will take place more around the trough of the 18.6-year cycle fluctuations in sediment transport. This could result in slightly lower sediment transport rates, which would make the selected period even somewhat conservative. Note that this is only expected to affect the time scale of developments around the island but not necessarily the extent of the effects.

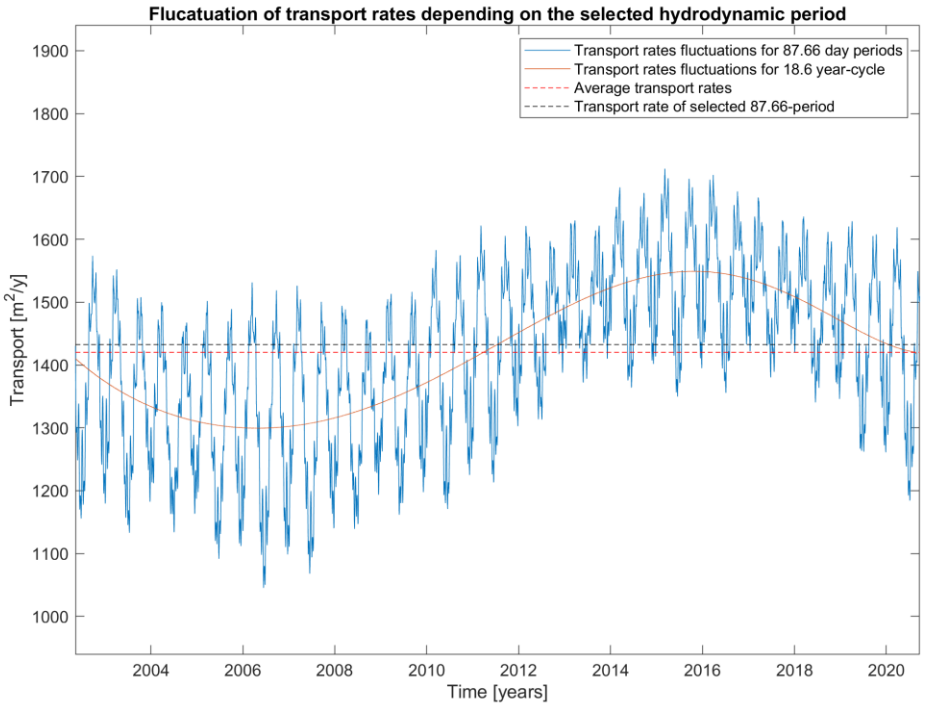

Figure 4-7. Analysis of sediment transport rate based on 19 year astronomical timeseries.

5 HYDRODYNAMIC COMPARISON FINEL2D-EXPLICIT AND FINEL2D-IMPLICIT

As explained in Chapter 3, the FINEL2D-explicit software does not explicitly incorporate turbulence. Thus, the effect of individual eddies, and the corresponding energy exchange, is not simulated. To validate the hydrodynamic results of the FINEL2D-explicit model, and to address the effect of turbulence on the flow around the MOG2 island, an identical hydrodynamic simulation including the MOG2 island at the West1 location with the FINEL2D-implicit software is carried out. This chapter serves to highlight the comparison between either model at the West1 location, and the obtained insight from the analysis. It is assumed the comparison would be similar for the other two island locations. Most of the results are presented as the difference between a simulation with and without the MOG2 island present. This is referred to as the 'disturbance of the flow due to the island' for the flow velocities, and the 'island impact on the bed shear stress' for the bed shear stresses.

5.1 Flow velocities

5.1.1 Typical flow profile

Figure 5-1 displays the disturbance of the flow due to the presence of the island for a typical ebb scenario (flow from North-East to South-West) in the FINEL2D-explicit model (left) and the FINEL2D-implicit model (right). The FINEL2D-explicit model shows clear zones of accelerated flow along the long sides of the island, and a clear, steady zone of decelerated flow downstream of the island. The results from the FINEL2D-implicit model correspond well with the results from the FINEL2D-explicit model, but show a more varying flow pattern downstream of the island, with alternating zones of accelerated and decelerated flow. This alternating pattern is caused by turbulent eddies, which form along the long-sides of the island and detach along the downstream corners of the island. These eddies combined are called the 'vortex train' on the lee-side of the island, and cause a much less stable zone of deceleration downstream of the island.

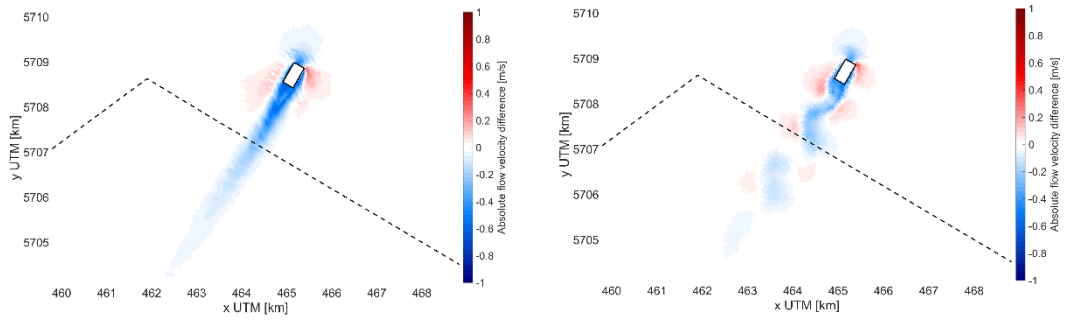

Figure 5-1: Disturbance of the flow (simulation with island – simulation without island) for a typical ebb scenario for the FINEL2D-explicit model (left), and the FINEL2D-implicit model (right).

5.1.2 Mean flow velocities

As the resolved turbulence in the FINEL2D-implicit model is largely variable in time, the implications of the additional turbulence can better be investigated using time-averaged properties and the variability of the flow. For this purpose, the mean flow disturbance over one spring-neap tidal cycle (~14 days) is shown in Figure 5-2 for both the FINEL2D-explicit (left) and FINEL2D-implicit (right) model.

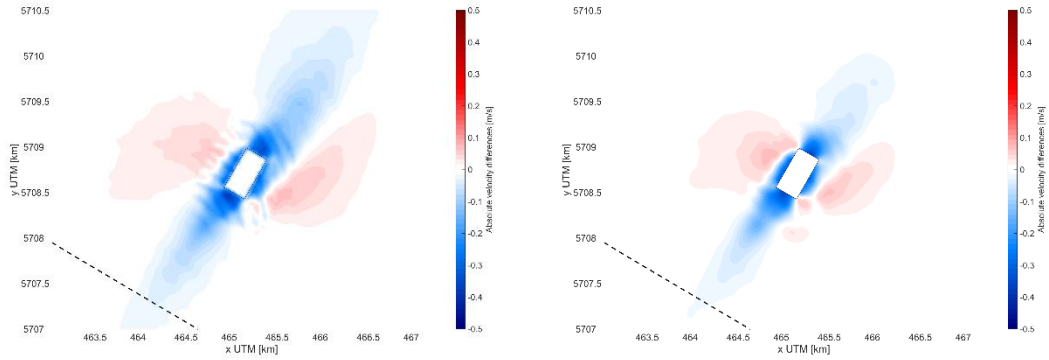

Figure 5-2: Mean disturbance of the flow (simulation with island – simulation without island) within one spring-neap tidal cycle (~14 days) for the FINEL2D-explicit model (left), and the FINEL2D-implicit model (right).

Figure 5-2 shows the expected mean disturbance of the island, with accelerated flows along the long sides of the island, and decelerated flow along the short sides. Furthermore, the figure shows the results from both simulations are very comparable. Nevertheless, it is observed that especially the decelerated velocity zones are larger in the FINEL2D-explicit model compared to the FINEL2D-implicit model. It should be kept in mind that, as shown in paragraph 3.4.2, the flow velocities resolved in the FINEL2D-implicit model are slightly lower compared to the FINEL2D-explicit model. Nevertheless, Figure 5-2 shows that the time-averaged effect of the inclusion of turbulence in the FINEL2D-implicit model yield a smaller disturbance of the hydrodynamics due to the island. A possible explanation for this phenomenon is the increased exchange of momentum due to the large-scale turbulence.

5.1.3 Flow velocity fluctuations

The process of averaging in time nullifies the influence of individual eddies on the flow pattern. Thus, to properly investigate the effect of turbulence on the flow, the variability of the flow may be computed on time step level. Nevertheless, in this specific scenario such a statistical analysis aimed to isolate the effect of turbulence is difficult due to the time-varying flow velocities induced by the tides. In the context of this study, an indication of the variability of the flow due to the turbulence is sufficient. This is achieved by considering the maximum absolute flow velocity disturbances introduced by the island over a period of one spring-neap tidal cycle. These maximum absolute flow velocity disturbances are shown in Figure 5-3 for the FINEL2D-explicit model (left) and the FINEL2D-implicit model (Right).

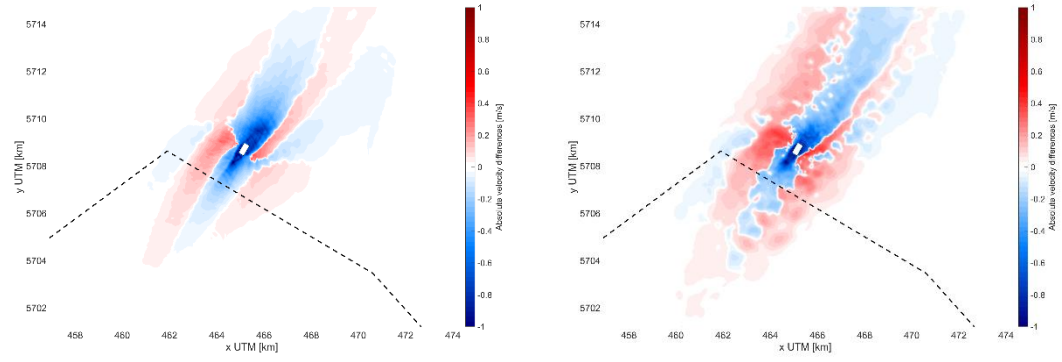

Figure 5-3: Maximum disturbance of the flow (simulation with island – simulation without island) within one spring-neap tidal cycle (~14 days) for the FINEL2D-explicit model (left), and the FINEL2D-implicit model (right).

Again, Figure 5-3 shows good correspondence between the results from the FINEL2D-explicit and FINEL2D-implicit model. Nevertheless, it is observed that the maximum flow velocity differences in

FINEL2D-explicit are both lower in magnitude and more compact in space compared to the maximum flow velocity differences in FINEL2D-implicit. This is especially true for the maximum flow accelerations due to the island indicated in red in Figure 5-3, and to a lesser extent for the maximum flow decelerations indicated in blue in Figure 5-3.

Though no proper turbulent properties can be derived from Figure 5-3, it does portray the larger variability of the flow with the inclusion of turbulence. Possible implications of this larger variability of the flow lie in a more dynamic behaviour of the sand. The alternate pattern of flow acceleration and deceleration caused by the vortex train can yield a more dynamic pattern of erosion and sedimentation compared to the FINEL2D-explicit model.

5.2 Bed shear stresses

5.2.1 Definition

The bed shear stresses form the bridge between hydrodynamics and morphodynamics within numerical models. Thus, the difference in bed shear stresses between a simulation with and without island of both models are compared to one another to serve as a proxy for the zones of erosion and sedimentation.

Within the scope of this report, the bed shear stress is derived from the hydrodynamic simulations based on the method (*Soulsby, 1997)*, with the corresponding equations shown in Eq 1 and Eq 2.

$$\tau_b = \rho_w \cdot C_d \cdot \sqrt{U_x^2 + U_y^2}^2 \qquad \text{Eq 1}$$

$$C_d = \frac{g}{C^2} = \frac{g}{\left(18 \log\left(\frac{12(H+z)}{k_s}\right)\right)^2} \qquad \textit{Eq 2}$$

With:

τ_b = Bed Shear stress $\left[\frac{N}{m^2}\right]$

ρ_w = Density of salt water = 1025 $\left[\frac{kg}{m^3}\right]$

U_i = Flow velocity component in I direction $\left[\frac{m}{s}\right]$

C_d = Drag coefficient $[-]$

g = Gravitational acceleration = 9.81 $\left[\frac{m}{s^2}\right]$

k_s = Roughness height $[m]$

H = Water level $[m]$

z = Bed level $[m]$

Though this method is not identical to the calculation of the bed shear stress within the morphological models, the scope of this section is to compare bed shear stress differences due to the island between the FINEL2D-explicit and FINEL2D-implicit simulations, rather than to look at the absolute values of the bed shear stress. For this purpose, the method as described above is considered sufficient.

5.2.2 Bed shear stresses around peak spring tide

Images of the impact of the MOG2 island on the bed shear stress for both the FINEL2D-explicit and FINEL2D-implicit model are shown per hour for the peak tidal cycle in Figure A- 1 to Figure A- 12 in Appendix A. Recall that the impact of the MOG2 island on the bed shear stress is defined as the bed shear stress in a simulation with the MOG2 island minus the bed shear stress in a simulation without the MOG2 island.

Looking through Figure A- 1 to Figure A- 12, it is evident the results from the FINEL2D-explicit and FINEL2D-implicit model are similar, with the exception of the formation of the vortex train on the lee-side of the island in the FINEL2D-implicit model. Both the extent and magnitude of the bed shear stress differences are alike in either simulation.

The process of the peak tidal cycle can be described with the following sequence for both models:

- Ebb (Figure A- 1 and Figure A- 2). The peak ebb flow velocities flow from the North-East towards the South-West, making the south-western side of the island the leeside. The blockage of the flow due to the MOG2 island is especially visible towards the South-West of the island. The contraction of the streamlines of the flow, and the corresponding flow accelerations, follow the long-sides of the island. Nevertheless, as the island is not perfectly aligned with the flow, the increased bed shear stresses are most predominant along the West side of the island. For the FINEL2D-implicit model, Figure A- 1shows the initial creation of the vortex train on the leeside of the island.
- Slack tide ebb to flood (Figure A- 3 to Figure A- 5**)**. In Figure A- 3 a zone of lower bed shear stress can be seen to form at the eastern side of the island in both simulations. This zone of decelerated flow is transported downstream (in north-eastern direction) with the rotation of the tide in Figure A- 4 and Figure A- 5, creating a large zone of lower bed shear stresses relatively far North-East of the MOG2 island.
- Flood (Figure A- 6 to Figure A- 9). The peak flood flow velocities flow from the South-West towards the Nort-East, making the north-eastern side of the island the leeside. The blockage of the flow due to the MOG2 island is especially visible towards the North-East of the island. Similar to the Ebb situation, the contraction of the streamlines and the corresponding accelerations follow the long-sides of the island. As the island is not perfectly aligned with the flood flow, the increased bed shear stresses are most predominant along the East side of the island.
- Slack tide flood to ebb (Figure A- 10 to Figure A- 12). Similar to the slack tide from ebb to flood, a large zone of lower bed shear stress can be seen to form North-West of the island in Figure A- 10. This zone is transported downstream (in South-Western direction) with the rotation of the tide in Figure A- 11 and Figure A- 12**,** creating a large zone of lower bed shear stresses relatively far South-West of the MOG2 island.

To conclude, the bed shear stresses are shown to compare well within the tidal cycles for the FINEL2D-explicit and FINEL2D-implicit model, with the exception of the eddy train, which is absent in the FINEL2D-explicit model. Furthermore, it is shown that larger zones of decreased bed shear stresses that are created close to the island can be transported further away from the island with the rotating tide.

5.3 Conclusion

In this chapter, a hydrodynamic simulation using the FINEL2D-explicit software package is compared to a hydrodynamic simulation using the FINEL2D-implicit software package at the West1 location to validate the results from the FINEL2D-explicit model, and to investigate the hydrodynamic profile around the island with and without explicit representation of turbulence.

It can be concluded the flow profiles around the island are similar. The inclusion of turbulence in the FINEL2D-implicit model show a vortex train forms at the lee-side of the island, which is absent in the FINEL2D-explicit model. Considering the time-averaged flow profile around the island for one spring-neap tidal cycle shows the nett effect of turbulence is a smaller zone of decelerated flow in the mean velocity profile around the MOG2 island, but an increase in the variability of the flow.

The impact of the island on the bed shear stresses for peak ebb and peak flood in one spring-neap tidal cycle was investigated. It is concluded the impact of the island on the bed shear stresses is similar between both simulations. Furthermore, it was shown that in in both the slack period between ebb and flood and the slack period between flood and ebb, a relatively large zone of decreased bed shear stresses is instantiated relatively far away from the island. All in all, the comparison between the two solvers shows that a long term morphological simulation with the FINEL2D-explicit model will yield reliable results.

6 HYDRODYNAMIC MODELLING RESULTS

This chapter serves to highlight the hydrodynamic results from the EIA modelling of the MOG2 island for all three island locations. The hydrodynamic results are separated into the island impact on current, island impact on waves, and island impact on bed shear stress. The island impact on waves is thoroughly addressed for the West1 location as the most extensive wave data is available at the West1 location, see IMDC, CDR, Svasek (2022a). The island impact on bed shear stresses is divided in a summer condition (tide-dominated) and a winter condition (tide + 1/year wave). These conditions should be interpreted as indicative for the impact of the island in these periods.

6.1 West1 location

6.1.1 Island impact on current

The flow disturbance caused by the island is further investigated by analysing the mean flow velocity pattern over one spring-neap tidal cycle at four moments in time: immediately after construction and 1, 4, 10 years after construction. The results are depicted in Figure 6-1 to Figure 6-4, including the tidal ellipses at several points around the island.

The mean flow velocity magnitude around West1 location equals approximately 0.5 m/s. In the direct vicinity of the island the flow deceleration in the leesides of the island is clearly visible when considering the mean velocities around the island (middle figures). The flow accelerations along the island long-side are less visible but can clearly be seen in the flow difference figures (right figures). The flow accelerations are at maximum 30% of the mean flow velocity immediately after construction of the island. 10 years after construction this value decreases to a maximum of 10% of the mean flow velocity.

Directly after construction (Figure 6-1) the flow velocity differences are most significant as no adaption of the surrounding seabed to construction of the island has taken place. The morphological changes in the subsequent years reduce the magnitude of these differences in flow velocity. After 4 years (Figure 6-4) the flow accelerations along the island long-sides have decreased significantly. Furthermore, the area and magnitude of the flow decelerations have decreased as well. Between T = 4 years (Figure 6-3) and T = 10 years (Figure 6-4) the flow disturbance due to the presence of the island remains more or less the same, indicating the system is approaching an equilibrium.

The impact of the MOG2 island on the direction of the tidal flow is limited. Significant differences are only found in the direct vicinity of the island, similar to the flow accelerations and decelerations.

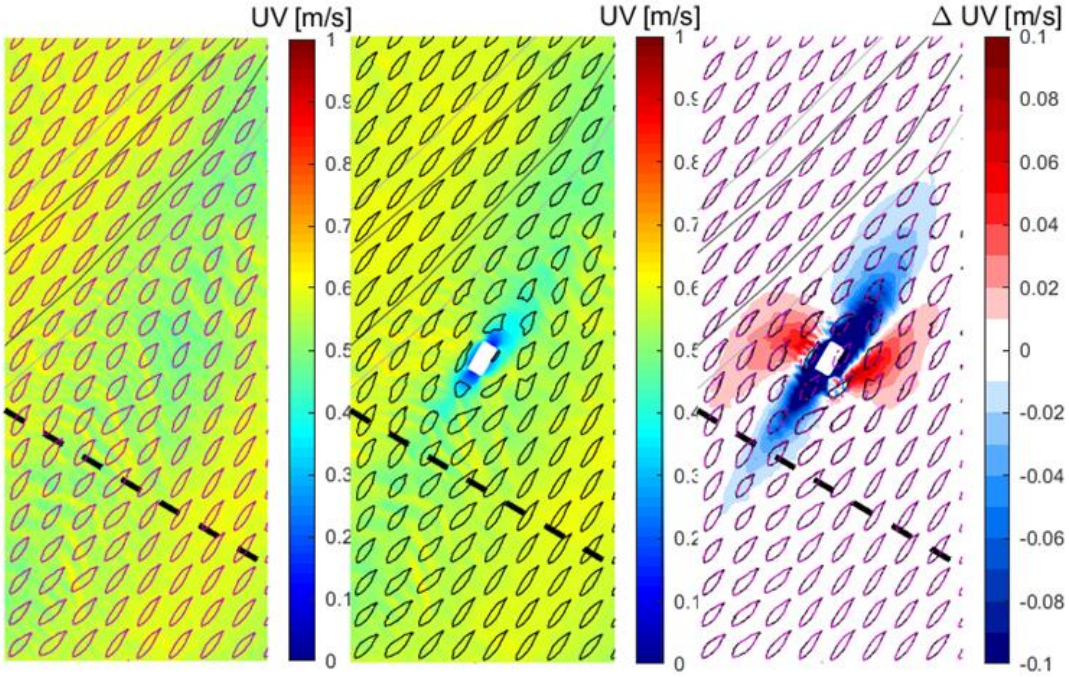

Figure 6-1: Mean flow velocity for one spring-neap tidal cycle at the West1 location immediately after construction for a scenario without island (left), with island (middle), and the difference (right). The figures include the tidal ellipses without island (purple) and with island (black).

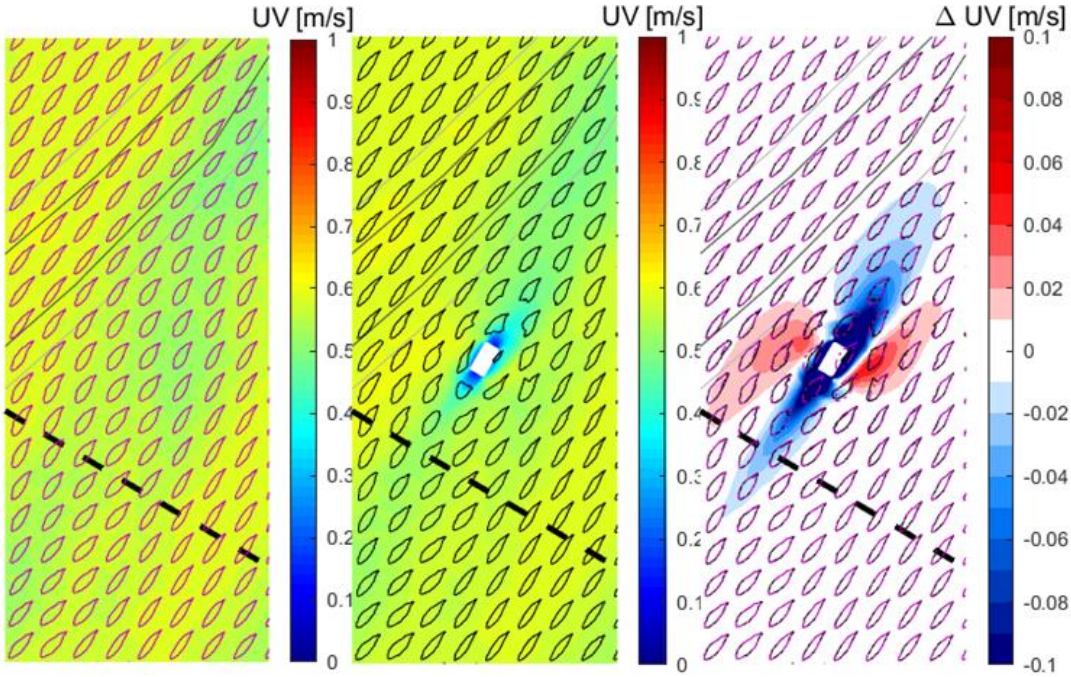

Figure 6-2: Mean flow velocity for one spring-neap tidal cycle at the West1 location after T = 1 year after construction for a scenario without island (left), with island (middle), and the difference (right). The figures include the tidal ellipses without island (purple) and with island (black).

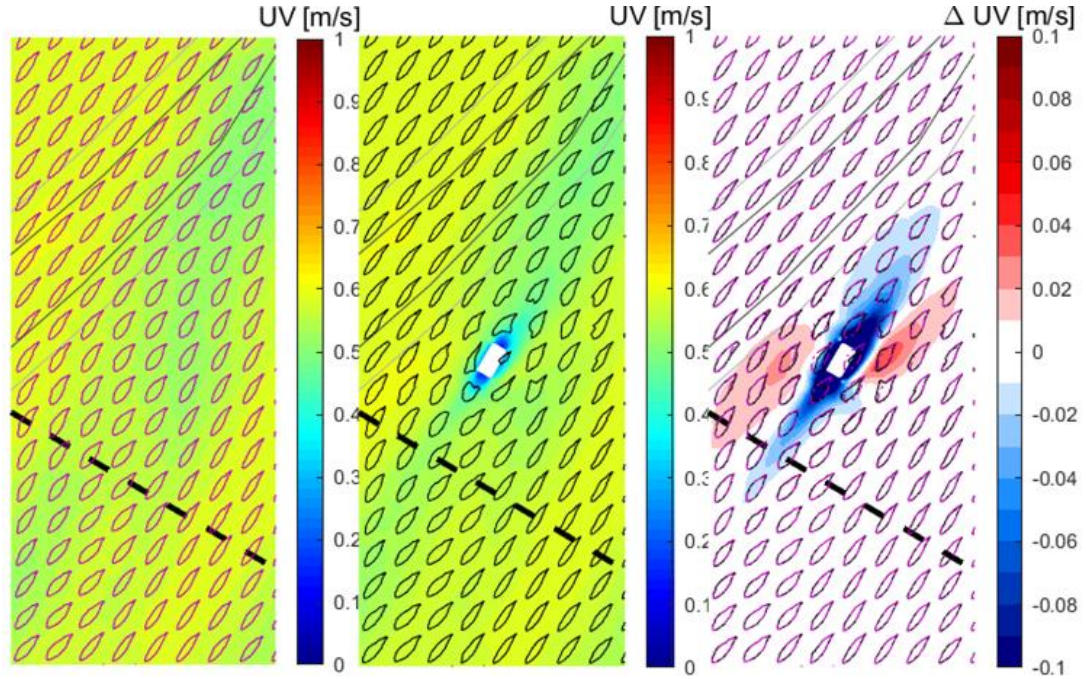

Figure 6-3: Mean flow velocity for one spring-neap tidal cycle at the West1 location after T = 4 years after construction for a scenario without island (left), with island (middle), and the difference (right). The figures include the tidal ellipses without island (purple) and with island (black).

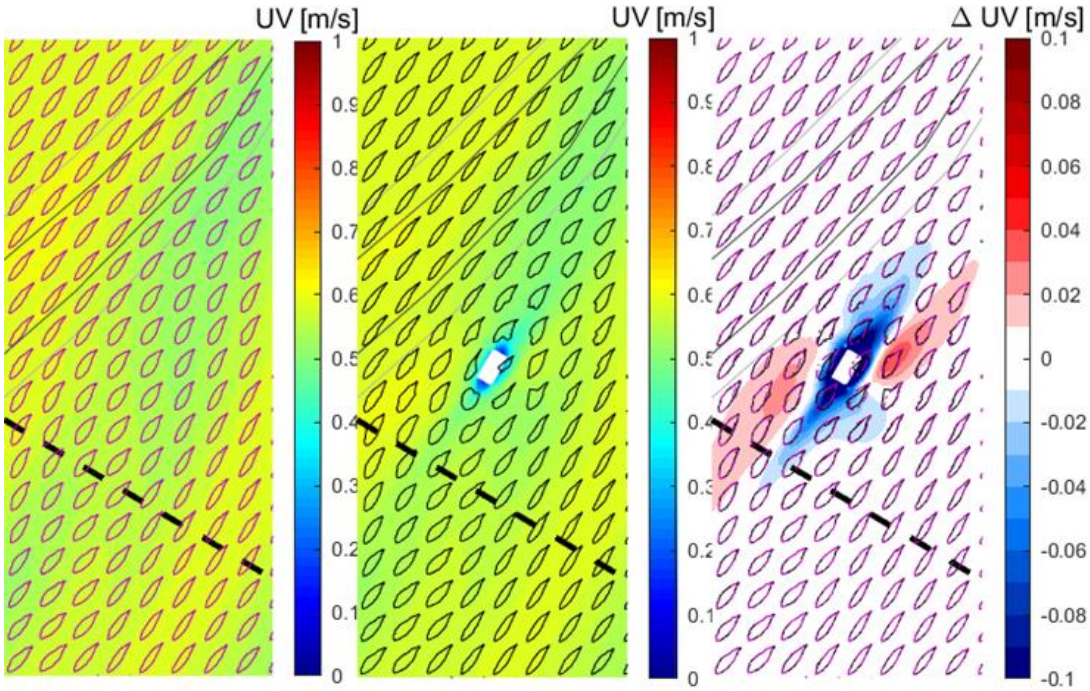

Figure 6-4: Mean flow velocity for one spring-neap tidal cycle at the West1 location after T = 10 years after construction for a scenario without island (left), with island (middle), and the difference (right). The figures include the tidal ellipses without island (purple) and with island (black).

6.1.2 Island impact on waves

The islands impact on waves is investigated for a 1/year wave condition of H_s=4.5, T_p=9.3 s and a direction of 352.5 °N. A 1/year wave condition is considered representative as a wave height that does affect the bed at these depths but is not expected to cause very significant bed changes in the reference situation.

In Figure 6-5 to Figure 6-8 the wave height in a reference situation, a situation with the island and the difference is presented, for the bathymetry just after construction of the island, and after 1 year, 4 years and 10 years after construction of the island. The island reflects the waves, inducing a higher wave height (~0.5m) on the exposed sides of the island. The wave height is increased with more than 1% over a distance of ~18km. Behind the island the wave height is significantly reduced (>1m). At a distance of almost 5 km the reduction in wave height falls to only 1%. The direction of the waves is only affected in the lee of the island.

Over time a scour pit develops around the island (chapter 7), which reduces the area where the wave height is affected in size. Nevertheless, in general it can be stated that because of the large depth around the island the differences are relatively small.

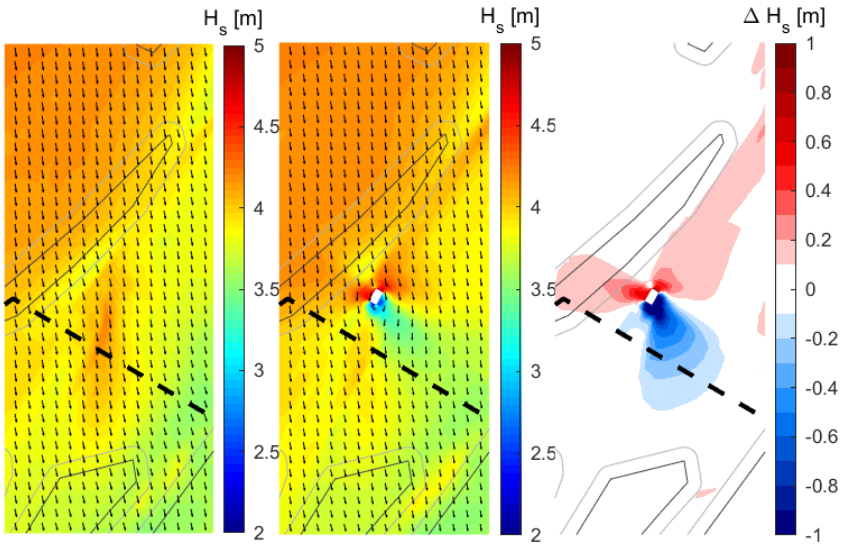

Figure 6-5: Wave height in reference situation (left), with island (middle) and difference (right). For a bathymetry just after construction of the island at the West1 location

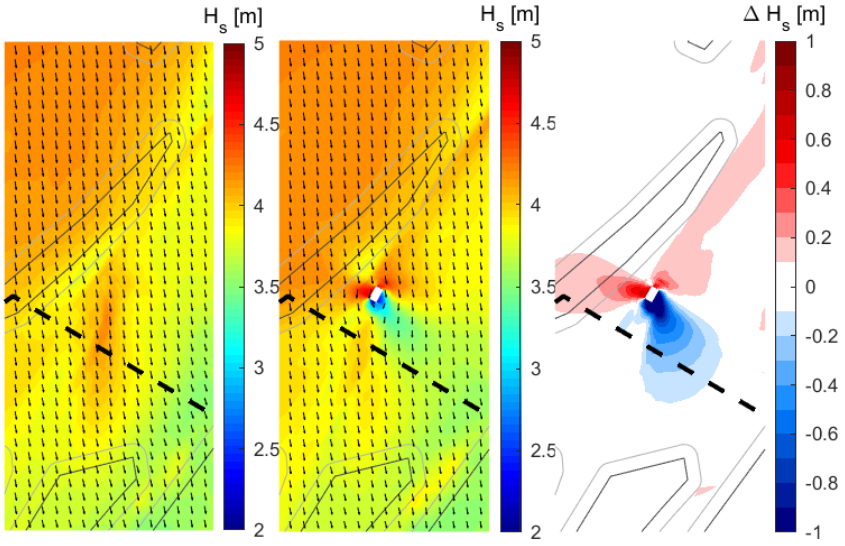

Figure 6-6: Wave height in reference situation (left), with island (middle) and difference (right). For a bathymetry 1 year after construction of the island at the West1 location.

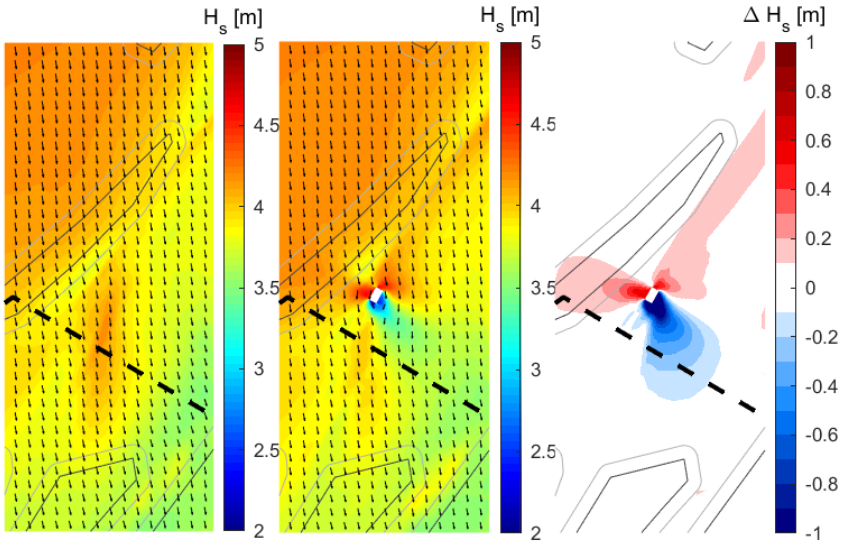

Figure 6-7: Wave height in reference situation (left), with island (middle) and difference (right). For a bathymetry 4 years after construction of the island at the West1 location.

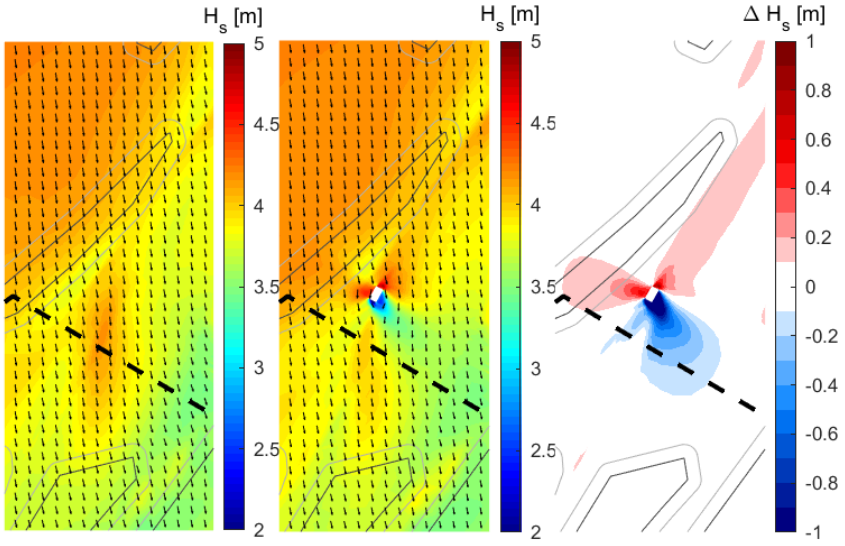

Figure 6-8: Wave height in reference situation (left), with island (middle) and difference (right). For a bathymetry 10 years after construction of the island at the West1 location.

6.1.3 Island impact in bed shear stresses

The 1/year wave condition as used in the winter condition is equal to the wave condition from Section 6.1.2. Soulsby (1997) is used to calculate the bed shear stress under the combined force of waves and currents.

Summer conditions

The island impact on the bed shear stress as averaged over one spring-neap tidal cycle in summer, assuming a tidal current only, at four moments in time (T = 0, 1, 4, 10 years) are shown in Figure 6-9 to Figure 6-12. The mean bed shear stress in summer around the West1 location equals approximately 0.4 N/m^2. Due to the presence of the island the bed shear stresses increase and decrease corresponding to the flow accelerations and decelerations as discussed in Section 6.1.1. The maximum bed shear stress increase equals 42% of the mean bed shear stress immediately after construction of the island. 10 years after construction this value decreases to a maximum of 14% of the mean bed shear stress. Flow over the scour protection is excluded from this analysis.

10 years after construction increased bed shear stress >10% can be found up to 1 km away from the island center, whereas decreased bed shear stress <-10% can be found up to 2 km away from the island center. Directly after construction approximately 245 Ha is affected with bed shear stress changes > 10% of the mean bed shear stress in summer conditions. After 10 years this area is reduced to 110 Ha. These areas exclude the scour protection. The areas with bed shear stress disturbances larger than 10% almost exclusively comprise of bed shear stress decreases.

Due to the quadratic relationship between the bed shear stress and the flow velocity, the trend of the bed shear stresses (Figure 6-9 to Figure 6-12) shows large resemblance to the trend of the flow velocities, Section 6.1.1. Directly after construction of the island (Figure 6-9) the bed shear stress differences are highest. At T = 4 years (Figure 6-11) the magnitude of the bed shear stress increases has fallen significantly due to morphological feedback. Furthermore, the extent of the bed shear stress decreases in the wakes of the island have decreased as well. Between T = 4 years (Figure 6-11)

and T = 10 years (Figure 6-12) relatively little changes are observed, indicating the system is approaching an equilibrium.

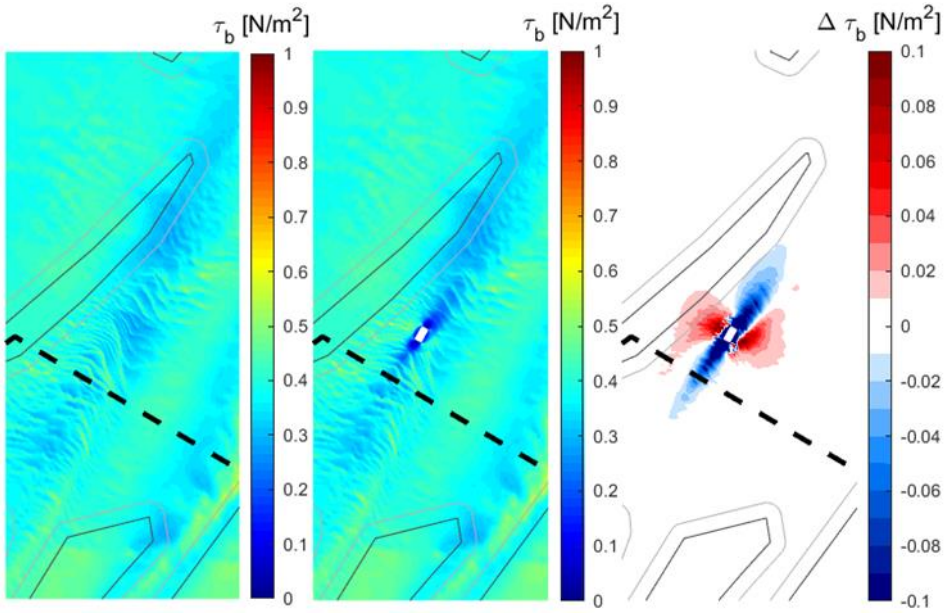

Figure 6-9: Mean bed shear stress for one spring-neap tidal cycle with summer conditions immediately after construction for a scenario without island (left), with island (middle), and the difference (right) at the West1 location.

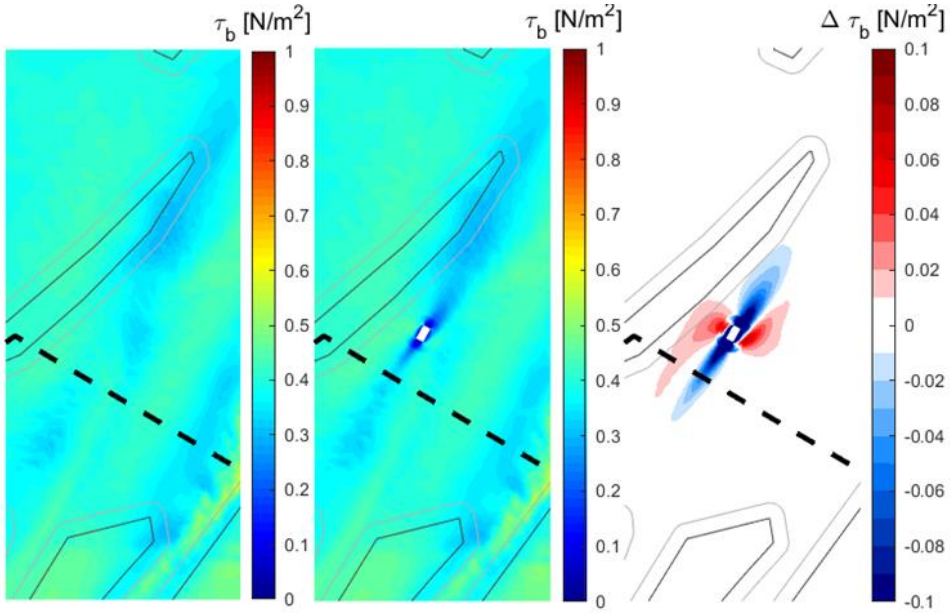

Figure 6-10: Mean bed shear stress for one spring-neap tidal cycle with summer conditions at T = 1 year after construction for a scenario without island (left), with island (middle), and the difference (right) at the West1 location.

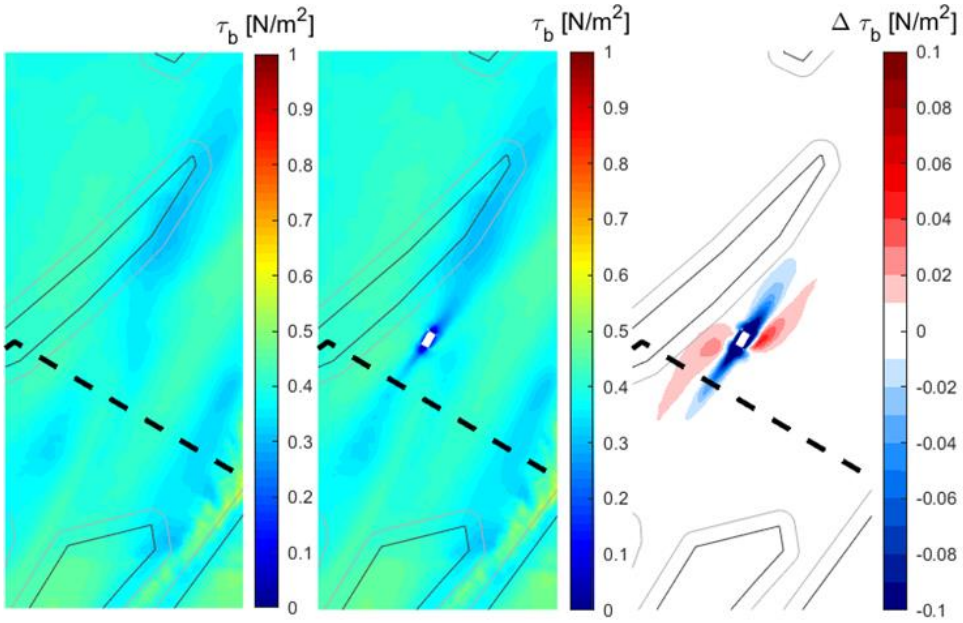

Figure 6-11: Mean bed shear stress for one spring-neap tidal cycle with summer conditions at T = 4 years after construction for a scenario without island (left), with island (middle), and the difference (right) at the West1 location.

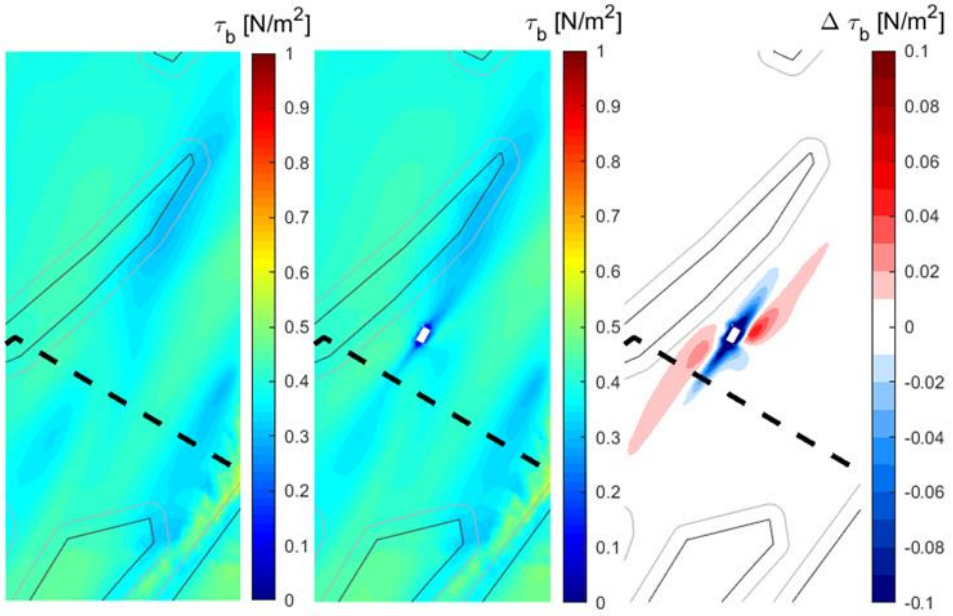

Figure 6-12: Mean bed shear stress for one spring-neap tidal cycle with summer conditions at T = 10 years after construction for a scenario without island (left), with island (middle), and the difference (right) at the West1 location.

Winter conditions

The island impact on the bed shear stress during a 1/year storm and average tidal conditions is derived by combining the shear stresses under both waves and currents with the formula of Soulsby

(1997). This winter condition is presented at four moments in time (T = 0, 1, 4, 10 years)[5] in Figure 6-13 to Figure 6-16. The mean bed shear stress in winter around the West1 location equals approximately 0.5 N/m^2. Due to the presence of the island the bed shear stresses increase and decrease corresponding to the flow accelerations and decelerations. The maximum bed shear stress increase equals 43% of the mean bed shear stress immediately after construction of the island. This value decreases to 19% of the mean bed shear stress 10 years after construction of the island. The point of maximum bed shear stress increases is located further away from the north-eastern corner of the island (compared to summer conditions), corresponding with the reflection of the waves.

10 years after construction increased bed shear stress >10% can be found up to 1.5 km away from the island center, whereas decreased bed shear stress <-10% can be found up to 2 km away from the island center. Directly after construction the absolute mean bed shear stresses change with more than 10% over an area of approximately 245 Ha. After 10 years this area is reduced to 190 Ha. These areas exclude the scour protection. The decrease in affected area through time is smaller compared to summer conditions as the morphological adaptations towards the new equilibrium are dominated by the continuous tidal currents rather than the instantaneous waves. As such, instantaneous events such as the 1/yr wave condition can still yield bed shear stress changes over a relatively large area.

The bed shear stress disturbance of the MOG2 island in winter conditions is more severe compared to summer conditions, both in magnitude (+20%) and extent of the disturbances (after 10 years). Nevertheless, the majority of the bed shear stresses are an effect of the tidal current.

Due to wave sheltering of the island the bed shear stresses towards the south-east are significantly lowered in a relatively large area. Furthermore, due to reflection along the northern side of the island the bed shear stresses are increased in a long stretch towards the northeast. This coincides with the increase in significant wave height as analysed in Section 6.1.2.The combined pattern of waves and currents will be different for waves from other directions but it is not expected that this will strongly influence the magnitude of the areas with more than 10% change.

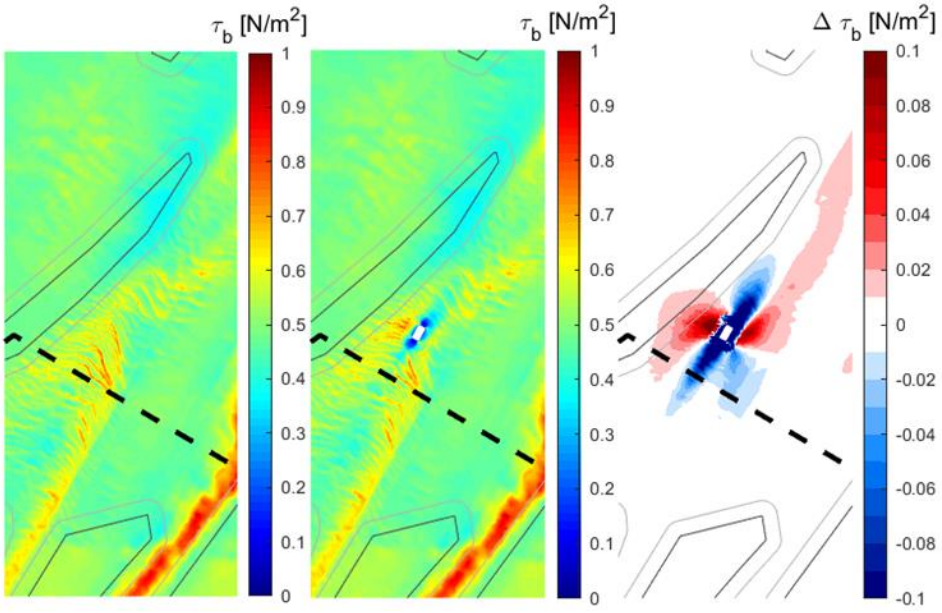

Figure 6-13: Mean bed shear stress for one spring-neap tidal cycle with winter conditions immediately after construction for a scenario without island (left), with island (middle), and the difference (right) at the West1 location.

[5] Note that the bed levels for the hydraulic simulations at these times are derived from a morphological computation as presented in chapter 7. In this computation the effect of waves is not included because it is shown that waves have only a limited impact on the bed level changes (paragraph 7.6).

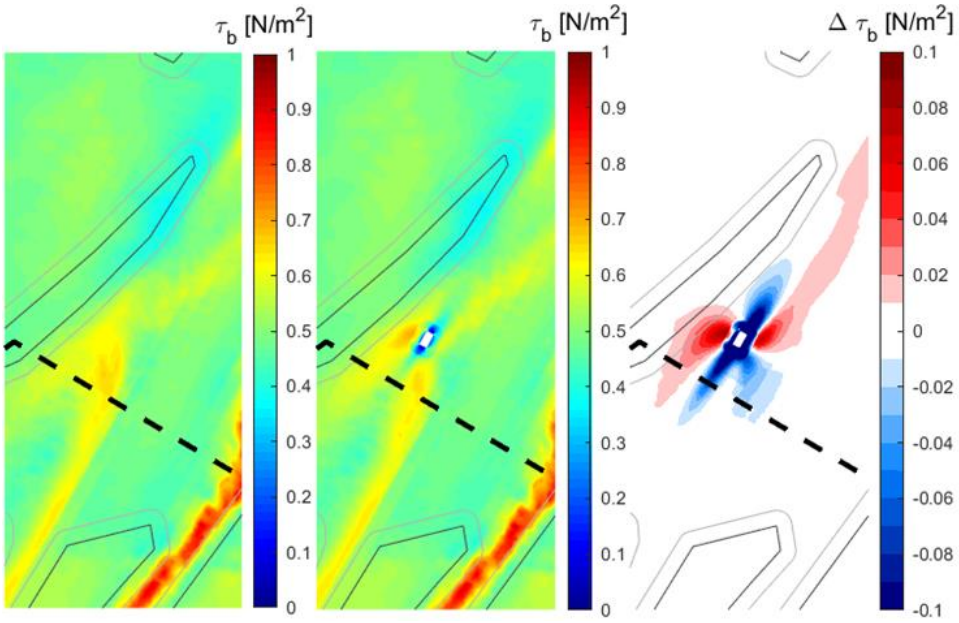

Figure 6-14: Mean bed shear stress for one spring-neap tidal cycle with winter conditions at T = 1 year after construction for a scenario without island (left), with island (middle), and the difference (right) at the West1 location.

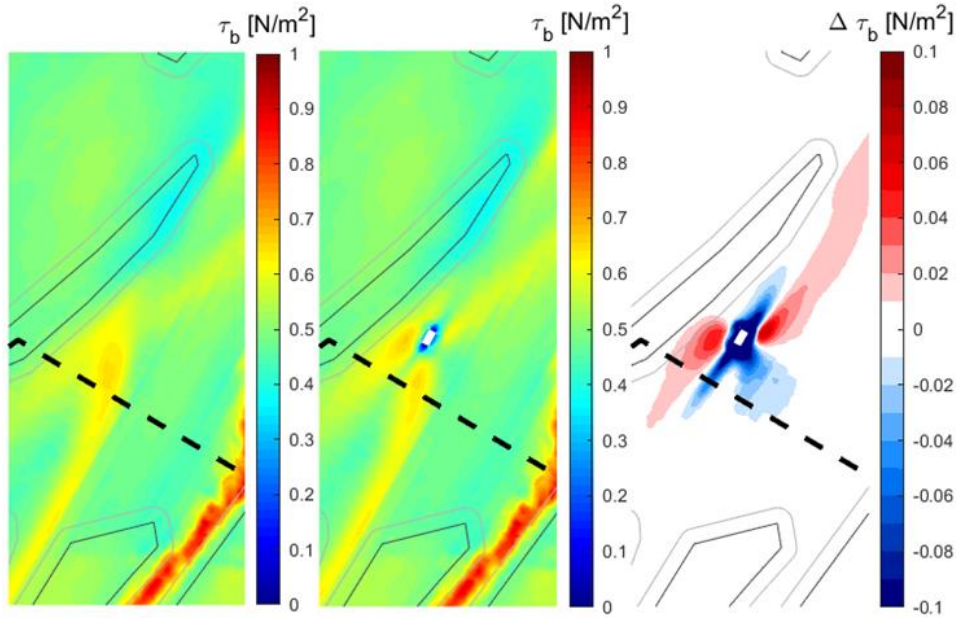

Figure 6-15: Mean bed shear stress for one spring-neap tidal cycle with winter conditions at T = 4 years after construction for a scenario without island (left), with island (middle), and the difference (right) at the West1 location.

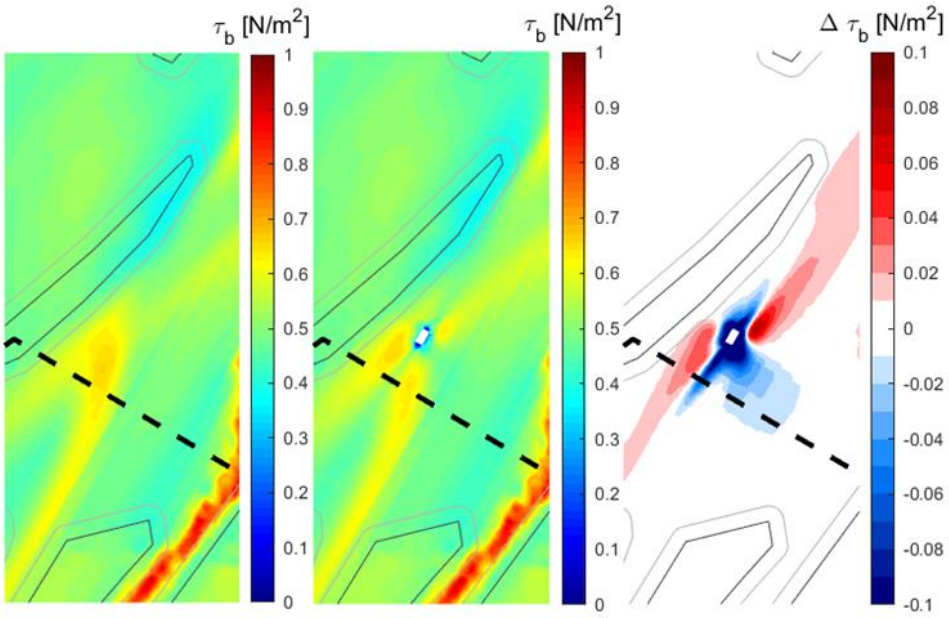

Figure 6-16: Mean bed shear stress for one spring-neap tidal cycle with winter conditions at T = 10 years after construction for a scenario without island (left), with island (middle), and the difference (right) at the West1 location.

6.2 West2 location

The wave sheltering effect of the island is not expected to be different for an island of similar shape and orientation at the West 2 location. At the West1 location it is shown that bed shear stresses at these depths are predominantly induced by the tidal current. For the deeper located West2 location it is expected that the effect of waves on the bed shear stress is even lower. For this reason, for the West2 location the assessment focusses on current and current-induced bed shear stresses only but it should be noted that under 1/yr storm conditions shear stresses might be approximately 20% higher.

6.2.1 Island impact on current

The flow disturbance caused by the island is further investigated by analysing the mean flow velocity pattern over one spring-neap tidal cycle at four moments in time: immediately after construction and 1, 4, 10 years after construction. The results are depicted in Figure 6-17 to Figure 6-20, including the tidal ellipses at several points around the island.

The mean flow velocity magnitude around the West2 location equals approximately 0.5 m/s. In the direct vicinity of the island the flow deceleration along the leesides of the island are clearly visible when considering the mean velocities around the island (middle figures). The flow accelerations along the island long-side are less visible but can clearly be seen in the flow difference figures (right figures). The flow accelerations are at maximum 15% of the mean flow velocity immediately after construction of the island. 10 years after construction this value increases to a maximum of 8% of the mean flow velocity. This excludes the flow on the bed protection.

Directly after construction (Figure 6-1) the flow velocity differences are most significant as no adaption of the surrounding seabed to the island has taken place. The morphological changes in the subsequent years decrease the magnitude of these flow velocity differences. After T = 4 years (Figure 6-4) the flow accelerations along the island long-sides have decreased significantly. Furthermore, the area and magnitude of the flow decelerations have decreased as well. Between T = 4 years (Figure 6-3) and T = 10 years (Figure 6-4) the flow disturbance due to the presence of the island remains more or less the same, indicating the system is approaching an equilibrium.

The impact of the MOG2 island on the direction of the tidal flow is limited. Significant differences are only found in the direct vicinity of the island, similar to the flow accelerations and decelerations.

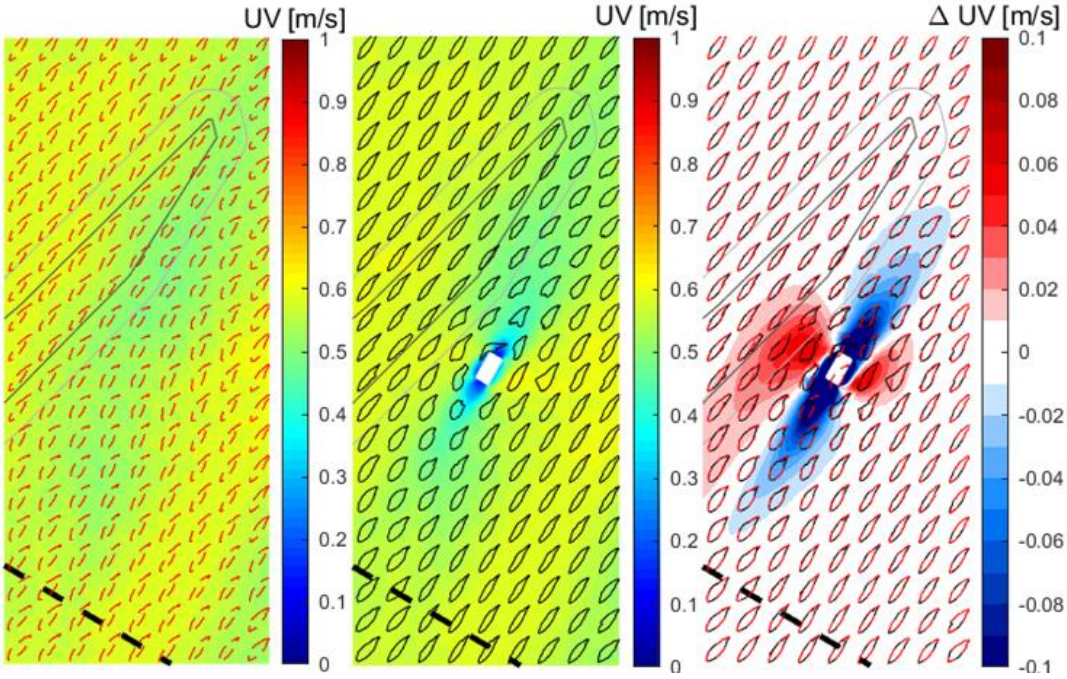

Figure 6-17: Mean flow velocity for one spring-neap tidal cycle at the West2 location immediately after construction for a scenario without island (left), with island (middle), and the difference (right). The figures include the tidal ellipses without island (purple) and with island (black).

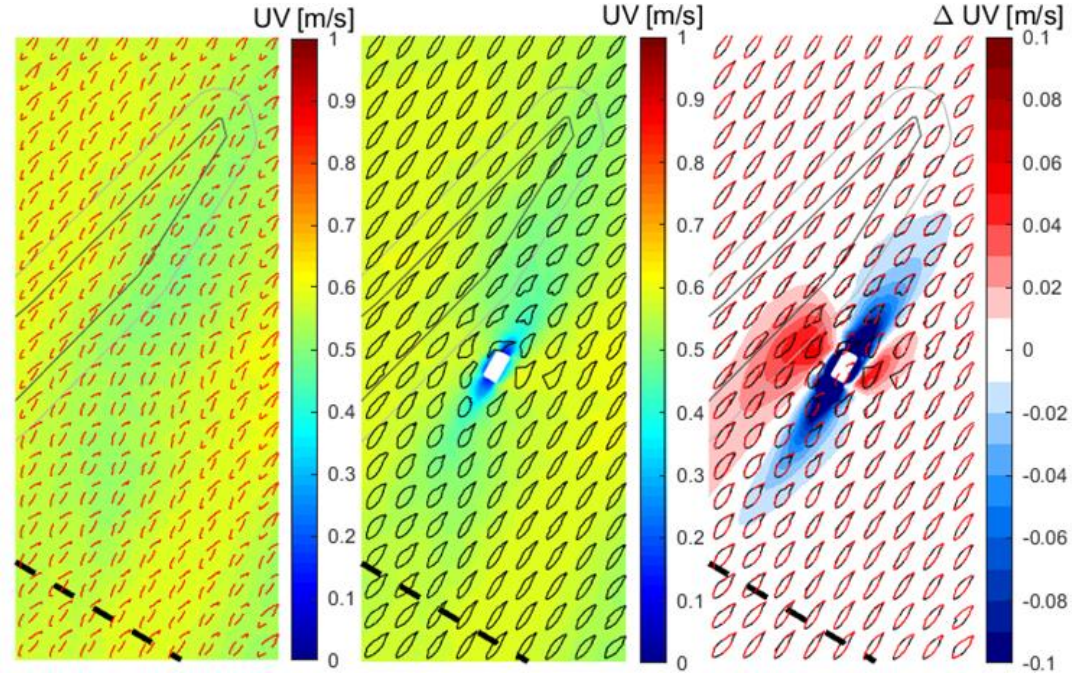

Figure 6-18: Mean flow velocity for one spring-neap tidal cycle at the West2 location after T = 1 year after construction for a scenario without island (left), with island (middle), and the difference (right). The figures include the tidal ellipses without island (purple) and with island (black).

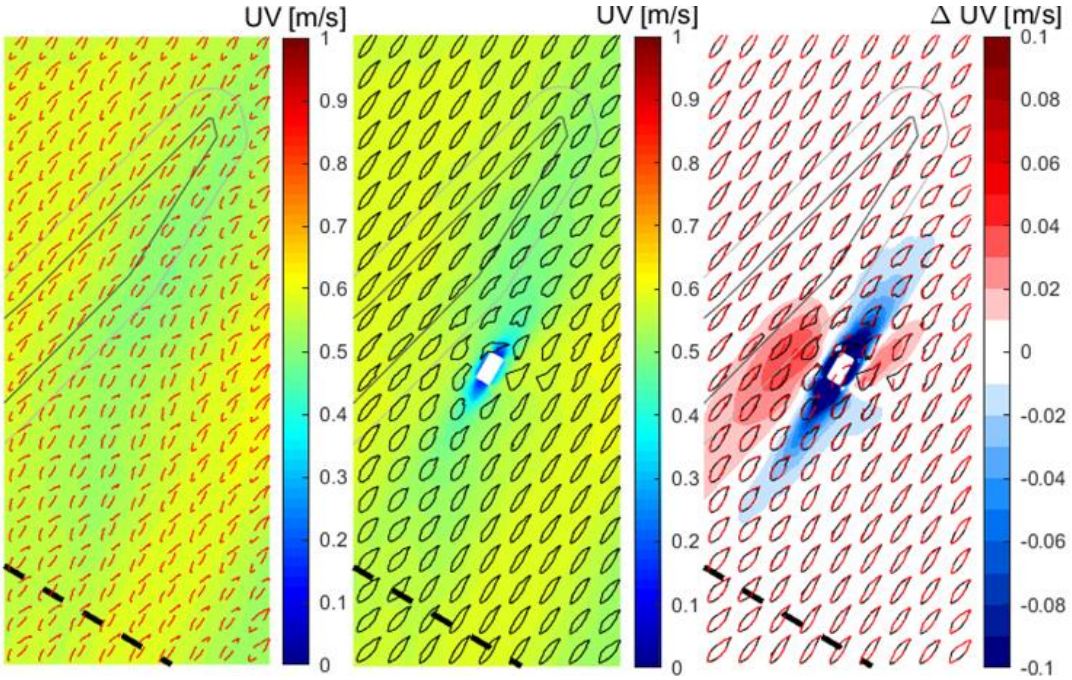

Figure 6-19: Mean flow velocity for one spring-neap tidal cycle at the West2 location after T = 4 years after construction for a scenario without island (left), with island (middle), and the difference (right). The figures include the tidal ellipses without island (purple) and with island (black).

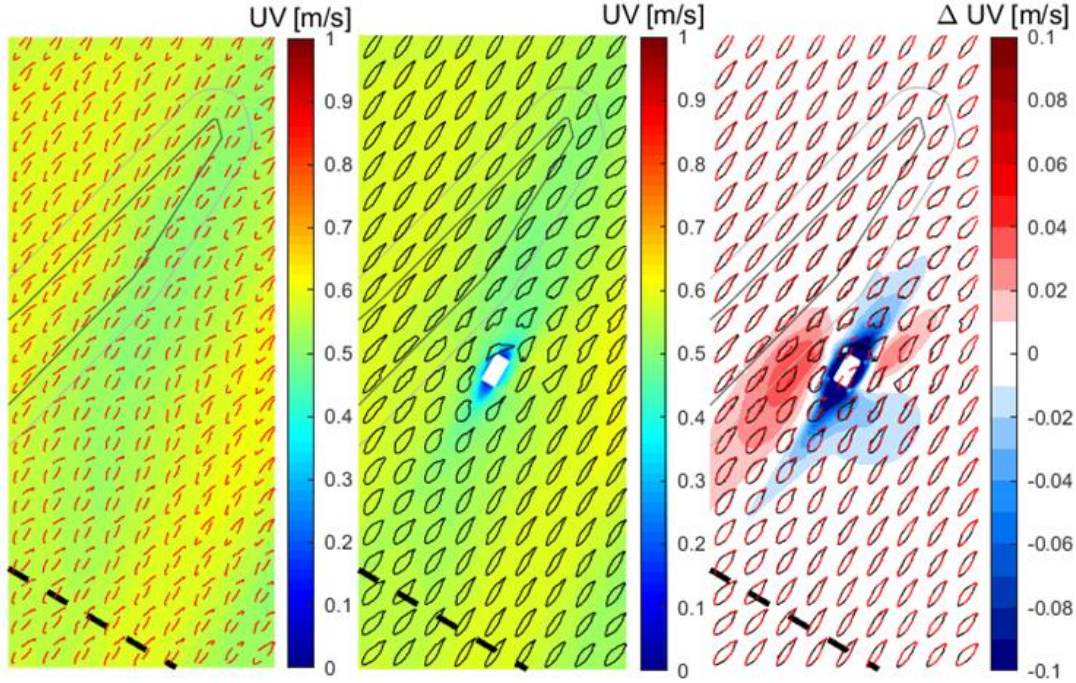

Figure 6-20: Mean flow velocity for one spring-neap tidal cycle at the West2 location after T = 10 years after construction for a scenario without island (left), with island (middle), and the difference (right). The figures include the tidal ellipses without island (purple) and with island (black).

6.2.2 Island impact on bed shear stress

The island impact on the bed shear stress as averaged over one spring-neap tidal cycle in summer, assuming a tidal current only, at four moments in time (T = 0, 1, 4, 10 years) are shown in Figure 6-21 to Figure 6-24. The mean bed shear stress in summer around the West1 location equals approximately 0.4 N/m^2. Due to the presence of the island the bed shear stresses increase and decrease corresponding to the flow accelerations and decelerations as discussed earlier. The maximum bed shear stress increase equals 40% of the mean bed shear stress immediately after construction of the island. 10 years after construction this value increases to a maximum of 10% of the mean bed shear stress. This analysis excludes the flow over the scour protection.

10 years after construction increased bed shear stress >10% can be found up to 1 km away from the island center, whereas decreased bed shear stress <-10% can be found up to 2 km away from the island center. Directly after construction approximately 280 Ha is affected with bed shear stress changes > 10% of the mean bed shear stress in summer conditions. After 10 years this area is reduced to 85 Ha. These areas exclude the scour protection. The areas with bed shear stress disturbances larger than 10% almost exclusively comprise of bed shear stress decreases.

Due to the quadratic relationship between the bed shear stress and the flow velocity, the trend of the bed shear stresses Figure 6-21 to Figure 6-24 is similar to trend of the flow velocity in time. Directly after construction of the island (Figure 6-9) the bed shear stress differences are highest. At T = 4 years (Figure 6-23) the magnitude of the bed shear stress increases has fallen significantly due to morphological feedback. Furthermore, the extent of the bed shear stress decreases in the wakes of the island have decreased as well. Between T = 4 years (Figure 6-23) and T = 10 years (Figure 6-24) relatively little changes are observed, indicating the system is approaching an equilibrium.

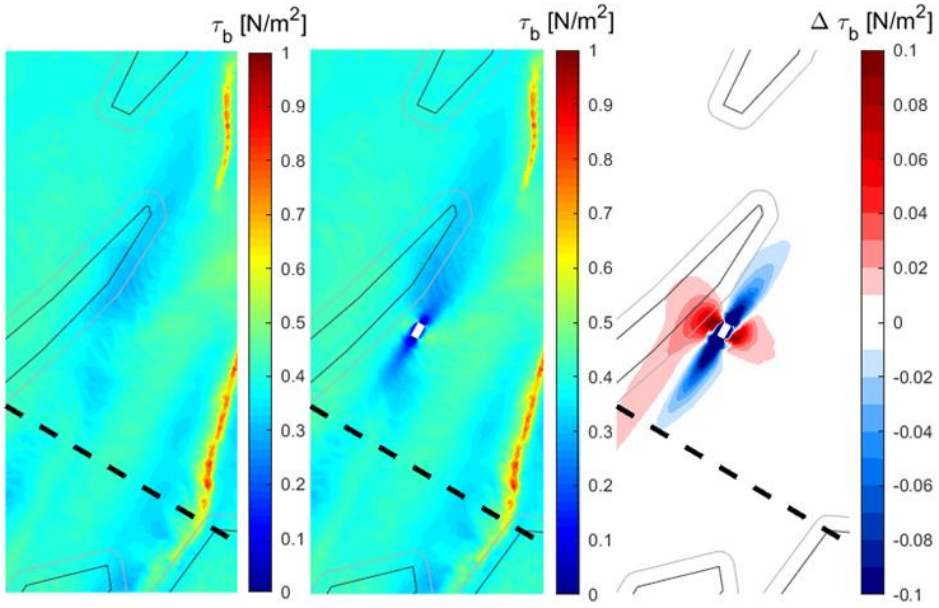

Figure 6-21: Mean bed shear stress for one spring-neap tidal cycle with summer conditions immediately after construction for a scenario without island (left), with island (middle), and the difference (right) at the West2 location.

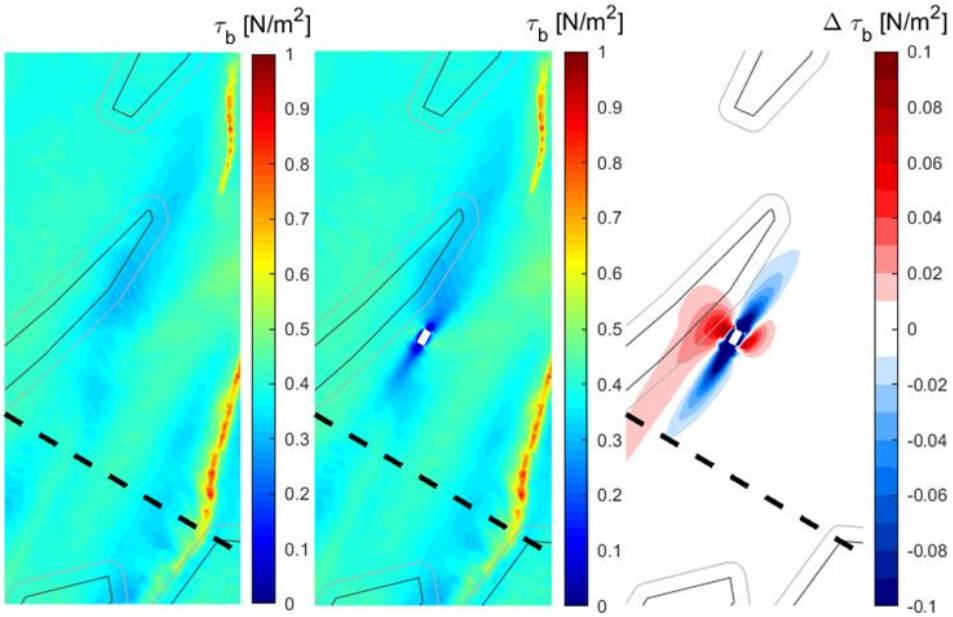

Figure 6-22: Mean bed shear stress for one spring-neap tidal cycle with summer conditions at T = 1 year after construction for a scenario without island (left), with island (middle), and the difference (right) at the West2 location.

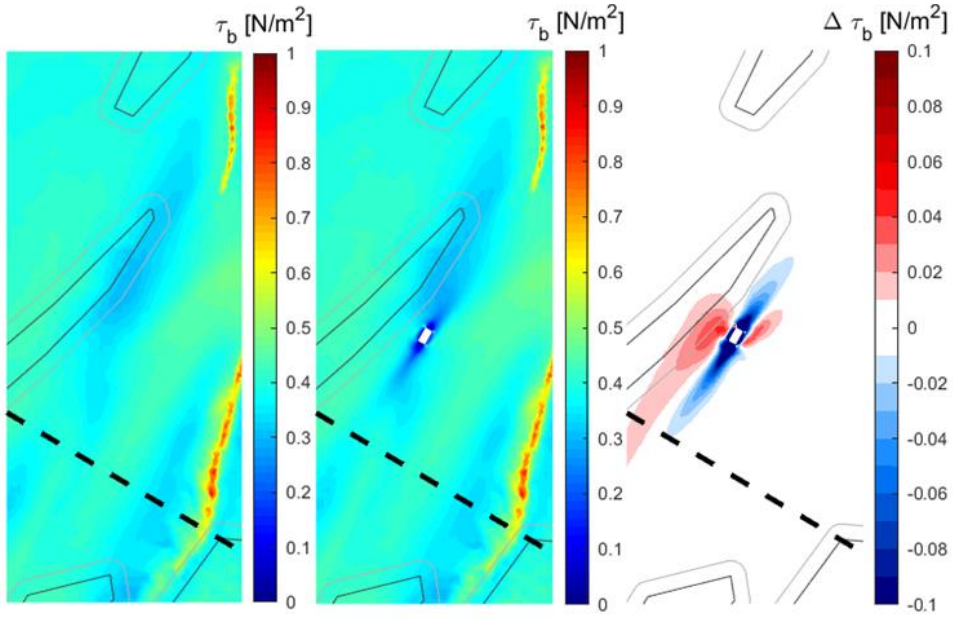

Figure 6-23: Mean bed shear stress for one spring-neap tidal cycle with summer conditions at T = 4 years after construction for a scenario without island (left), with island (middle), and the difference (right) at the West2 location.

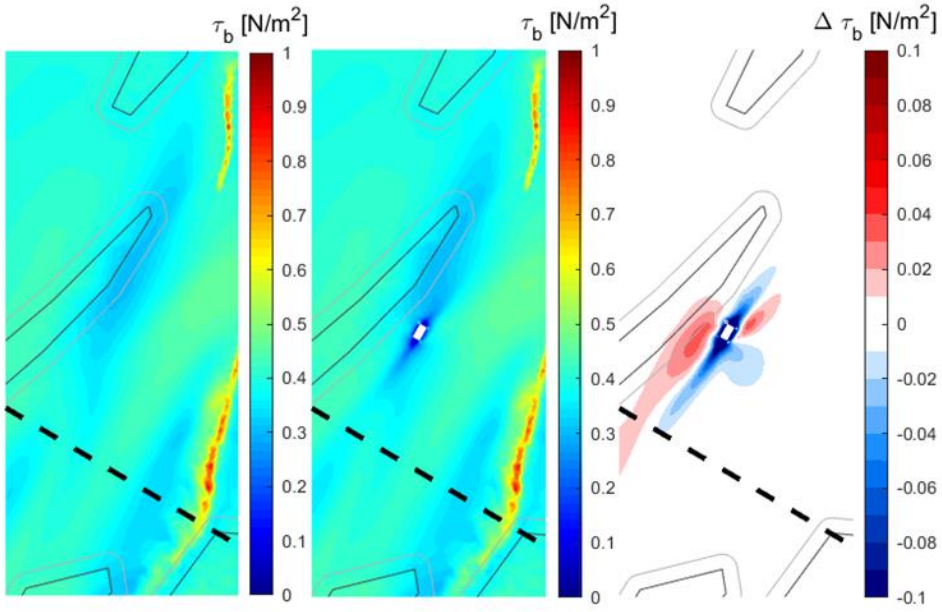

Figure 6-24: Mean bed shear stress for one spring-neap tidal cycle with summer conditions at T = 10 years after construction for a scenario without island (left), with island (middle), and the difference (right) at the West2 location.

6.3 Noord location

The wave sheltering effect of the island is not expected to be different for an island of similar shape and orientation at the Noord location. At the West1 location it is shown that bed shear stresses at these depths are predominantly induced by the tidal current. For the deeper located Noord location it is expected that the effect of waves on the bed shear stress is even lower. For this reason, for the Noord location the assessment focusses on current and current-induced bed shear stresses only but it should be noted that under 1/yr storm conditions shear stresses might be up to 20% higher.

6.3.1 Island impact on current

The flow disturbance caused by the island is further investigated by analysing the mean flow velocity pattern over one spring-neap tidal cycle at four moments in time: immediately after construction and 1, 4, 10 years after construction. The results are depicted in Figure 6-25 to Figure 6-28, including the tidal ellipses at several points around the island.

The mean flow velocity magnitude around Noord location equals approximately 0.5 m/s. In the direct vicinity of the island the flow deceleration along the leesides of the island are clearly visible when considering the mean velocities around the island (middle figures). The flow accelerations along the island long-side are less visible but can clearly be seen in the flow difference figures (right figures). The flow accelerations are at maximum 20% of the mean flow velocity immediately after construction of the island. 10 years after construction this value decreases to a maximum of 14% of the mean flow velocity.

Directly after construction (Figure 6-25) the flow velocity differences are most significant as no adaption of the surrounding seabed to the island has taken place. The morphological changes in the subsequent years decrease the magnitude of these flow velocity differences. After T = 4 years (Figure 6-27) the flow accelerations along the island long-sides have decreased significantly. Furthermore, the area and magnitude of the flow decelerations have decreased as well. Between T = 4 years (Figure 6-27) and T = 10 years (Figure 6-28) the flow disturbance due to the presence of the island remains more or less the same, indicating the system is approaching an equilibrium.

The impact of the MOG2 island on the direction of the tidal flow is limited. Significant differences are only found in the direct vicinity of the island, similar to the flow accelerations and decelerations.

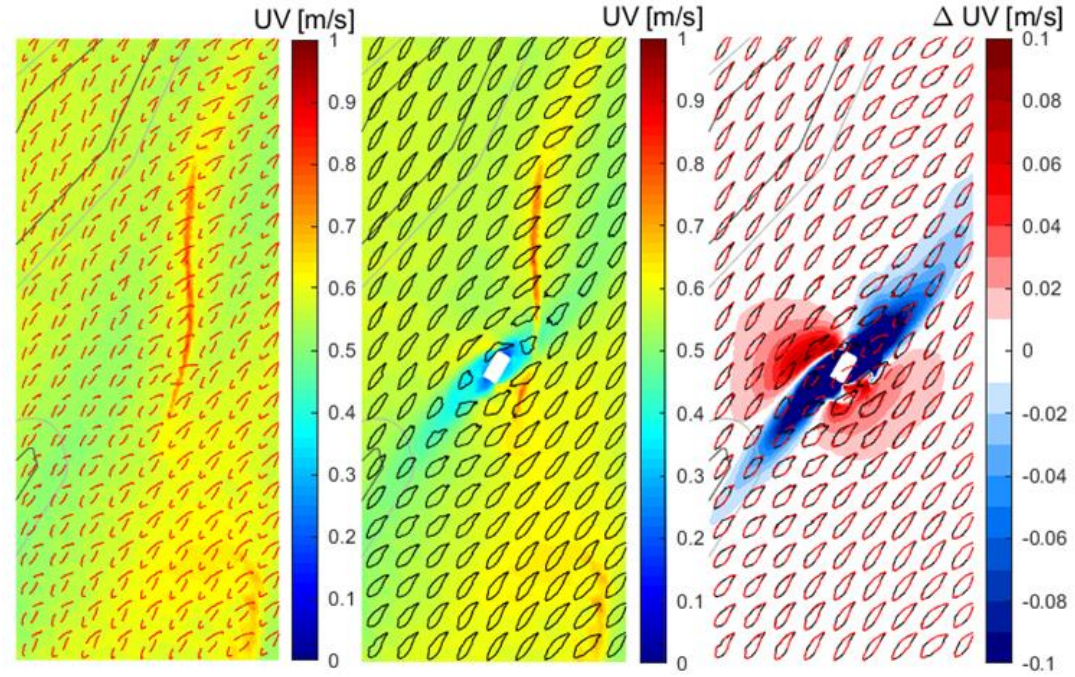

Figure 6-25: Mean flow velocity for one spring-neap tidal cycle at the Noord location immediately after construction for a scenario without island (left), with island (middle), and the difference (right). The figures include the tidal ellipses without island (purple) and with island (black).

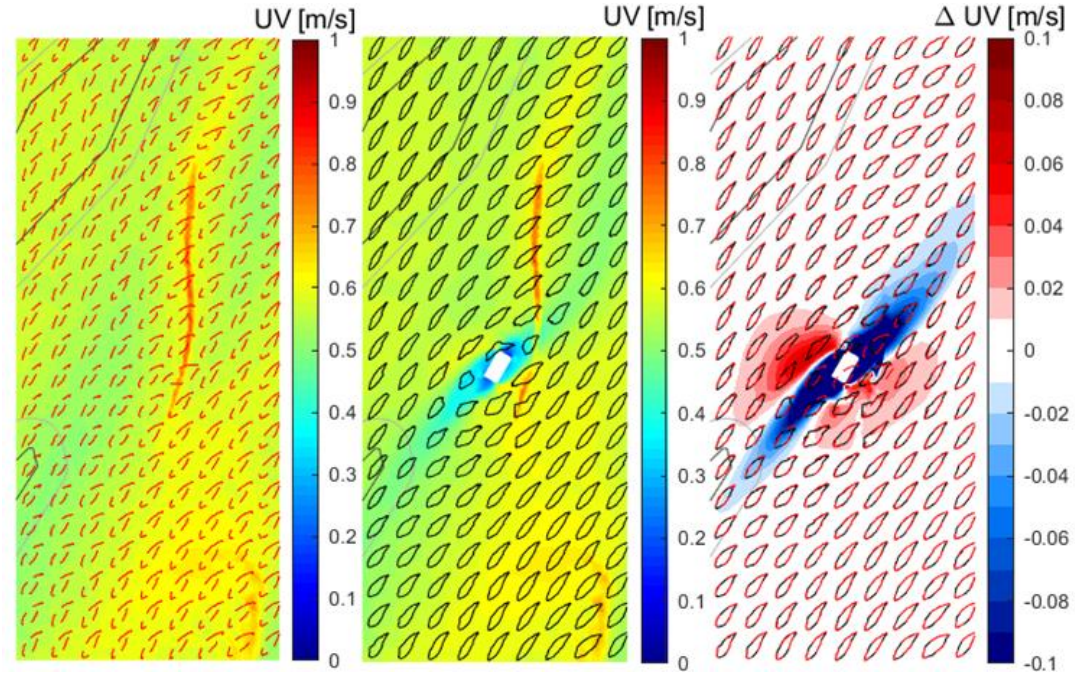

Figure 6-26: Mean flow velocity for one spring-neap tidal cycle at the Noord location after T = 1 year after construction for a scenario without island (left), with island (middle), and the difference (right). The figures include the tidal ellipses without island (purple) and with island (black).

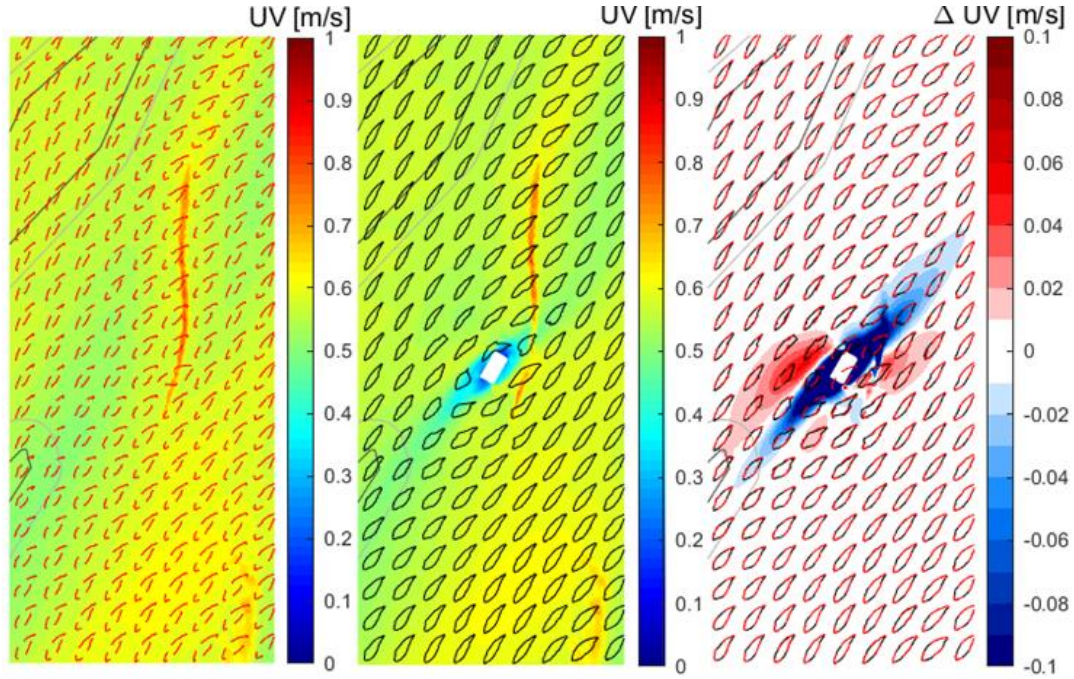

Figure 6-27: Mean flow velocity for one spring-neap tidal cycle at the Noord location after T = 4 years after construction for a scenario without island (left), with island (middle), and the difference (right). The figures include the tidal ellipses without island (purple) and with island (black).

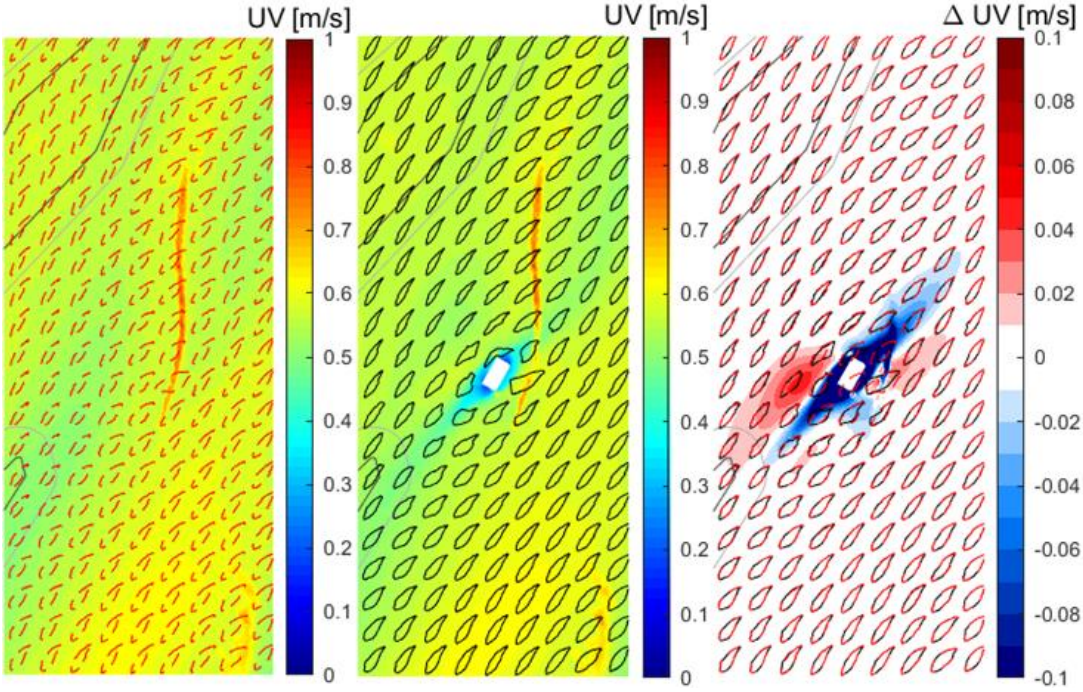

Figure 6-28: Mean flow velocity for one spring-neap tidal cycle at the Noord location after T = 10 years after construction for a scenario without island (left), with island (middle), and the difference (right). The figures include the tidal ellipses without island (purple) and with island (black).

6.3.2 Island impact on bed shear stress

The island impact on the bed shear stress as averaged over one spring-neap tidal cycle in summer, assuming a tidal current only, at four moments in time (T = 0, 1, 4, 10 years) are shown in Figure 6-29 to Figure 6-32. The mean bed shear stress in summer around the Noord location equals approximately 0.33 N/m^2. Due to the presence of the island the bed shear stresses increase and decrease corresponding to the flow accelerations and decelerations as discussed earlier. The maximum bed shear stress increase equals 62% of the mean bed shear stress immediately after construction of the island. Note that this increase leads to similar values of maximum shear stresses compared to the other island locations. 10 years after construction this value decreases to a maximum of 10% of the mean bed shear stress. This analysis excludes flow over the scour protection.

10 years after construction increased bed shear stress >10% can be found up to 1.25 km away from the island center, whereas decreased bed shear stress <-10% can be found up to 2 km away from the island center. Directly after construction approximately 350 Ha is affected with bed shear stress changes > 10% of the mean bed shear stress in summer conditions. After 10 years this area is reduced to 120 Ha. These areas exclude the scour protection. It is remarked that these areas are affected by the Noordhinderbank, which is kept at a fixed position within the simulations. As a result, the morphological feedback is absent around the Noordhinderbank and bed shear stresses remain high throughout the simulations. This is not a realistic development but a limitation of models available. However, it does indicate that significant impact of the island on the Noordhinderbank cannot be ruled out at the Noord location.

Due to the quadratic relationship between the bed shear stress and the flow velocity, the change in time visible in Figure 6-21 to Figure 6-24 shows large resemblance to the trend of the flow velocities in time. Directly after construction of the island (Figure 6-9) the bed shear stress differences are highest. At T = 4 years (Figure 6-23) the magnitude of the bed shear stress increases has fallen significantly due to morphological feedback. Furthermore, the extent of the bed shear stress decreases in the wakes of the island have decreased as well. Between T = 4 years (Figure 6-23) and T = 10 years (Figure 6-24) relatively little changes, indicating the system is approaching an equilibrium.

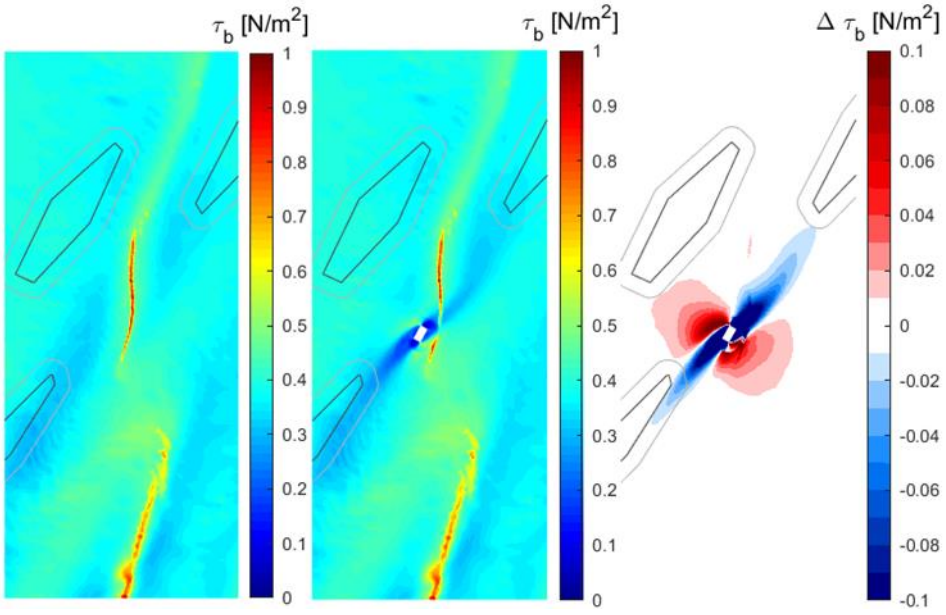

Figure 6-29: Mean bed shear stress for one spring-neap tidal cycle with summer conditions immediately after construction for a scenario without island (left), with island (middle), and the difference (right) at the Noord location.

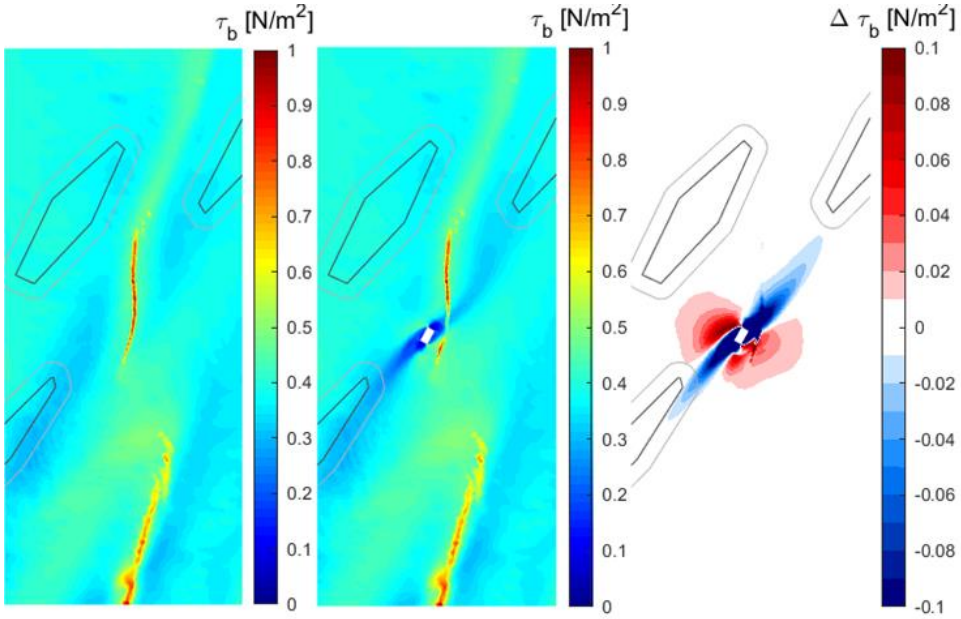

Figure 6-30: Mean bed shear stress for one spring-neap tidal cycle with summer conditions at T = 1 year after construction for a scenario without island (left), with island (middle), and the difference (right) at the Noord location.

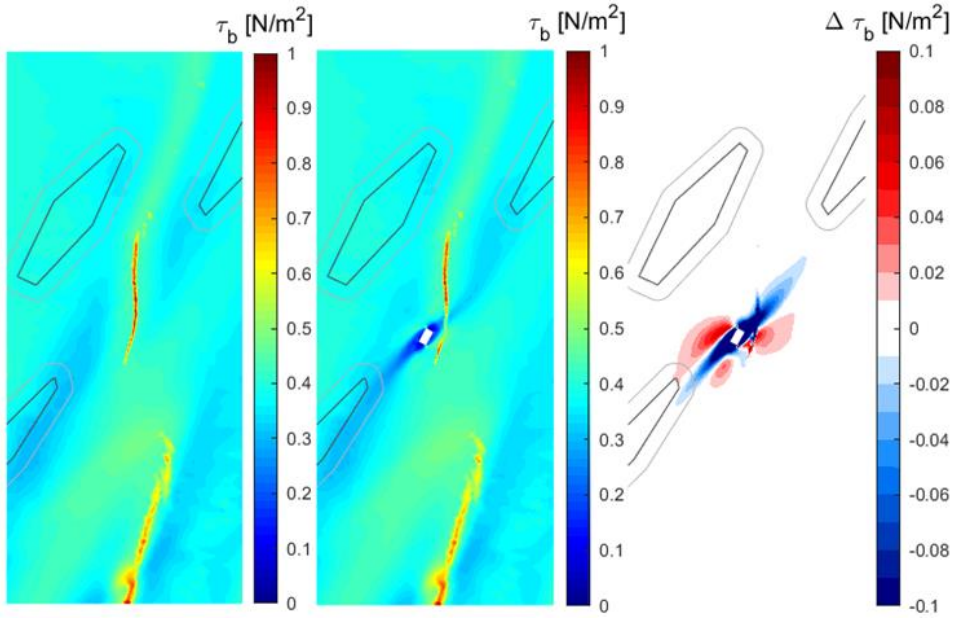

Figure 6-31: Mean bed shear stress for one spring-neap tidal cycle with summer conditions at T = 4 years after construction for a scenario without island (left), with island (middle), and the difference (right) at the Noord location.

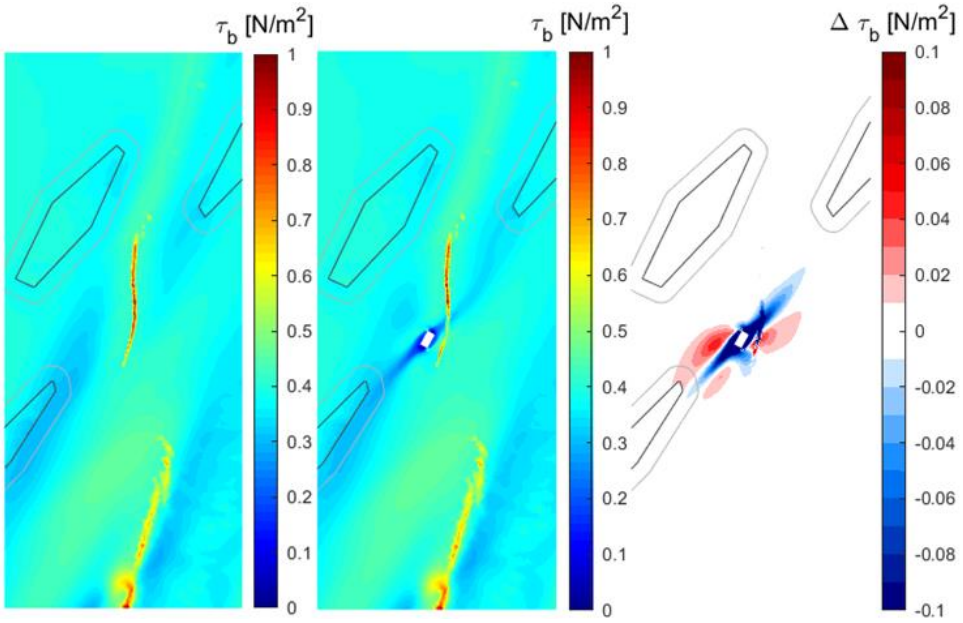

Figure 6-32: Mean bed shear stress for one spring-neap tidal cycle with summer conditions at T = 10 years after construction for a scenario without island (left), with island (middle), and the difference (right) at the Noord location.

7 MORPHOLOGICAL MODELLING RESULTS

In this chapter the morphological modelling results are predicted for the island design including pre-scour dredging unless stated otherwise.

7.1 Sediment concentration patterns

The effect of the island on the sediment concentrations around the island can be subdivided in three typical stages. First, a pattern of reduced sediment concentrations in the lee of the island and two higher concentration areas along the long sides of the island occurring with the peak ebb and flood flow (left panels in Figure 7-1). The high concentration areas correspond to the flow acceleration zones with increased bed shear stress, as discussed in the previous chapter. In the second stage, these high concentration areas are spread over a larger area further away from the island caused by the counterclockwise rotation of the flow and shedding of eddies at the onset to slack tide (left panels in Figure 7-1 red areas further from the island). In the final stage, closer to slack tide, sediment concentrations are reducing, indicating that the sediment is being deposited further away from the island (right panels in Figure 7-1).

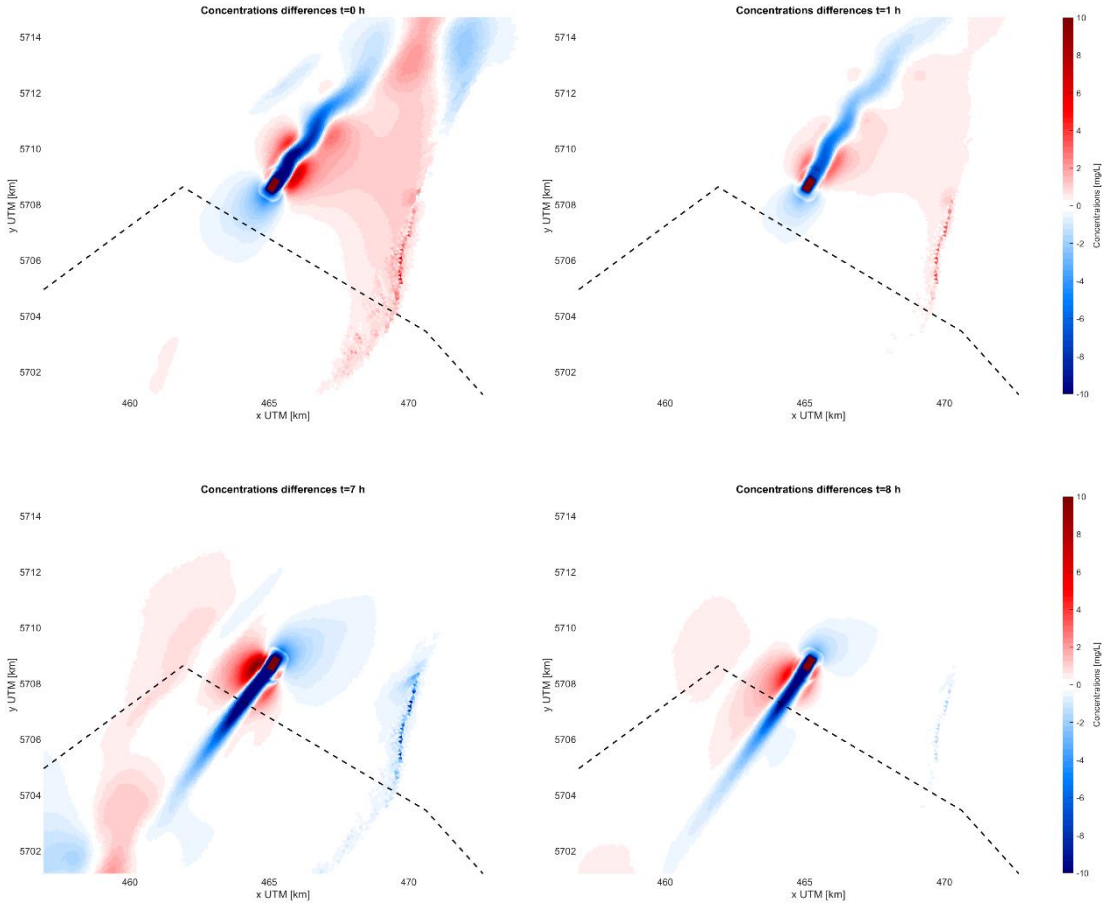

Figure 7-1: Sediment concentration increase relative to a situation without island. At peak flood (top left), just before slack flood (top right), at peak ebb (bottom left),and just before slack tide ebb (bottom right) for the West1 location.

7.2 Local erosion and sedimentation

Within the scope of the local erosion and sedimentation, erosion is defined as locations where 1m erosion or more occurs, and sedimentation is defined as locations where 1m sedimentation or more occurs. These thresholds are defined to isolate the local morphological changes, and to remove secondary effects such as the autonomous effect of the model.

The flow acceleration zones with high bed shear stress and high sediment concentrations result in erosion over the long sides of the island and sedimentation in the direct lee of the island (the short edges), Figure 7-2. Areas with a sedimentation thickness of more than one meter stay within a distance of 1.5 km of the island for the West 1 and 2 locations and within a distance of 2 km for the Noord location. The relatively shallow situation of the West1 location results in a lower intensity of the erosion and sedimentation. At the Noord location the erosion sedimentation pattern is stronger and has a different orientation than the long axis of the island. This is an indication that the main flow direction deviates from the island's orientation. In paragraph 7.4 the consequences of a better alignment with the flow orientation are investigated.

From the scour holes over the long sides of the island significant amounts of sediment are transported. This erosion is not growing linearly with time. The most severe erosion occurs in the first years after construction (including pre-scour dredging), and gradually decreases in subsequent years as it moves to an equilibrium. This effect is depicted in Figure 7-3, showing the eroded volumes over time for the three island locations. The eroded volume is strongly influenced by the phase (spring/neap) of the tide within the simulations. In the simulations, one spring-neap cycle is stretched over a year (first 2 years of the simulation) or even two years (next 8 years of the simulation) as morphological acceleration is used. In reality, periods of stronger erosion will be alternated with periods of lesser erosion on a weekly basis. To filter out this effect, the data is fitted to an exponentially decaying curve, which is depicted Figure 7-3 together with the whole-year data points of the simulation. For all three island locations, the affected sediment volumes and affected areas after 1, 4 and 10 years are summarized in Table 7-1 for the erosion and in Table 7-2 for the sedimentation. Figures after 1 and 4 years can be found in Appendix B.

The distance over which the island leads to a lower seabed of more than >0.5m grows with time. After the first year this distance is 450, 485 and 640 m for the West1, West 2 and Noord location respectively. While after 10 years this distance has approximately doubled to 900, 1270 and 1085 m for the West1, West 2 and Noord location respectively.

The maximum scour occurs at the northwest corner of the island for the West1 and West2 location, and at the south-east corner of the island for the Noord location. For all three locations, the maximum in scour hole depth is reached after approximately 7 years. Afterwards, a slight backfill of the maximum point of the scour hole occurs, which is strongest at the West1 location. The maximum scour depths through time equal 12.1 m for the West1 location, 14.9 m for the West2 location, and 12.1 m for the Noord location. At the end of the 10 year simulation period, these depths are reduced to 10.4 m at the West1 location, 14.3 m at the West2 location, and 12 m at the Noord location. It is noted that the purpose of the performed simulations was to address the long term impact of the MOG2 island on areas such as the gravel beds. Thus, the employed numerical grid is relatively coarse close to the MOG2 island, and not necessarily designed to accurately calculate maximum scour hole depths. Though it is expected any grid-related uncertainties fall within the uncertainty band of these types of morphological simulations, the results are portrayed for indicative purposes.

Note that in the simulations, only one sediment grain size of medium-coarse sand is taken into account. In reality, fine material is also present in the bed material which is eroded in the scour holes. The spreading of these fines is further investigated in (IMDC, 2022).

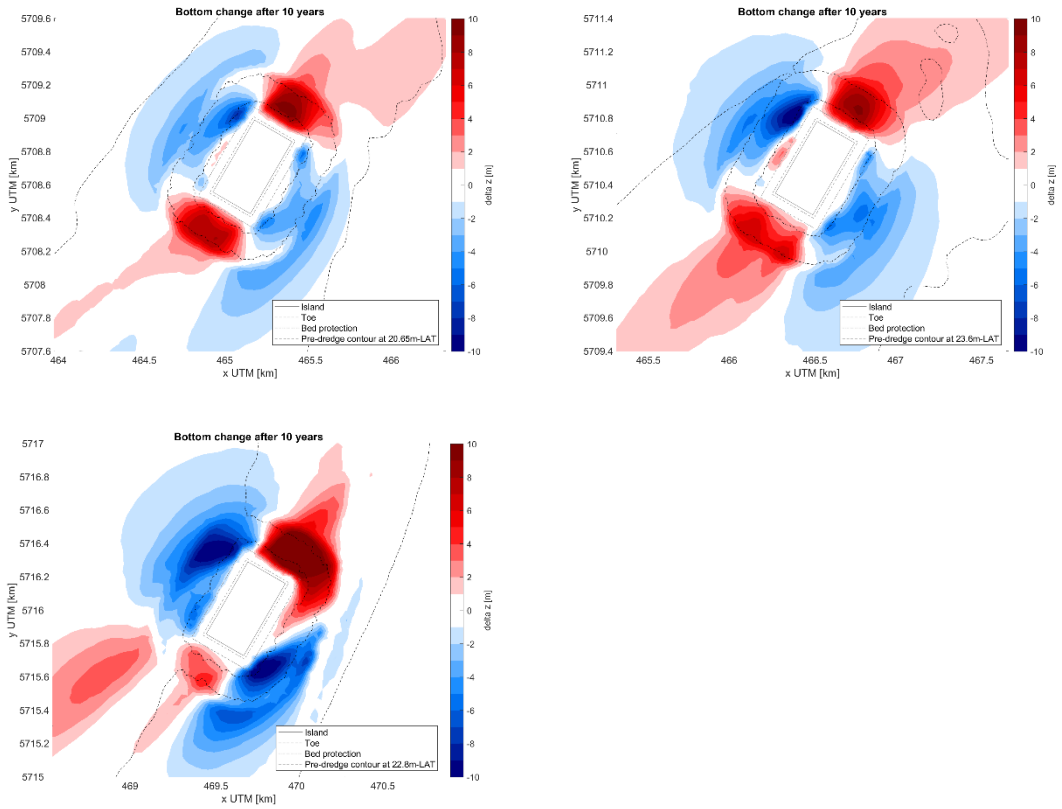

Figure 7-2: Local erosion and sedimentation pattern after 10 years for location West1 (top left), West2 (top right) and Noord (bottom left). The contours of the island, the pre-dredge design, and the local bathymetry are outlined in the figures.

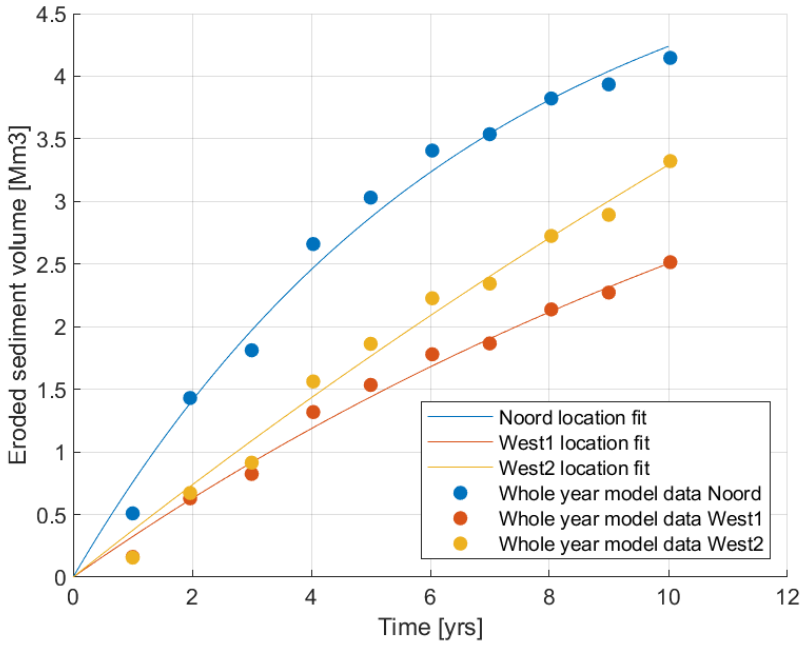

Figure 7-3: Eroded sediment volume in time for the different locations. Continuous lines depict the volume from an exponential decay fit to filter out spring-neap fluctuations, dots indicate the yearly model results used for these fits.

Table 7-1: Erosion volumes and areas at different moments in time close to the MOG2 island (after island construction with pre-scour dredging)

	West1	West2	Noord
Local eroded volume after 0.5 yr[6] [Mm³]	0.2	0.2	0.4
Local eroded area after 0.5 yr [Ha]	7	7	24
Local eroded volume after 1 yr [Mm³]	0.3	0.3	0.5
Local eroded area after 1 yr [Ha]	11	10	30
Local eroded volume after 4 yr [Mm³]	1.4	1.6	2.7
Local eroded area after 4 yr [Ha]	65	75	98
Local eroded volume after 10 yr [Mm³]	2.6	3.4	4.2
Local eroded area after 10 yr [Ha]	124	155	130

Table 7-2: Sedimentation volumes and areas at different moments in time close to the MOG2 island (after island construction with pre-scour dredging)

	West1	West2	Noord
Local sedimentation volume after 1 yr [Mm³]	0	0	0.1
Local sedimentation area after 1 yr [Ha]	2	0	9
Local sedimentation volume after 4 yr [Mm³]	0.7	1.1	1.7
Local sedimentation area after 4 yr [Ha]	35	71	82
Local sedimentation volume after 10 yr [Mm³]	2	3.8	3.5
Local sedimentation area after 10 yr [Ha]	89	163	125

7.3 Gravel bed impact

After 10 years, the islands impact is predicted to change the sandy bed with more than 10 cm over a distance of almost 10 km in the main direction of the tidal current, see Figure 7-4. The magnitude of the island impact varies per island location and is related to the local depth of the island, the local strength of the tidal current and the local orientation of the main current direction. As a result, the largest bed level changes are observed at the Noord location and the smallest at the West1 location.

Sedimentation further away from the island is caused by sediment picked-up around the island by the high bed-shear stresses in the flow acceleration zone. This sediment is transported over relatively long distances away from the island by the complex current pattern and deposited around slack tide. This results in three main areas of sedimentation for all three island locations: 1) a location about 1 km to the west-southwest of each island location, 2) a long stretched location to the south west and 3) a location to the north east that starts in the lee of the island but expands further in north east direction. Dependent on the local bathymetry this pattern varies slightly in shape and complexity.

[6] Based on exponentially decaying fit through whole-year data

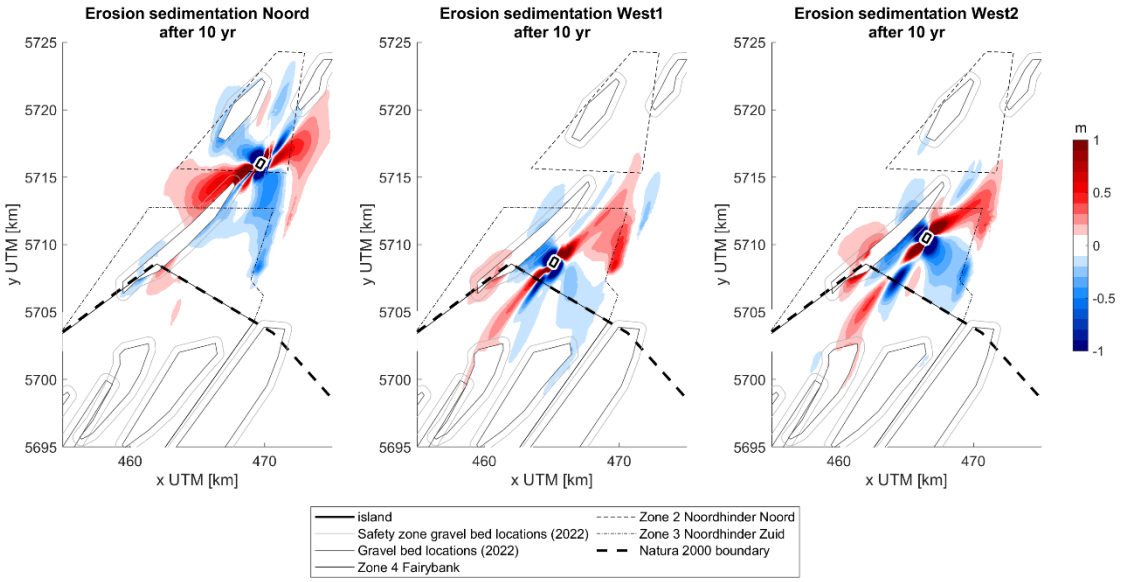

Figure 7-4: Erosion sedimentation pattern around the island at location Noord (left), West1 (center) and West2 (right) relative to a simulation without island.

For the gravel beds a thin layer of 2 cm of sand can already have a significant impact on the ecology. The sedimentation on the gravel beds because of the placement of the MOG2 island is investigated using this 2 cm threshold, and after a time period of 10 years. In Figure 7-5, the contours within which 2 cm or more sedimentation has occurred due to the MOG2 island are depicted for all three island locations. There are several zones where the island causes over 2 cm sedimentation on the gravel beds blue/green and red contour lines, but only in zones where also sedimentation is predicted in the autonomous simulations (indicated with cyan shaded area).

In Figure 7-6 the sedimentation contours for 1 cm of sedimentation are depicted. These contours cover a slightly larger area compared to the 2 cm contour lines in Figure 7-5 but the general outline is similar. It is concluded in Section 4.3 that in a simulation without the MOG2 island present, sedimentation can be observed at several locations on the gravel beds: indicating either poor local model performance or an inaccurate estimation of gravel bed extent. These locations are highlighted as the Cyan areas in Figure 7-5 and Figure 7-6. In both figures, it can be observed that the island only impacts the gravel beds at locations where in the autonomous prediction 2 cm or more sedimentation occurs as well. It should be noted that 2 and 1 cm after 10 years is equal to sedimentation of respectively 2 and 1 mm a year and this is an accuracy level that is not often attributed to morphological models on this time and spatial scale.

In Figure 7-7 the development of the 2 cm contour in time is depicted. The contours grow fast in the first few years, but slow down over time. The contour after 10 years is only marginally wider than the contour after 7.5 years. To the southeast of the West2 location the sedimentation is migrating over time rather than extending.

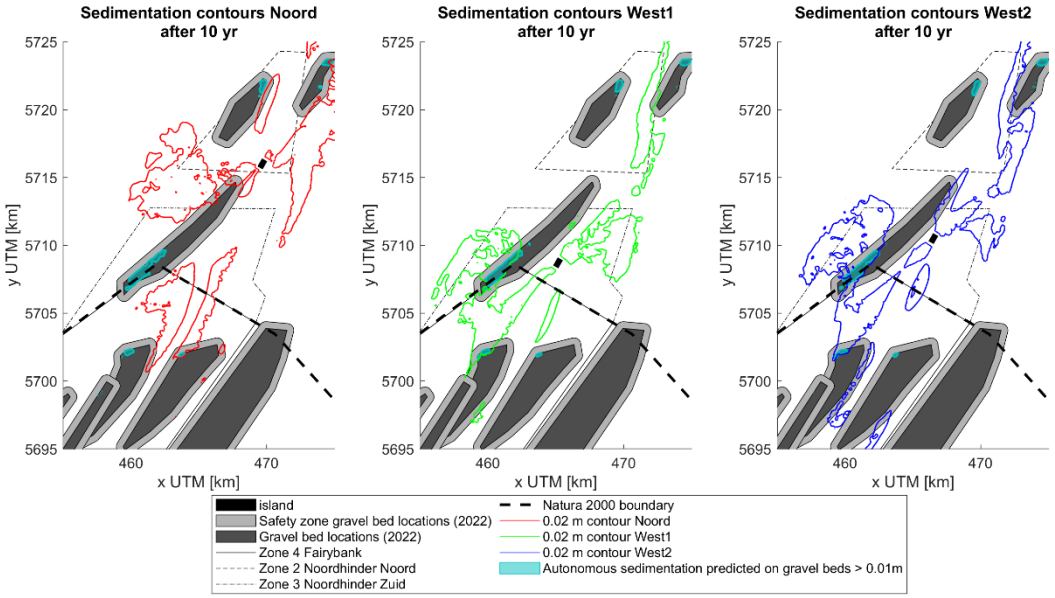

Figure 7-5: Sedimentation contours around the island locations, for more than 2 cm of sedimentation as effect of the island, after 10 years.

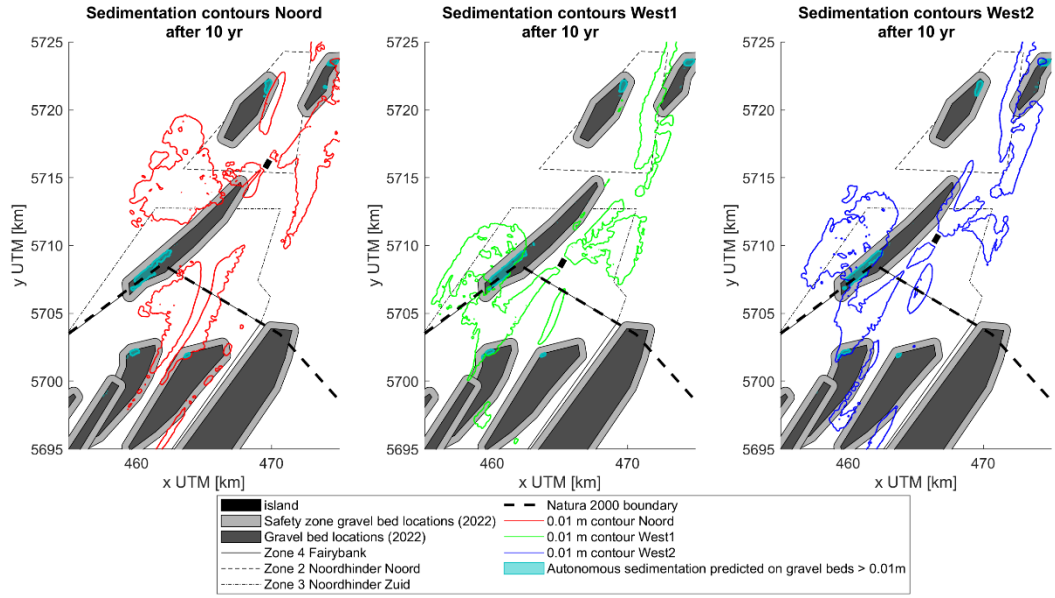

Figure 7-6: Sedimentation contours around the island locations, for more than 1 cm of sedimentation as effect of the island, after 10 years.

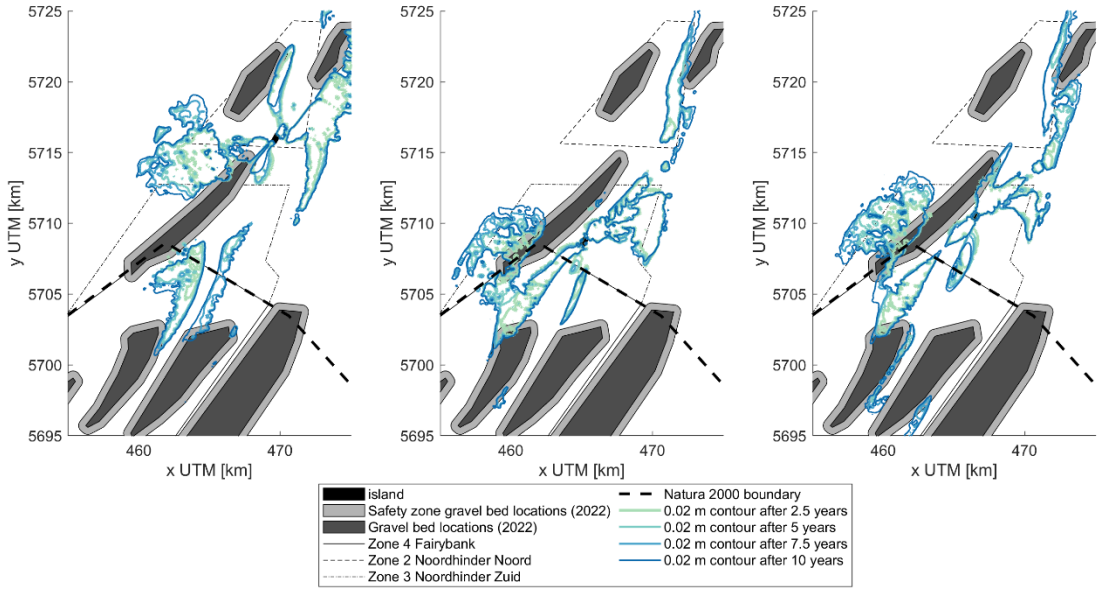

Figure 7-7: Sedimentation contours around the island locations after 2.5, 5, 7.5 and 10 years, for more than 2 cm of sedimentation as effect of the island.

7.4 Sensitivity to orientation North location

The island is oriented with a direction of 30 °N at all three locations. While the main current direction varies for each island location. Especially at the Noord location this orientation is misaligned with the main current direction of the tide of approximately 50 °N. To assess the consequences of a more optimal island orientation a 1 year simulation with an island orientation of 50 °N is carried out at location Noord. A comparison of the 2 cm sedimentation contour after 1 year with an orientation of 30 °N and 50 °N shows that the extent of the sedimentation induced by the island can be reduced by almost 50% by choosing an optimal alignment with the tidal current direction, Figure 7-8**Error! Reference source not found.**. It is expected that these differences might be a bit less pronounced after 10 years, but the general impact of the island will still be reduced by changing the orientation to 30 °N for the North location. The reduction of impact on the gravel beds is small (<5%) on this time scale but that is mainly because the sedimentation area has not reached the gravel areas yet.

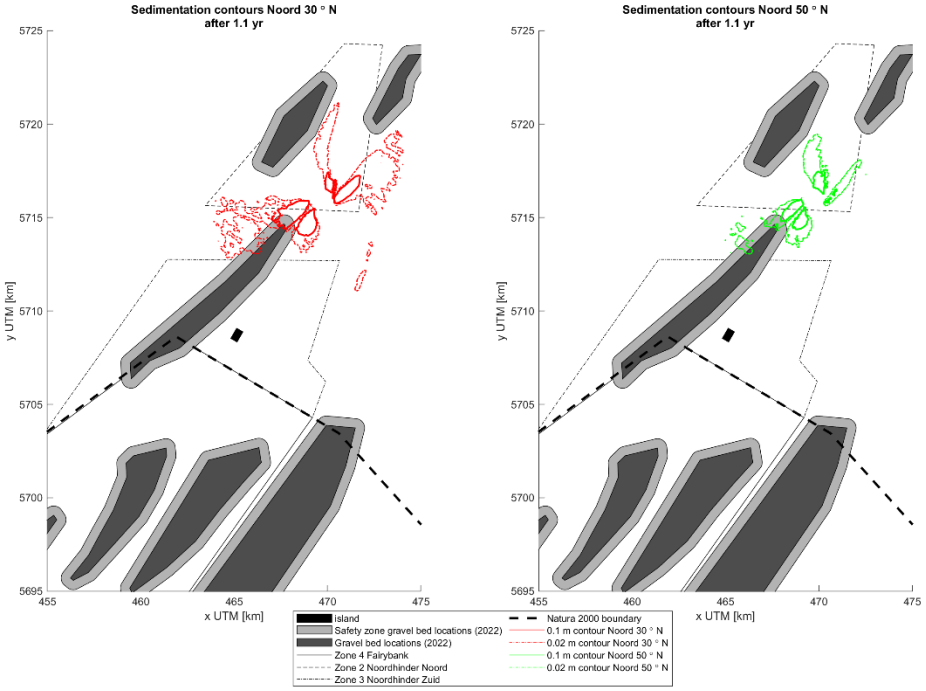

Figure 7-8: Sedimentation contours around the Noord location with an island orientation of 30 °N (left) and an orientation of 50 °N (right), for more than 2 and 10 cm of sedimentation due to the island, after 1.1 year.

7.5 Effect of pre-dredge design West1 location

The design includes a pre-dredged volume of 2 to 3 million m^3 at locations where erosion is expected to limit sedimentation induced by the island. The effectiveness of this measure is investigated by comparing a simulation with pre-dredge design and one without. The results after 2 years are presented in Figure 7-14. Close to the island the effect of pre-dredging is significant. The shape of the sedimentation areas is reduced in extent and thickness. The area of the 2 cm contour is reduced by 10% and the 10cm contour by 25% in size. This means that further away from the island, the sedimentation remains similar, but that closer to the island where the sedimentation is thicker the effect of pre-dredging is more significant. Around the gravel areas the reduction in size is a bit less than 10%.

7.6 Model sensitivities

The computational results contain a certain degree of uncertainty. This uncertainty is introduced by model inputs, model calibration, limitations of the model and choices in schematization in the model. As a result of a lack of morphological calibration data, the order of magnitude and even the direction of sediment transport remain uncertain, even with the validations which have been performed. The autonomous movement of sand dunes and ridges cannot be represented in longer term 2D computations which can also affect model outcomes. The used transport formulae and parameter settings also contribute to uncertainties in the results. Especially for the gravel bed impact these uncertainties are highly relevant because of the limited amount of sedimentation of only 1 or 2 cm which can have significant impact on the gravel bed areas.

This paragraph serves to assess the sensitivity of the model to these uncertain factors and to assess the range of conservativity in the predictions.

7.6.1 Transport formula

One of the most impactful model settings is the choice for the transport formula. The sensitivity of scour development around the island for to application of the Soulsby van Rijn (2007) and Engelund-Hansen formula (1967) was already presented in the morphological modelling report for the MOG2 tender design (Svašek & IMDC, 2022d). It was concluded that the transport formula does not significantly change the pattern or intensity of scour, but it does affect the timescale over which it develops.

The comparison between the transport formula's has been performed anew, focussing on the sedimentation patterns relevant for the gravel bed impact. The result is shown in Figure 7-9. Like the comparison from the tender design study, the sedimentation patterns resulting from either transport formula show a time discrepancy. Considering the 2 cm contour, the sedimentation calculated with the Engelund-Hansen formula after 10 years (Figure 7-9) is more resemblant of the sedimentation calculated with the Soulsby & van Rijn formula after 5 years (Figure 7-7). As such, a large discrepancy between the extent of the 2cm sedimentation contour as resolved from the Soulsby & van Rijn formula and the Engelund-Hansen formula is visible in Figure 7-9. The comparison between the two formulae as made in the morphological modelling report for the MOG2 tender design was extended for a period up to 20 and showed that the discrepancy between the morphological changes calculated with either formula decreases with time. It is theorized that a similar process is at play considering the sedimentation on the gravel beds. This leads to the conclusion that the sedimentation on the gravel beds can also occur after a longer time scale.

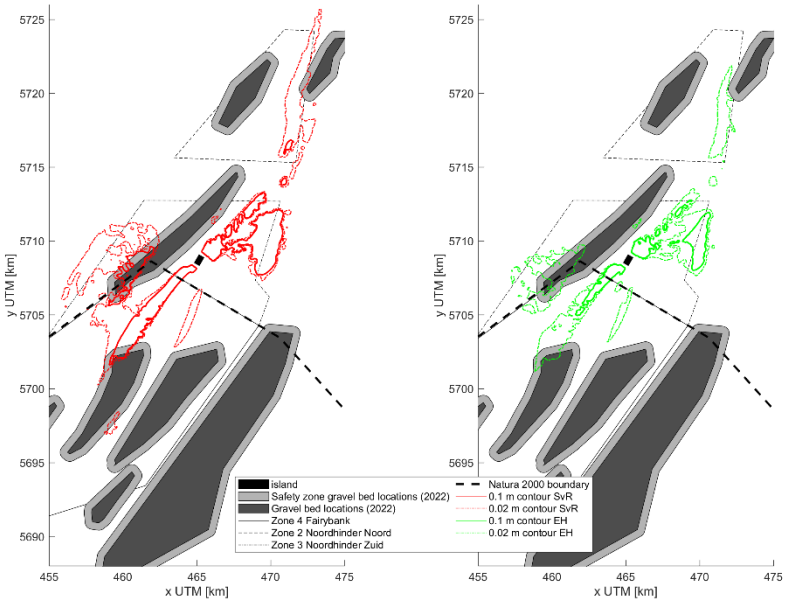

Figure 7-9: Sedimentation contours around the West1 island, for more than 2 and 10 cm of sedimentation as effect of the island, after 10 years for the Soulsby van Rijn (2007) (left) and Engelund-Hansen transport equations (right).

7.6.2 Grain size

In Svašek & IMDC (2022d) it was concluded that the extent of the morphological changes reached significant distances from the MOG2 island. Considering only one sediment grain size is employed within the simulations, this indicates the chosen sediment grain size should be representative of a relatively large area around the MOG2 island. To maintain a conservative approach, it was decided to employ the finest sediment grain size which was found in the proximity of the three potential island locations (West1, West2, North). As such, the grain size around the North location (d_{50}=312/d_{90}=581 µm) was employed within all simulations. To validate the conservative nature of this assumption a sensitivity computation with a representative grain size for the direct proximity of the West locations (d_{50}=409/d_{90}=1420 µm) was executed. The result is visualized in Figure 7-10. It is concluded that the coarser material is deposited close to the island and thus reduces the impact of the island on the gravel beds. Nevertheless, the differences are insignificant in comparison to other uncertainties such as the sediment transport formula.

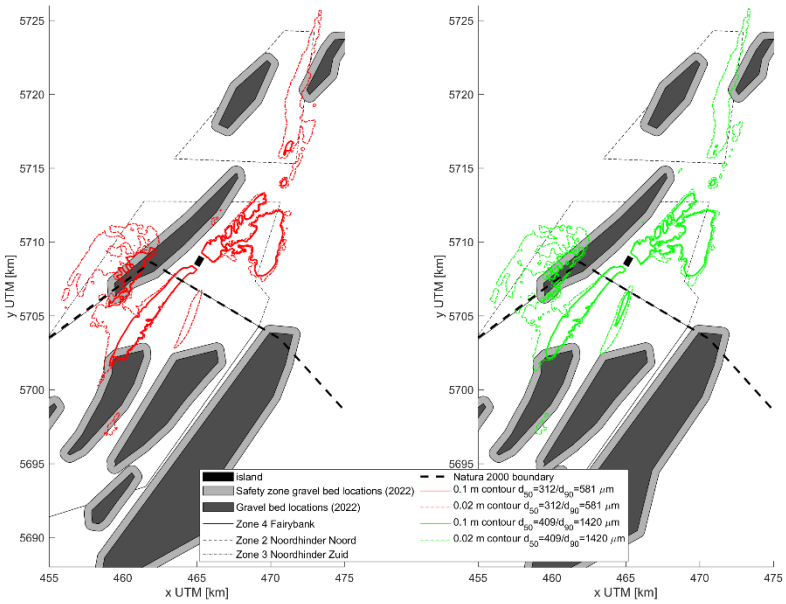

Figure 7-10: Sedimentation contours around the West1 island, for more than 2 and 10 cm of sedimentation as effect of the island, after 10 years for a grainsize distribution of d_{50}=312/d_{90}=581 µm (left) and d_{50}=409/d_{90}=1420 µm (right).

7.6.3 Waves

Within the morphological computations the wave forcing is excluded as previous studies found that the tide is the main transport mechanism at water depths such as around the MOG2 island. This is further confirmed by the analysis from section 6.3. To further verify the assumption that waves yield an insignificant effect on the morphological changes around the MOG2 island, a sensitivity computation with waves is carried out. Within this simulation the wave model is used as presented in paragraph 3.5. A representative wave climate of 17 conditions is derived to properly represent the sediment stirring introduced by waves in an average year around the West1 location. The derivation of this wave climate and the resulting conditions can be found in Appendix C. The results of the

simulation with waves compared to a simulation without waves is presented in Figure 7-11. It is concluded that waves have limited effect on the sedimentation on the gravel beds.

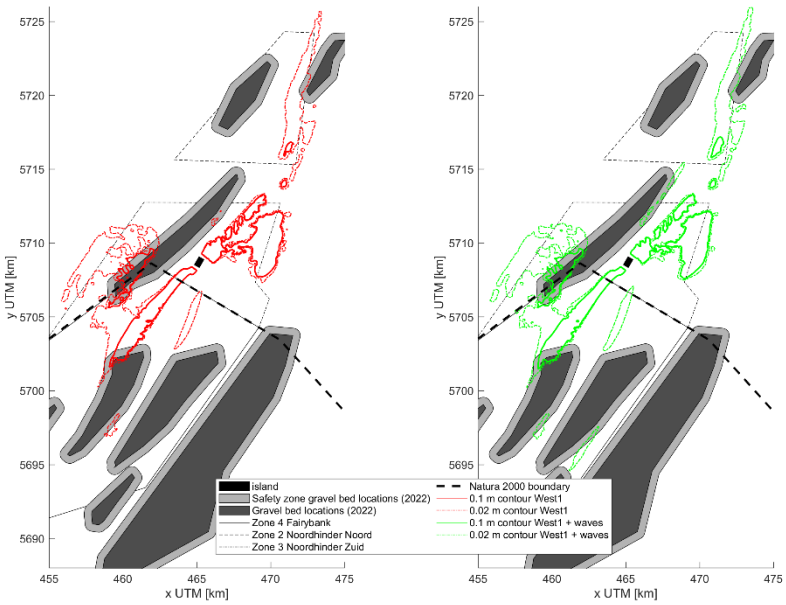

Figure 7-11: Sedimentation contours around the West1 island, for more than 2 and 10 cm of sedimentation as effect of the island, after 10 years for a simulation without waves (left), and a simulation with waves (right).

7.6.4 Roughness of the gravel areas

Within the simulations the gravel areas are assumed to be non-erodible. This leads to a more realistic sedimentation erosion pattern. In addition, and not incorporated in the standard model runs, the bed roughness of the gravel is also higher. An increased roughness induces additional turbulence over the bed which keeps more sand in suspension. Furthermore, higher roughness leads to a higher transport over the gravel bed (and a gradient over the gravel beds boundary). This is a three-dimensional effect and thus requires parametrization to be included in a 2D model. The Soulsby van Rijn formula (Soulsby,1997) has no suitable parameter to include this effect. The Engelund-Hansen formula does include such a parameter. Therefore, a sensitivity computation with the Engelund Hansen transport formula is executed to address the effect of the higher roughness on the gravel beds. The roughness height of the gravel areas is set to 12 cm and compared to a Engelund Hansen computation without extra roughness (roughness height = 7.7 cm). The 12 cm corresponds to gravel with a d_{90} of 4 cm, which is a realistic estimate based on gravel found in several vibrocore samples surrounding the gravel areas (TILES data portal). Both simulations are compared in Figure 7-12. The computation shows that especially for the southern gravel area affected by the island, this transport gradient removes all sediment that might be deposited on the gravel area. Indicating that the simulations presented in paragraph 7.3 are conservative in this regard.

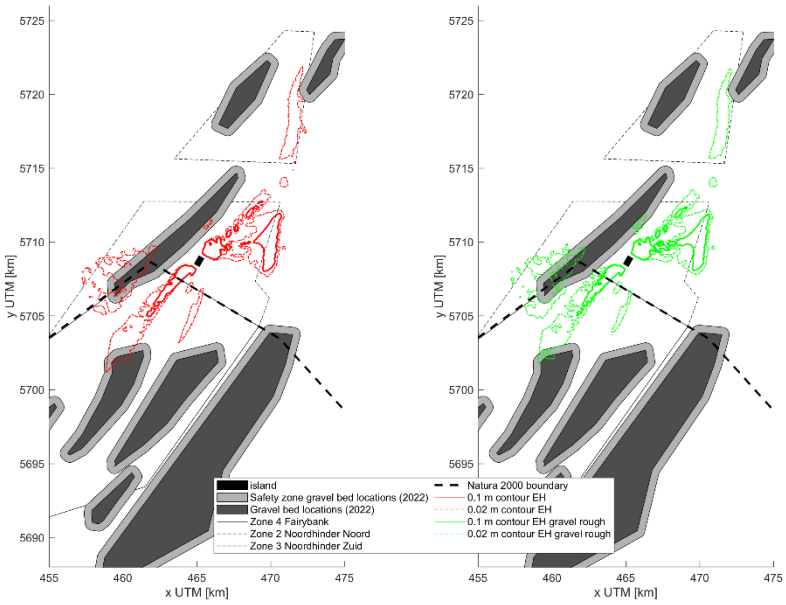

Figure 7-12: Sedimentation contours around the West1 island, for more than 2 and 10 cm of sedimentation as effect of the island, after 10 years for simulation with Engelund-Hansen transport formula (left) and with Engelund-Hansen transport formula and an increased gravel bed roughness.

7.6.5 Morphological acceleration

To speed up computations the morphological acceleration is set to 25 in the first two years and to 50 in the next 8. To assess the sensitivity of the results a computation with an acceleration of 12.5 is performed. The results after 5 years are presented in Figure 7-12 and show that this has no effect on the sedimentation pattern.

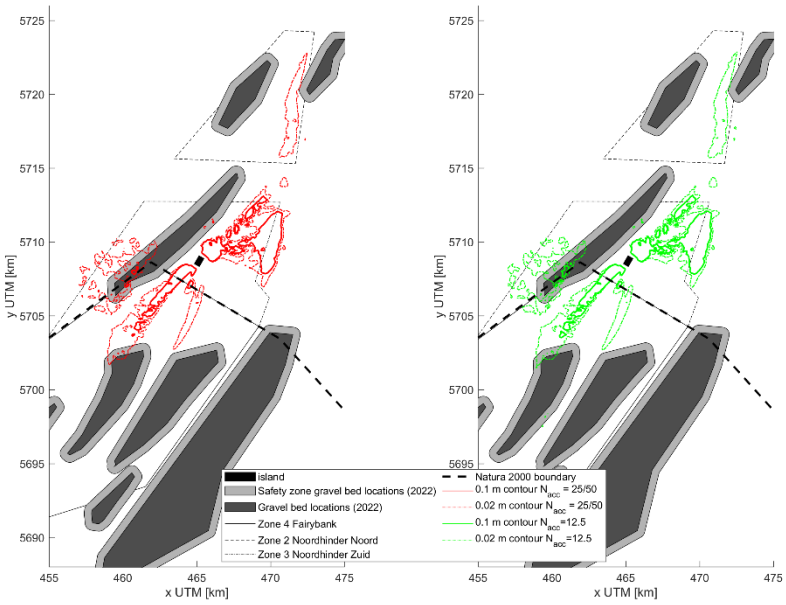

Figure 7-13: Sedimentation contours around the West1 island, for more than 2 and 10 cm of sedimentation as effect of the island, after 5 years for simulation with a morphological acceleration of 25 in the first two years and 50 in the next 8 (left) and a morphological acceleration of 12.5.

7.6.6 Spin-up

As is discussed in chapter 4, the model tends to smooth out the sand waves in the model because the 3d processes that create these sand waves are absent in the model used. The smoothing of the sand waves artificially increases the sediment transport tin the model. To eliminate this effect the model uses a morphological spin-up of 2 years. Nevertheless, after these two years an equilibrium is not reached, nor is this desired. A severe smoothing of the surrounding bathymetry include smoothing of larger bed forms, which can affect the propagation of the tide. In (Svasek & IMDC, 2022d) it was shown that the scour pit development around the island is insensitive to whether a morphological spin-up period is applied. Assessing this computation for the sedimentation on the gravel areas the conclusion is similar.

7.7 Discussion

Predictions of 1 to 2cm sedimentation can be considered on the limits/outside of the range of model accuracy. In general, morphological computations are considered to be quite uncertain. Even calibrated models can easily be 50-100% off. Also predicting migration of bed forms is not feasible with long term morphological models, which introduces additional uncertainty. This should be considered when interpreting the 1 and 2 cm contours as depicted in this chapter. Gladly, the sensitivity analysis shows that the model assumptions made are in general conservative.

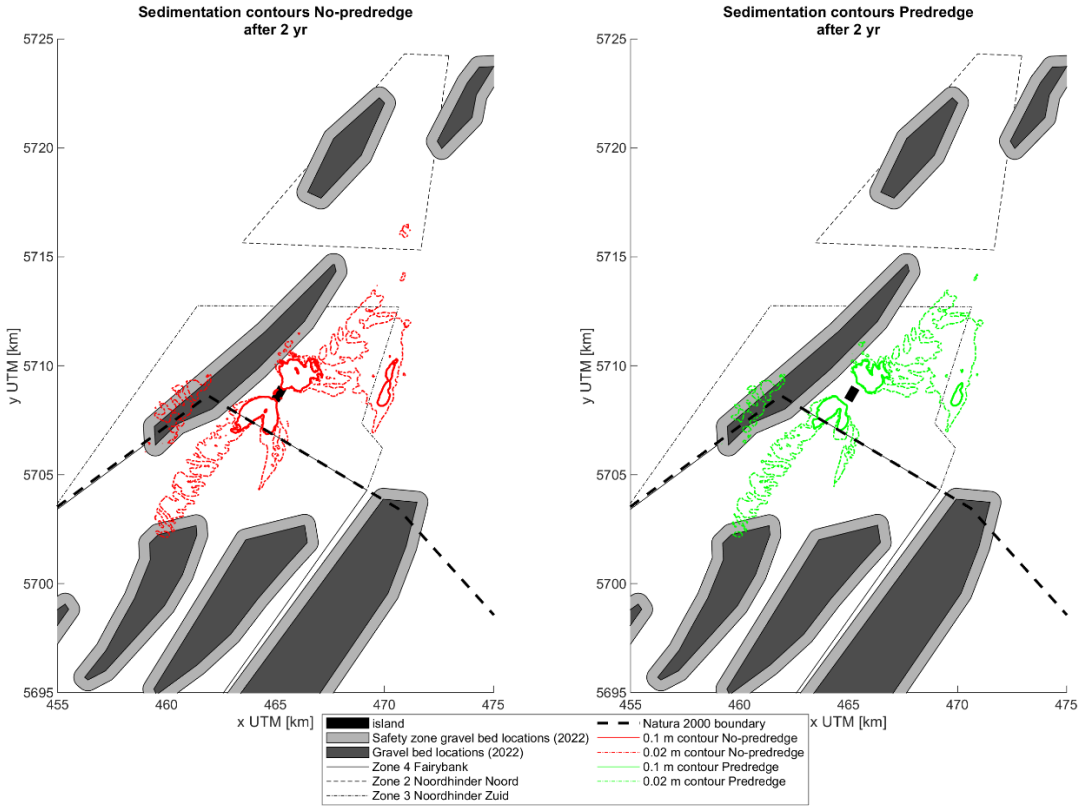

Figure 7-14: Sedimentation contours around the West1 location without pre-dredging (left) and with pre-dredging (right), for more than 2 and 10 cm of sedimentation due to the island, after 2 years.

8 CONCLUSIONS

This report assesses the environmental impact of the MOG2 island, mostly in the context of the impact on the surrounding gravel beds. Several conclusions can be drawn from the shown analyses within this report, which are discussed below.

8.1 Calculation method

The morphological impact assessment is performed with the two dimensional hydromorphological model FINEL2D. The model includes tidal water level variations and velocities and computes the response of the sea bed accordingly. The hydrodynamic and morphological setup of the model is similar to that of the Design Study (*IMDC, CDR, Svasek, 2022b*). This model can represent measured water levels and current velocities at various locations near the project location accurately.

In total, 10 morphological years are simulated. For the long-term EIA simulations, conservative-realistic sediment characteristics (d50/d90) are used, combined with the Soulsby&vanRijn sediment transport equation (*Soulsby, 1997*). The gravel beds (type 1) are simulated as non-erosive layers to simulate the reduced mobility of these gravel particles as opposed to the surrounding mobile sandy beds.

To isolate the environmental impact of the MOG2 island, results of simulations with the MOG2 island are always presented relative to an identical simulation without the MOG2 island.

8.2 Model (in)accuracies / limitations

When interpreting the results presented in this report several model (in)accuracies and limitations should be considered.

First, the applied explicit solver does not resolve turbulent diffusion and to increase confidence in the morphological results, the effect of this model limitation has been investigated. To this end the hydrodynamic results of the morphological model with an explicit solver were compared to the hydrodynamic results with an implicit solver that included a more realistic amount of eddy diffusivity. Comparison of both models showed similar flow and shear stress patterns increasing confidence in the morphology predictions.

Second, sand dunes, and ripples are (often) migrating bedforms and their dynamics are a complex coupling of detailed three-dimensional hydro and morphodynamic processes. As a result, predicting migration of bed forms is not feasible with long term morphological models, which introduces uncertainty in the computations presented. The influence of bed forms on the island effect has been largely eliminated from the calculations by spinning up the model bathymetry (which smooths out smaller bed forms) and only then implementing the island and its effects. Moreover, sensitivity computations have shown that the results are quite insensitive to this effect.

Third, several gravel bed locations were shown to attract sediment in simulations without the MOG2 island. This sedimentation is either an indication of reduced model quality in these areas or an indication of a local inaccurate demarcation of the estimated gravel bed areas. Sensitivity computations show that less sedimentation occurs on the gravel areas when they are rougher. The limitations of the model regarding the difference in sediment transport over the gravel areas and the sandy bed could be contributing to these inaccuracies.

Next, the Soulsby&vanRijn sediment transport equation (*Soulsby, 1997*) is known to yield significantly higher sediment transport compared to other transport equations (*IMDC, CDR, Svasek, 2022b)*. As a result, using a different transport formula can lead to different erosion -sedimentation patterns. Nevertheless, these pattern differences reduce with time. Indicating that the uncertainty within the transport equation mainly affects the time-scale of the erosion and sedimentation. Thus,

the time period of 10 morphological years as presented in this report remains uncertain, and the resulting morphological developments may likely correspond to longer time periods.

Finally, for the gravel beds a thin layer of sand can already have a significant impact on the ecology. Prediction of 1 to 2cm sedimentation is on the limits/outside of the range of prediction accuracy. In general morphology computations are considered to be quite uncertain. Sensitivity analysis shows that the model assumptions made are in general conservative.

8.3 Local scour around the island

In this study the spreading of the sediment that is eroded from the scour holes around the island is modelled by assuming locally characteristic sediment properties. Nevertheless, within this eroded volume also fine material is present that has the potential to travel long distances which is not modelled in this modelling study. Within the framework of the EIA the dispersion of fines is assessed by IMDC (2022), but the local scour as modelled in this study serves as an input.

The local erosion around the MOG2 island is largely variable depending on the island location. The highest local impact was simulated at the Noord location due to the large local water depth and the discrepancy between the flow direction and the island orientation. The lowest local impact was simulated at the West1 location. For all locations the scour is strongest in the first year and reduces with time.

At the Noord location, it was shown an orientation of 50 degrees rather than 30 degrees could yield a significant reduction in the sedimentation in the initial year after the placement of the island. Furthermore, it was shown that pre-dredging around the island has a large impact on the sedimentation in the direct vicinity of the island, but only limited impact on the extent of the 2 cm sedimentation contour relevant for the impact on gravel beds.

8.4 Gravel bed impact

Sedimentation of more than 1 cm in 10 years on the gravel beds is limited. Most of the gravel bed areas remain uninfluenced by the MOG2 island. The gravel bed locations on which more than 1 cm of sedimentation is predicted due to the placement of the MOG2 island coincide with gravel bed locations that attract more than 1 cm of sediment in the autonomous simulation. Thus, no additional sedimentation areas on the gravel beds are introduced with the placement of the island within the simulations.

Sedimentation relatively far away from the island occurs in three stages. First, sediment is stirred-up in the zones of accelerated flow around the island during maximum ebb or flood flow. Second, this sediment spreads out and is transported with the rotating tide. Finally, the sediment is deposited around slack tide.

Over time, it was shown the sedimentation areas expand rapidly in the first 2 years. However, after approximately 7.5 years, the sedimentation area remains relatively constant.

Although different locations have a large impact on the erosion and deposition effects directly around the island (see next section), the different locations are not significantly distinctive with regard to the impact on the gravel beds.

REFERENCES

Engelund, F., & Hansen, E. (1967). A monograph on sediment transport in alluvial streams. Technical University of Denmark 0stervoldgade 10, Copenhagen K.

Glaister, P., (1993). Flux difference splitting for open-channel flows. International Journal for Numerical Methods in Fluids 16: p. 629-654.

Hervouet, J.M., (2007). Hydrodynamics of Free-Surface Flows: Modelling with the Finite Element Method. Appendix A, Tide-generating force. John Wiley & Sons.

Hughes, T.J.R., (1987). The finite element method. Englewood Cliff. New Jersey: Prentice-Hall.

IMDC. (2022). Pluimmodellering MER MOG2. I/RA/11614/22.125/TWO/.

Labeur, R.J. (2009). Finite element modelling of transport and non-hydrostatic flow in environmental fluid mechanics. Ph.D. Thesis, Delft University of Technology, Delft

Labeur, R.J., Wells, G.N. (2012). Energy stable and momentum conservative interface stabilised Finite Element Method for the incompressible Navier-Stokes equations. SIAM Journal on Scientific Computing, 34(2), A889-A913

Overes, P. (2021). Modeling Sand Wave Field Dynamics in the North Sea using Delft3D Flexible Mesh.

Ralston, M. L., & Jennrich, R. I. (1978). DUD, a derivative-free algorithm for nonlinear least squares. Technometrics, 20(1), 7-14.

Schrama, E.J.O., (2020). Lecture Notes on Planetary sciences and Satellite Orbit Determination. Delft University of Technology, Faculty of Aerospace, Astrodynamics and Satellite missions.

Soulsby, R.L., (1997). Dynamics of marine sands: a manual for practical applications. Thomas Telford, London.

Svasek, IMDC, CDR (2021). Data GAP analysis Site Conditions. Report. Reference, 2094/U21376/E/YAT.

Svasek, (2022a). MOG-II Island Metocean Report. Report. Reference, MOG-II-SVA-IIZIR-00002.

Svasek, CDR, (2022b). MOG-II Island Wave&Current Scour Protection assessment. Note. Reference, MOG2/CDR/LEDIN-00003_v1.0.

Svasek, (2022c). MOG-II eliminated alternatives. Memorandum. Reference, 2094/U22391/A/YSTE.

Svasek, IMDC (2022d). MOG-II Morphological study MOG2 island tender design Report. Reference: MOG2-SVA-LEMIN-00001

Van Lancker, V., & Baeye, M. (2015). Wave glider monitoring of sediment transport and dredge plumes in a shallow marine sandbank environment. PloS one, 10(6), e0128948.

Van Rijn, L. C. (1984). Sediment transport. Journal of hydraulic engineering, 110(12), 1733-1754.

A BED SHEAR STRESSES OVER ONE PEAK TIDAL CYCLE

This Appendix serves as visual support for Chapter 5. In the images, the difference in bed shear stress between a hydrodynamical simulation with the MOG2 island and a hydrodynamical simulation without the MOG2 island is shown for a model using the FINEL2D-explicit software package (left images) and for a model using the FINEL2D-implicit software package (right images). The most important difference between either software package is the inclusion of a turbulence model in the FINEL2D-implicit software package.

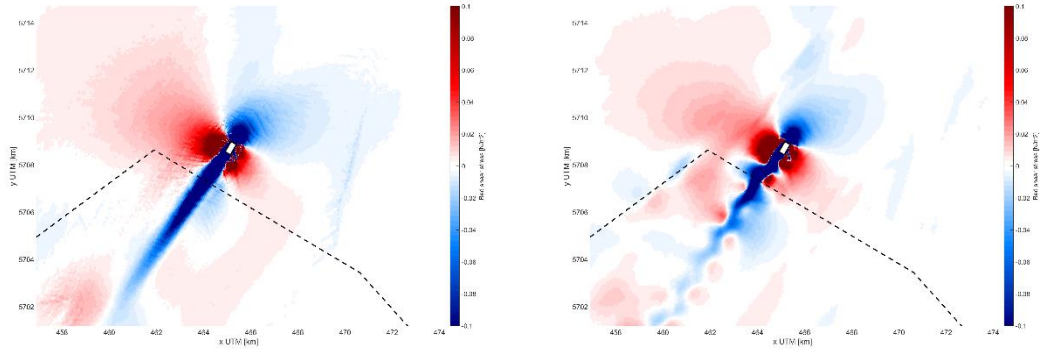

Figure A- 1: Bed shear stress FINEL2D-explicit (left) and FINEL2D-implicit (right) at T = 0 h

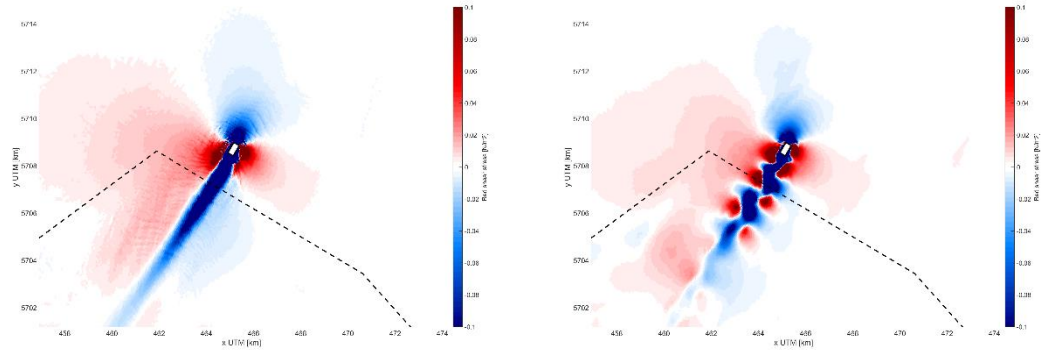

Figure A- 2: Bed shear stress FINEL2D-explicit (left) and FINEL2D-implicit (right) at T = 1 h

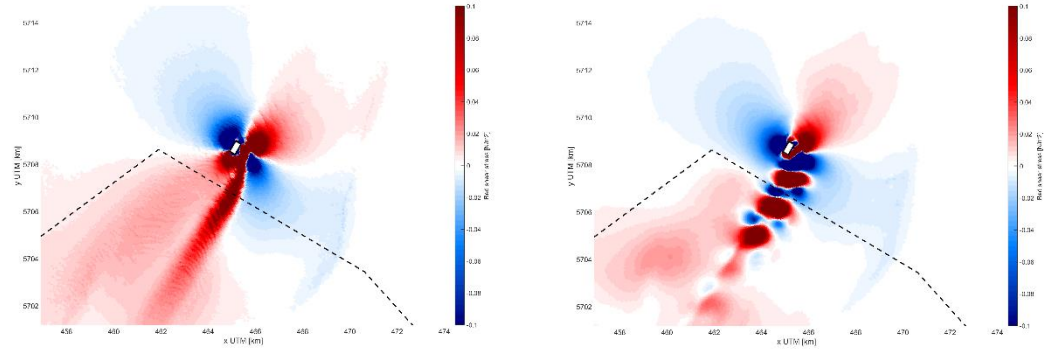

Figure A- 3: Bed shear stress FINEL2D-explicit (left) and FINEL2D-implicit (right) at T = 2 h

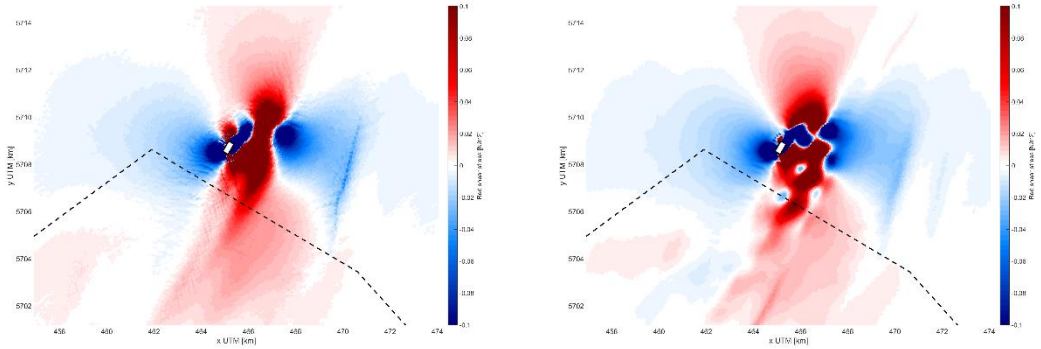

Figure A- 4: Bed shear stress FINEL2D-explicit (left) and FINEL2D-implicit (right) at T = 3 h

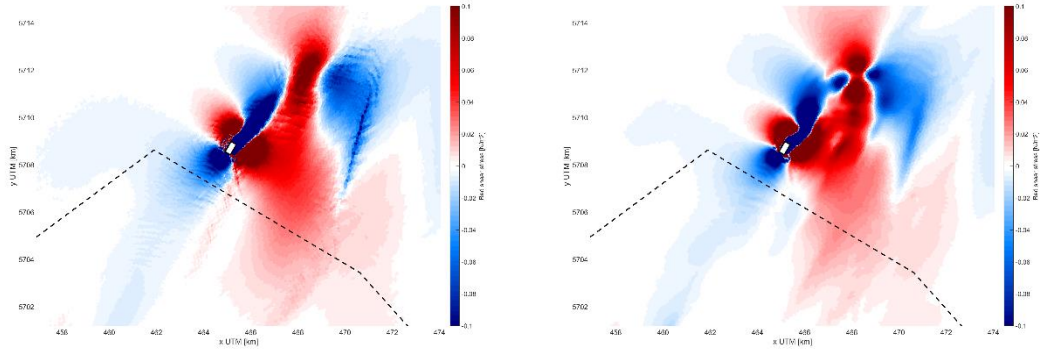

Figure A- 5: Bed shear stress FINEL2D-explicit (left) and FINEL2D-implicit (right) at T = 4 h

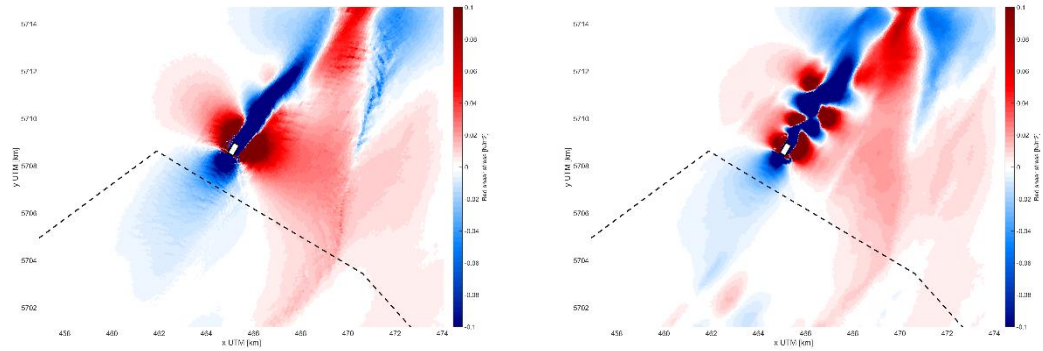

Figure A- 6: Bed shear stress FINEL2D-explicit (left) and FINEL2D-implicit (right) at T = 5 h

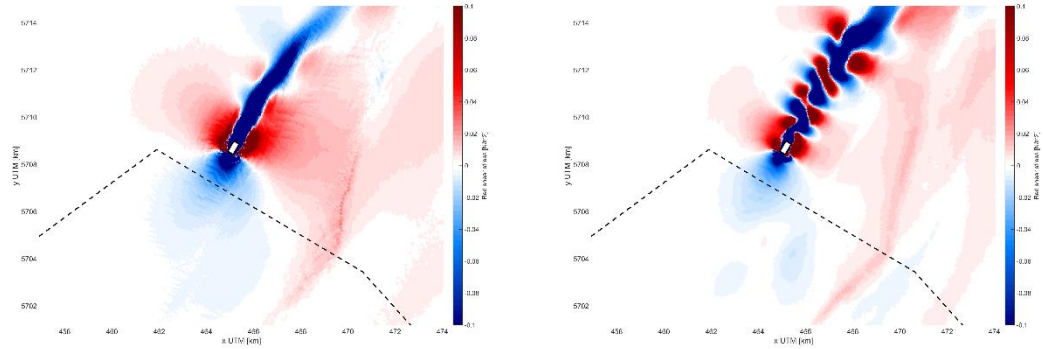

Figure A- 7: Bed shear stress FINEL2D-explicit (left) and FINEL2D-implicit (right) at T = 6 h

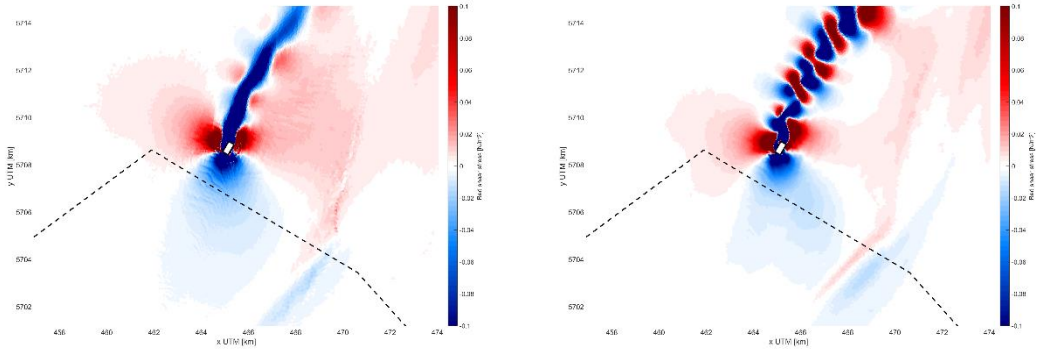

Figure A- 8: Bed shear stress FINEL2D-explicit (left) and FINEL2D-implicit (right) at T = 7 h

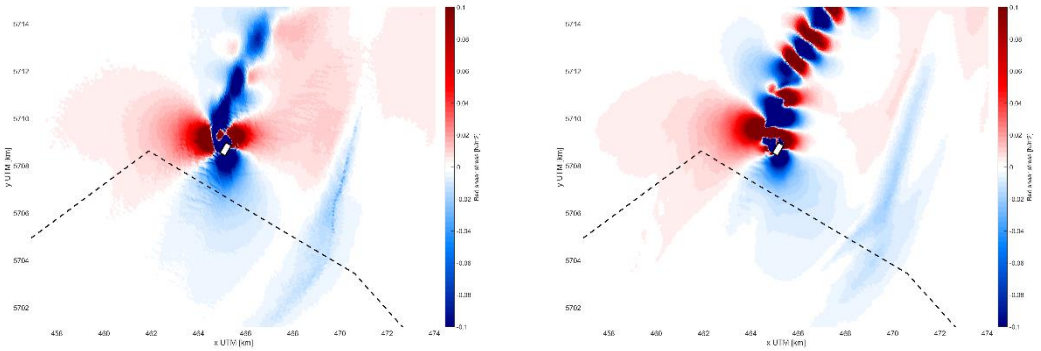

Figure A- 9: Bed shear stress FINEL2D-explicit (left) and FINEL2D-implicit (right) at T = 8 h

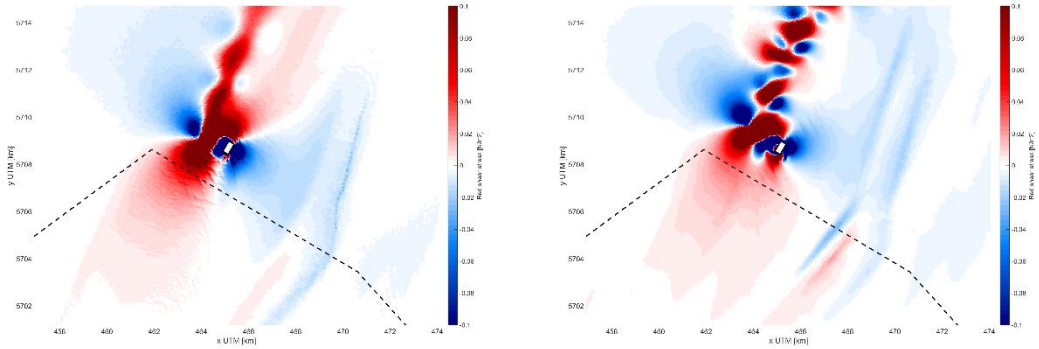

Figure A- 10: Bed shear stress FINEL2D-explicit (left) and FINEL2D-implicit (right) at T = 9 h

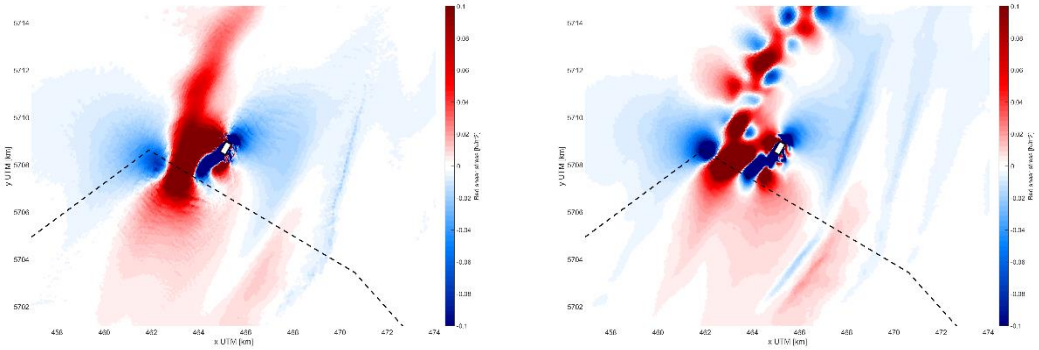

Figure A- 11: Bed shear stress FINEL2D-explicit (left) and FINEL2D-implicit (right) at T = 10 h

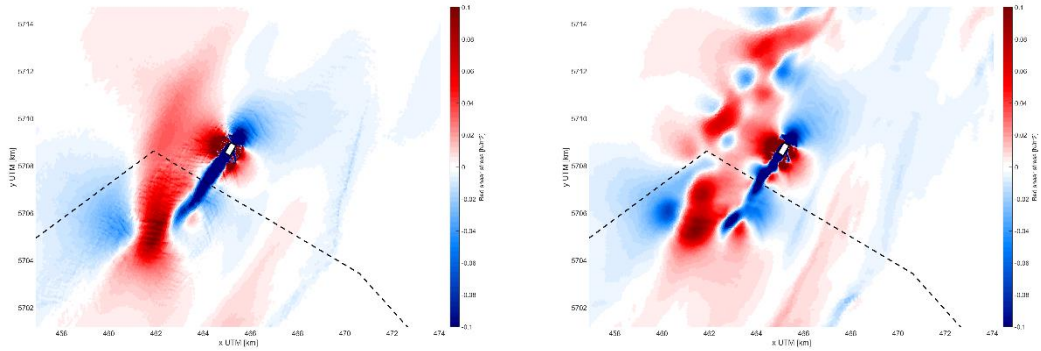

Figure A- 12: Bed shear stress FINEL2D-explicit (left) and FINEL2D-implicit (right) at T = 11 h

B LOCAL EROSION SEDIMENTATION

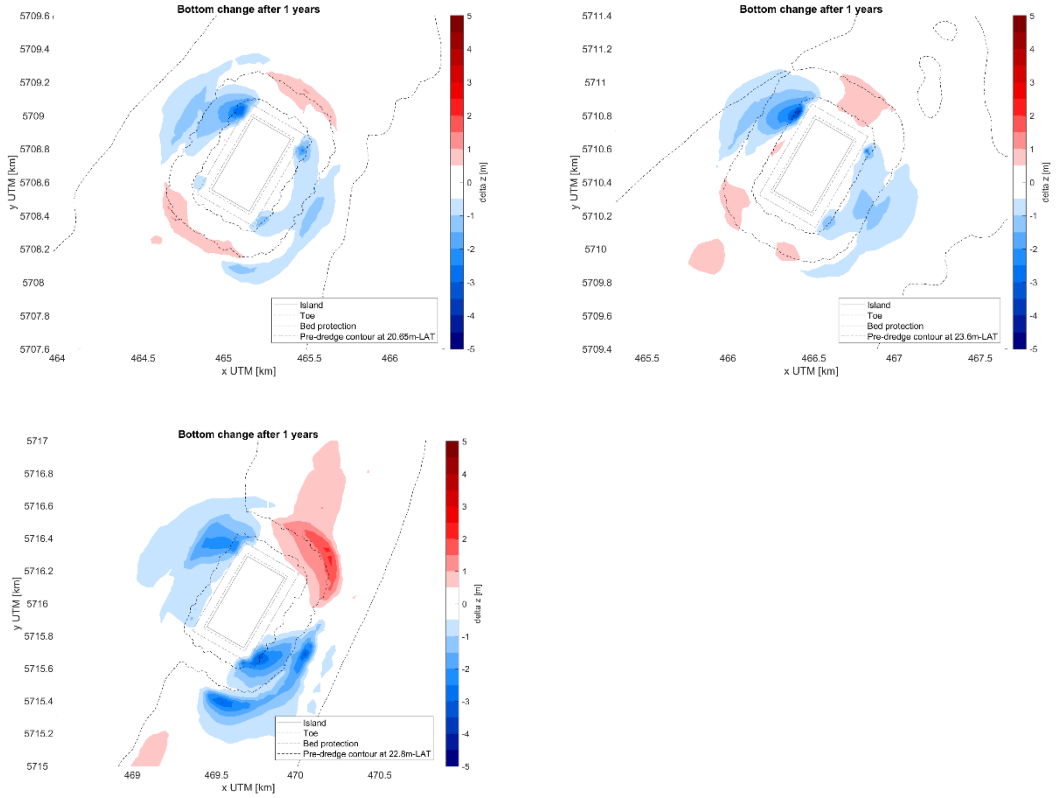

Figure B- 1: Local erosion and sedimentation pattern after 1 years for location West1 (top left), West2 (top right) and Noord (bottom left). The contours of the island, the pre-dredge design, and the local bathymetry are outlined in the figures.

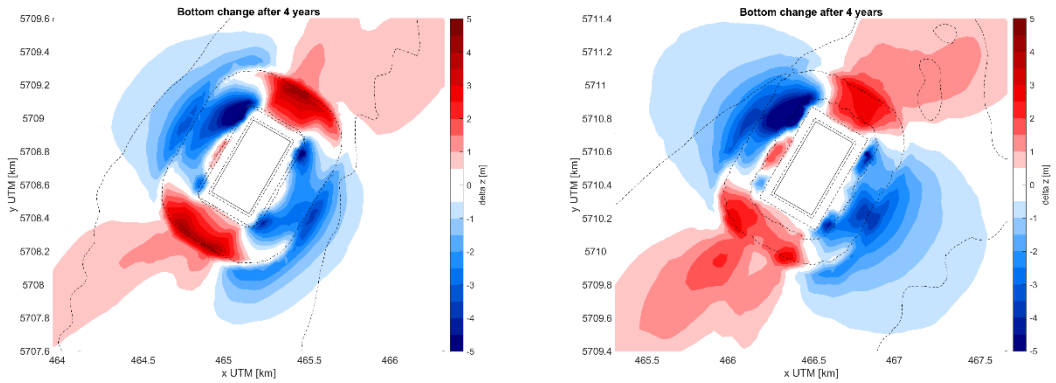

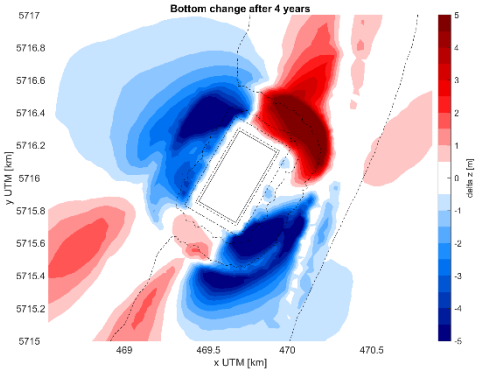

Figure B- 2: Local erosion and sedimentation pattern after 4 years for location West1 (top left), West2 (top right) and Noord (bottom left). The contours of the island, the pre-dredge design, and the local bathymetry are outlined in the figures.

C DERIVATION REPRESENTATIVE WAVE CLIMATE

Besides the currents, the waves also generate stirring of the sediment at the bottom of the sea. The morphological computations use a morphological acceleration factor to speed up the computation. For this reason a real observed wave signal cannot be imposed as a representative wave signal. A representative wave climate needs to be deducted from observed measurements. For this reason 40 years of wave data of the West location is used as derived in IMDC, CDR, Svašek (2022a).

The sediment transport formula that is used is the morphological computations is the Soulsby-Van Rijn formula for het transport of non-cohesive sediment, see Soulsby (1997):

$$q = u(A_{sb} + A_{ss}) \cdot \left(\left(u^2 + \frac{0.018 u_{rms}^2}{C_d} \right)^{0.5} - u_c \right)^{2.4} \cdot (1 - \alpha_b m) \qquad \text{Eq 3}$$

q	Volumetric sediment flux	[m^3/s]
u	Depth averaged flow velocity	[m/s]
A_{sb}, A_{ss}	Bed and suspended load multiplication factors	[-]
u_{rms}	Orbital velocity at the bottom	[m/s]
u_c	Critical velocity for movement of sediment	[m/s]
C_d	Drag coefficient	[-]
α_b	Bed slope coefficient (=1.6)	[-]
m	Bed slope in direction of current, defined as tan(β)	[-]

The part of Eq 3 between the power 2.4 can be considered as the stirring factor. This part is used in the derivation of the representative wave climate. A depth of 17m is assumed, together with a d_{50} grainsize of 350 µm and a d_{90} of 500 µm, which are required to calculate the u_c.

In the stirring part both a current and a wave stirring is present in combination with a critical threshold for movement of sediment. It is thus necessary to consider the stirring of the waves in combination with a velocity in order to get a representative wave climate. For this purpose a representative tidal signal is chosen out of several tidal signals of several locations in the direct vicinity of the project site.

The wave time series consists of 40 years of data at the West location with a time interval of 30 minutes. Every 30 minutes that a wave measurement is available the stirring is calculated over a complete representative tide keeping the wave parameters constant for this specific time period. The average stirring over this tide is now taken as the representative stirring of the combination of both wave and current.

The goal is to make a wave climate using blocks of 12 hours, where the wave height is kept constant. Using a spring-neap cycle (approx. 14 days) 28 blocks are available to impose waves in the morphodynamic computations.

Using the obtained stirring timeseries a pivot table is constructed where the significant wave height is used against the wave direction. From this table, 17 wave classes are defined, which are shown in Table C- 1.Several conditions are represented with a zero wave height. This indicates that for this

specific condition the stirring caused by waves is negligible compared to the stirring caused by currents. Thus, the wave condition can be ignored. This is roughly 43% of the time.

The wave period in Table C- 1 is obtained by generating a fit between the observed wave height and peak period so that the significant wave height is accompanied by a realistic peak wave period. The wave direction equals the average of the observed wave direction within each wave class.

Table C- 1: Definition of wave classes

Segment	Wave condition	Percentage	Number blocks	Wave height (Hs)	Wave period (Tp)	Wave direction [deg N]
345-15	Daily	17.9%	5	1.42	5.6	2
345-15	Storm	3.6%	1	2.88	8.7	359
15-45	Daily	10.7%	3	0	0	0
15-45	Storm	3.6%	1	2.36	7.6	27
45-105	Daily	7.1%	2	1.44	5.6	71
105-180	Daily	3.6%	1	1.79	6.3	154
180-210	Daily	3.6%	1	0	0	0
210-240	Daily	14.3%	4	0	0	0
210-240	Storm	3.6%	1	2.73	8.4	229
240-285	Daily	14.3%	4	0	0	0
240-285	Storm	3.6%	1	2.5	7.8	259
285-345	Daily	10.7%	3	1.17	5.1	318
285-345	Storm	3.6%	1	2.6	8.1	317


SVAŠEK
HYDRAULICS
COASTAL, HARBOUR AND RIVER CONSULTANTS